

This is a non peer reviewed preprint submitted to EarthArxiv.

Geophysical and Geochemical Constraints on Magma Storage Depths along the Cascade Arc: Knowns and Unknowns

Penny E Wieser^{1,2*}, Adam J.R. Kent², Christy B. Till³, Geoff A. Abers⁴

1. **Corresponding author:** Penny_wieser@berkeley.edu, 541-908-4572. Department of Earth and Planetary Sciences, McCone Hall, UC Berkeley, 94720, USA
2. College of Earth, Ocean and Atmospheric Sciences, Oregon State University, 97331, USA
3. School of Earth and Space Exploration, Arizona State University, Tempe, AZ 85281, USA
4. Earth and Atmospheric Sciences, Cornell University, Ithaca, NY 14850, USA

We have submitted to G3 (geochemistry, geophysics, geosystems).

We welcome any feedback – think we've missed a study? Think we've misrepresented your work? Please let us know! That is why we are posting a preprint (email penny_wieser@berkeley.edu)

Geophysical and Geochemical Constraints on Magma Storage Depths along the Cascade Arc: Knowns and Unknowns

Penny E Wieser^{1,2*}, Adam J.R. Kent², Christy B. Till³, Geoff A. Abers⁴

1. **Corresponding author:** Penny_wieser@berkeley.edu, 541–908–4572. Department of Earth and Planetary Sciences, McCone Hall, UC Berkeley, 94720, USA

2. College of Earth, Ocean and Atmospheric Sciences, Oregon State University, 97331, USA

3. School of Earth and Space Exploration, Arizona State University, Tempe, AZ 85281, USA

4. Earth and Atmospheric Sciences, Cornell University, Ithaca, NY 14850, USA

Key Points (140 characters or less)

1. The availability of geophysical and petrological constraints on magma storage depths along the Cascade arc is highly variable.
2. Available geophysical, mineral-melt and melt inclusion constraints cluster at 0-15 km depth ($\sim 2 \pm 2$ kbar), consistent with global compilations
3. Investigating the potential for deeper storage of the most mafic magmas will require studies accounting for melt inclusion vapour bubble CO_2 .

Abstract (can only be 250 words)

The iconic volcanoes of the Cascade arc stretch from Lassen Volcanic Center in northern California, through Oregon and Washington, to the Garibaldi Volcanic Belt in British Columbia. Recent studies have reviewed differences in the distribution and eruptive volumes of vents, as well as variations in geochemical compositions and heat flux along strike (amongst other characteristics). We investigate whether these along-arc variations manifest as variations in magma storage conditions. We compile available constraints on magma storage depths from InSAR, geodetics, seismic inversions, and magnetotellurics for each major edifice, and compare these to melt inclusion saturation pressures, pressures calculated using mineral-only barometers, and constraints from experimental petrology. The availability of magma storage depth estimates varies greatly along the arc, with abundant geochemical and geophysical data available for some systems (e.g. Lassen Volcanic Center, Mt. St. Helens), and very limited data available for other volcanoes, including many which are classified as “very high threat” by the USGS (e.g., Glacier Peak, Mt. Baker, Mt. Hood, Three Sisters). Acknowledging the limitations of data availability and the large uncertainties associated with certain methods, available data is indicative of magma storage within the upper 15 km of the crust ($\sim 2 \pm 2$ kbar). These findings are consistent with previous work recognising barometric estimates cluster within the upper crust in many arcs worldwide. There are no clear offsets in magma storage between arc segments that are in extension, transtension or compression, although substantially more petrological work is needed for fine scale evaluation of storage pressures.

Plain language summary

The Cascade arc contains a number of large volcanoes which present a significant hazard to human populations and infrastructure (e.g. Mount St. Helens, Mount Rainier). Until now, there has been no wide-scale review of where magma (molten rock) is stored in the crust beneath these volcanoes, even though understanding where magma is stored is very important to help monitor unrest at these volcanoes, and to predict future activity. We compile all available data on magma storage for each volcano, and show that a number of volcanoes have had very few studies performed at them, despite the fact they present a significant risk to society. The (albeit sparse) available data suggests that most magma is stored at 0-15 km depth before eruption.

Introduction

Determining the depths at which magmas are stored in continental arcs is a key parameter to help inform models of the formation and evolution of the continental crust (e.g., Ducea et al., 2015; Lee and Anderson, 2015; Rudnick, 1995), as well as to aid our understanding of volcanic eruptions and hazards. For example, precise determinations of magma storage depths help to distinguish between end-member models, where magmas may be distributed in a mush zone spanning the entire crust (Cashman et al., 2017), or concentrated in distinct magma storage reservoirs (e.g. Kilauea Volcano, Poland et al., 2014; Wieser et al., 2021, Benzmianny Volcano, Turner et al., 2013). Magma storage depths also influence the eruptive style, size and frequency of volcanic eruptions (Huber et al., 2019), and can be used to help interpret signals of volcanic unrest in monitoring data (Pritchard et al., 2019). Integration of petrological and geophysical constraints on magma storage depths was identified as vital to improve our understanding of magma storage, staging and transport by the SZ4D initiative (Hilley et al., 2022).

The Cascade arc presents an interesting case study to investigate magma storage depths, because of the wide variability in volcanic morphology, melt composition, and parameters relating to magma production along the arc (Hildreth, 2007; Till et al., 2019). The Cascade arc trends North-South along the Western margin of the US and Canada, forming as a result of the eastward subduction of the Juan de Fuca and Gorda plates beneath the North American plate. Quaternary activity in the Cascades has occurred at >2300 individual vents, and at least 30 topographically prominent edifices representing longer-lived magmatic systems (Hildreth, 2007). These larger edifices stretch from Lassen Peak in North California (USA) to Mt. Meager in British Columbia (Canada) along an approximately linear trend, erupting mostly intermediate and silicic magmas (Fig. 1). The more distributed off-axis fields of smaller, often monogenetic vents are characterized by more mafic compositions (O'Hara et al., 2020). In addition to activity focused around the arc axis, there are also three prominent rear-arc volcanic fields (Simcoe Mountains, Newberry Volcano, and Medicine Lake; Donnelly-Nolan et al., 2008; Hildreth and Fierstein, 2015; Sherrod et al., 1997). These major off-axis volcanic fields are thought to be associated with the impingement of the Basin and Range extensional province on the eastern limit of Cascade volcanism (Guffanti and Weaver, 1988; Priest et al., 2013).

Volcanism in the Cascades presents a significant societal hazard. Fourteen Cascade edifices have been active since the late Holocene, and 11 are listed in the USGS National Volcanic Threat assessment as "Very high threat" (Mt. St. Helens, Mt. Rainier, Mt. Shasta, Mt. Hood, Three Sisters, Lassen Volcanic Center, Newberry Volcano, Mt. Baker, Glacier Peak, Crater Lake; Ewert et al., 2018). Two more (Mt. Adams and Medicine Lake) are listed as "High Threat" (Fig. 1).

Over the last few decades, a number of studies have reviewed various aspects of Cascade volcanism on an arc-scale. Hildreth (2007) provided a comprehensive summary of the number, location, and

distribution of quaternary vents, along with descriptions of eruptive activity and approximate volume estimates of different vents along the arc. Poland et al. (2017) reviewed geodetic data collected over several decades in the Cascades to investigate the diverse causes of surface deformation. From a geochemical perspective, Schmitt et al. (2008) and Pitcher and Kent (2019) reviewed the major, trace and isotopic composition of samples to assess compositional variability along the arc. Pitcher and Kent (2019) used data from >12,000 samples to identify six statistically distinct arc-segments on the basis of erupted compositions. Integrating geophysics and geochemistry, Till et al. (2019) examined variations in erupted volumes and compositions, heat budget, and seismic velocities along the Cascades to investigate the influence of crustal processes (e.g., tectonic stress state) vs. mantle processes (e.g., magma generation, variations in subduction parameters, mantle wedge dynamics) on Cascade variability.

While geophysical and petrological studies have been performed at individual centres to investigate the pressures, temperatures and timescales associated with the magmatic plumbing system, there has been no detailed arc-scale review of magma storage conditions. A brief compilation was presented by Dufek et al. (2022, their Fig. 3). However, data sources and uncertainty associated with each estimate were not discussed. Based on the correlation between long seismic phase velocities and crustal heat flow, Till et al. (2019) suggest that crustal seismic structure and heat flow are primarily controlled by magmatic processes and advection of heat occurring in the upper mantle/deepest crust. They also argued that the flux of mantle-derived basalt varies by a factor of two along strike in the Quaternary Cascades. In Ocean-Island Basalts, it has been shown that volcanoes with longer repose periods (taken as a proxy for the magma supply rate) tend to be characterized by deeper magma storage (Gleeson et al., 2021). This correlation may indicate that large melts fluxes are required to maintain active crustal storage reservoirs in the cooler upper crust. Thus, it may be expected that shallower magma storage depths are found in the region of the arc with higher mantle supply. Alternatively, magma storage in the Cascades may be controlled by crustal processes such as the crustal stress state, or prominent lithological or density boundaries within the crust (Chaussard and Amelung, 2014).

A number of methods have been used to determine magma storage depths in the Cascades and elsewhere. These can broadly be subdivided into geophysical and petrological methods. One common petrological method is mineral-only and mineral-melt barometry, which relies on pressure-sensitivity of the exchange of chemical components between minerals and the liquid from which they crystallize (or re-equilibrate with, Putirka, 2008). In the Cascades, equilibrium involving clinopyroxene (Cpx), orthopyroxene (Opx), amphibole (Amp) and liquid (Liq) compositions have been used to determine magma storage conditions (e.g., Cpx-Liq, Amp-Liq, Hollyday et al., 2020; Scruggs and Putirka, 2018). A second petrological method which has been applied to the cascades is melt inclusion barometry (e.g., Aster et al., 2016; Ruscitto et al., 2010; Wright et al., 2012), which relies on the strong relationship between pressure and the concentration of CO₂ and H₂O in a volatile-saturated silicate melt (e.g., Dixon, 1997; Ghiorso and Gualda, 2015; Shishkina et al., 2014). After measuring the volatile (and major element) contents of melt inclusions (MIs) at the time at which these pockets of melt were trapped within crystals, a mixed fluid solubility model can be used to calculate the minimum pressure at which the magma was volatile saturated. Finally, petrologic experiments on different melt compositions and observations of phase relations and compositions at different pressures, temperatures and fluid compositions can be compared to erupted products to determine the conditions of crystallization (e.g., Mandler et al., 2014; Quinn, 2014).

Geophysical methods for imaging magma bodies which have been applied to the Cascades include magnetotellurics (Bedrosian et al., 2018; Bowles-Martinez and Schultz, 2020), local seismic

tomography with earthquakes or controlled sources (e.g., Kiser et al., 2016; Moran et al., 1999; Ulberg et al., 2020; Zucca and Evans, 1992), seismic wavefield-based methods (e.g., (Flinders and Shen, 2017; Heath et al., 2018; Jiang et al., 2023) and geodesy (e.g., tilt, levelling, GPS and InSAR, Dzurisin et al., 2009; Mastin et al., 2008; Poland et al., 2017). Seismicity also provides an indicator of deformation associated with magma movement.

Here, we calculate and compile magma storage depths for each volcanic centre using these methods and available geochemical and geophysical datasets. This compilation provides insight into magma storage depths at each volcano and helps to identify regions where data is sparse and future work is warranted.

Methods

When compiling and collating magma storage depths along the arc into a single coherent database, it is important to ensure consistency between published depth estimates from different volcanoes. We discuss the approaches used below for each proxy to ensure consistency along-arc.

Melt inclusion saturation pressures

MI CO₂ and H₂O contents can be converted into a saturation pressure estimate using a volatile solubility model, which estimates the pressure at which a melt with a given major element composition, volatile content and temperature was volatile-saturated. However, Cascade MI studies have used a wide variety of solubility models (see Supporting Table S1). The basaltic version of the VolatileCalc model of Newman and Lowenstern (2002, adapted from Dixon, 1997), was used by Aster et al. (2016) and Le Voyer et al. (2010). The rhyolite version of VolatileCalc was used by Blundy and Cashman, (2005) and Wright et al. (2012). The solubility model of Papale et al. (2006) was used by Johnson and Cashman, (2020), Quinn, (2014), Ruscitto et al. (2010), and Venugopal et al. (2020), and the solubility model MagmaSat (Ghiorso and Gualda, 2015) was used by Walowski et al. (2019). Because of the limited compositional range spanned by the calibration dataset of many of these models, calculated saturation pressures can easily differ by a factor of 2 or more (Wieser et al., 2022a). Thus, the use of different models at different volcanoes adds considerable uncertainty to arc-scale compilations and could even introduce spurious along arc trends if one model is favoured in a particular arc section (perhaps because different research groups favouring different models target different geographical regions). For consistency, we use published major element and volatile contents (PEC-corrected where available) to recalculate all saturation pressures using the solubility model MagmaSat implemented in the Open-source Python3 tool VESIcal (Iacovino et al., 2021). Using available experimental data for andesitic and dacitic compositions, Wieser et al., (2022) show that MagmaSat is the most accurate solubility model. Similarly, once a saturation pressure is calculated, pressure is converted to depth using estimates of crustal density. Cascade MI studies have used a wide variety of crustal densities to convert pressures into depths in the crust ($\rho=2200 \text{ kg/m}^3$ by Bacon et al., 1992, $\rho=2800 \text{ kg/m}^3$ by Johnson and Cashman, 2020). Saturation pressures were converted into depths using a uniform crustal density of $\rho=2700 \text{ kg/m}^3$.

MI saturation pressures have other limitations. It is becoming increasingly apparent from Raman spectroscopic analyses that a large proportion of the total CO₂ in a MI is held within the vapour bubble in olivine-hosted MIs in arc magmas (e.g. Mironov et al., 2020; Moore et al., 2018, 2015). Accurate Raman measurements require each laboratory to carefully determine the relationship between Raman spectral features and CO₂ densities an optical apparatus where CO₂ gas is held at known temperature and pressure conditions (DeVitre et al., 2021; Lamadrid et al., 2017), or reference materials measured in a laboratory with an optical apparatus (e.g., Mironov et al., 2020, Wieser et al., 2021). Only the MI vapour bubbles from two cinder cones near Lassen Peak by Aster et al., (2016)

have been measured on a calibrated Raman system. Venugopal et al. (2020) perform Raman measurements but use a literature calibration line rather than an instrument-specific calibration. The fact that a large number of their bubbles yield CO₂ densities above the thermodynamical limit at room temperature indicates that their calibration may have overestimated CO₂ densities. Other studies reconstruct vapour bubbles using bubble growth models (Johnson and Cashman, 2020; Walowski et al., 2019). However, these reconstructions require a precise estimate of the amount of post-entrapment crystallization (PEC) experienced by MIs, which in turn, requires accurate estimates of the initial FeO_t content of each MI (Danyushevsky and Plechov, 2011). Estimating initial FeO_t is very challenging for monogenetic cones, where the fractionation path is not known because only a very narrow range of liquid compositions were erupted. The remaining studies of olivine-hosted MIs do not measure or reconstruct the vapour bubble (e.g. Ruscitto et al., 2010; Walowski et al., 2016). As a result, saturation pressures obtained from published MI data must be interpreted with extreme caution, due to uncertainty regarding total CO₂ contents, and solubility models.

To obtain a self-consistent database, we calculate saturation pressures using bubble CO₂ from Aster et al., (2016) for MI saturation pressures, and bubble + glass reconstructions from Venugopal et al. (2020), with the important caveat that these Raman measurements may have overestimated CO₂ because of the absence of an instrument-specific calibration. We do not use modelled bubble reconstructions, because of the wide variability of different approaches used, and the sensitivity of these methods to reliable estimates of the amount of PEC, H₂O-loss etc (and insufficient data is reported to perform such corrections). Thus, it is important to recognise that the other MI compilations we show are very much minimum estimates which would likely increase were bubble CO₂ accounted for.

Mineral barometry

For mineral-melt barometry, we compile Amp and Cpx compositions from a wide variety of studies, along with a smaller number of matched Opx-Cpx analyses. We perform all calculations using the open-source Python3 tool Thermobar (Wieser et al., 2022b). In many cases, we could not obtain contextual information of whether the analysis was taken at a core or rim. A notable exception is the data of Streck and Leeman, (2018) who overlay their measurements on thin section images. For Cpx-Opx, we calculate pressures by iterating Putirka (2008) eq36(T)-eq39(P) and eq37(T)-eq39(P). Using a new dataset of arc magmas not used to calibrate such models (Wieser et al., 2023a, 2023b) we find that these barometers behave poorly for Cpx with Mg#<0.68, and so we filter out such pairs.

As with MI saturation pressures, Cpx-based barometry in the Cascades has utilized a variety of models to convert measured phase compositions into pressures (and temperatures). Hollyday et al. (2020) and Scruggs and Putirka, (2018) use the Cpx-Liq barometry of Neave and Putirka, (2017) iterated with the Cpx-Liq thermometer of Putirka, (2008, eq33). Sas et al., (2017) use the Cpx-Liq barometer from Putirka, (2008, eq32c) with an unspecified thermometer. However, different Cpx-Liq barometers can yield pressures with offsets spanning the pressure equivalent to the entire thickness of the Cascade crust (3-12 kbar, ~10-45 km, Das and Nolet, 1998; see Wieser et al., 2023b). Additionally, Cpx-Liq barometry relies on pairing up whole-rock compositions with equilibrium Cpx compositions (Scruggs and Putirka, 2018), which is challenging in arc-like magma compositions where whole-rock compositions do not necessarily represent true liquids (e.g., Kent et al., 2010) and many equilibrium tests perform badly (Wieser et al., 2023b). Given that Cpx-only and Cpx-Liq barometers show similar performance for a dataset of arc-like experimental products (Wieser et al. 2023b), we avoid melt-matching complications by using the Cpx-only barometers of Jorgenson et al., (2022, hereafter J2022) and Wang et al. (2021, hereafter W2021). These two Cpx-only barometers show the best RMSE and R² values (J2022: R²=0.78, RMSE=1.9 kbar, W2021: R²=0.66, RMSE=2.4 kbar) and least systematic error

when applied to an experimental dataset of several hundred experiments relevant to arc magmas conducted at 0-17 kbar which were not used in model calibration (Wieser et al. 2023b). These RMSE mean that they can identify magma storage depths within a window spanning ~15-18 km at 1σ confidence. The relatively thick crust in the Cascades (Moho thicknesses of ~40-50 km, Kiser et al., 2016; Parsons et al., 1998; Shehata and Mizunaga, 2022, Jiang et al. 2022) means that Cpx-based barometry can roughly distinguish between upper, mid and lower crustal storage, but should not be taken as highly precise estimates. An additional complication with arc-scale compilations is that the quality of analyses in our mineral compilation is not known, as publications do not quote the analytical precision of each measurement. Analytical uncertainty related to the measurement of Na₂O in pyroxene can easily yield errors spanning 3-5 kbar on each individual Cpx measurement (Wieser et al., 2023a). Averaging multiple Cpx compositions at each volcano can help to mitigate these random analytical errors (Putirka et al., 1996), and results in a substantial improvement when applied to the experimental data investigated by Wieser et al. (2023b). Thus, we predominantly focus on median $\pm 1\sigma$ pressures calculated for each volcano.

Identifying equilibrium Amp-Liq pairs is even more challenging than for Cpx-Liq, because the only widely-used equilibrium test to assess equilibrium is the exchange of Fe-Mg ($K_{D_{Fe-Mg}}$). This can lead to a number of spurious matches, as magmas can follow very different trends in major element space and still yield the same Fe/Mg ratio in the liquid. Tests on a new calibration dataset show that the Amp-only barometer of Ridolfi, (2021, hereafter R2021) performs moderately well, as long as extreme care is taken to ensure that the barometer is being used within the P-T-X limits of the calibration (Wieser et al, in review). When displaying Amp-only pressures, we first filter for the compositional criteria of Ridolfi (2021, grey kernel plots, black crosses, Fig. 2-12). We also apply an additional filter to remove Amp with atomic proportions on the basis of 13 cations >6.8 For Si, and <1.1 for Al, as these lie outside the calibration range (green kernel and grey crosses, Fig., 2-12, see supporting Fig. S1-2). In general, this removes Amp with the lowest calculated pressures, pushing the median pressure substantially deeper. A large number of Amp at Lassen (N=260, Fig. 2) are excluded using this filter, affecting the interpretation of magma storage, but at other volcanoes this filter has a minor influence on the median pressure.

A final problem with literature compilations of mineral compositions is that a number of published analyses are labelled as Cpx are actually Amp or Opx or vice versa. To automatically sort through these, we use a sklearn support vector classification machine learning algorithm (linear kernel) trained on a compilation of Cpx, Amp, Opx, Plag, feldspar, apatite, and oxides (classification algorithm available in Thermobar, Wieser et al., 2022b). Analyses classified as pyroxenes are further filtered to only use analyses with cation sum between 3.95 and 4.05, and Ca/(Ca+Mg+Fe) ratios between 0.2 and 0.5 for Cpx and 0-0.06 for Opx (excluding pigeonites). We filter out Amp with cation sums outside of 15-16.

We also compile experimental constraints where directly relevant to a specific Cascade edifice. We quote these pressures as published.

Reference levels

MI saturation pressure and mineral barometers yield pressures, which are then converted to depths (H) using assumptions about crustal density ($P=\rho gH$) or a crustal density model. In contrast, geophysical methods generally determine depths relative to a variety of reference levels. We abbreviate these as: below sea level (bsl), below ground level (bgl), below average station level (basl), or reference level unknown (rlu). When comparing geophysical depths to one another, and to petrological estimates, it is important to account for different reference levels. For consistency, we adjust all measures to yield depth below the summit of each volcano. This means that geophysical

estimates will match petrological estimates of pressure if the magma chamber is centrally-located. However, given evidence for magma reservoirs being offset from the volcanoes summit (Lerner et al. 2020), this correction could lead to a systematic offset between petrological and geophysical estimates. To allow visual assessment of these possible offsets, we include a topographic profile across each major edifice on each diagram, extracted from the ASTER global digital elevation model V003 using QGIS (NASA/METI/AIST/Japan Space Systems And U.S./Japan ASTER Science Team, 2019; QGIS.org, 2022). In reality, petrological and geophysical estimates could be displaced from one another by a vertical distance equivalent to the topographic profile shown.

Seismic data coverage

To obtain the km-scale resolution required to image magma bodies using seismic or magnetotelluric methods, it is normally necessary to obtain data using short-term high-density array deployments (e.g., Bedrosian et al., 2018; Kiser et al., 2018; Zucca and Evans, 1992). At relatively well-monitored volcanoes such as Mt. Rainier and Mt. St. Helens, these arrays can be used in conjunction with permanent volcano-monitoring networks (e.g., Moran et al., 1999; Ulberg et al., 2020; Waite and Moran, 2009). However, as permanent monitoring networks are densified, and older 1- or 3-component seismometers are replaced with modern broadband seismometers, the potential for a new generation of imaging using just permanent installations increases (both through increased station density, and the potential for wavefield-based imaging methods using broadband data). For example, broadband data enables ambient-noise imaging, which provides high-accuracy estimates of shear-wave velocity (V_s) at the upper-crustal depths where magma storage frequently occurs (e.g., Crosbie et al., 2019; Jiang et al., 2022). New stations require permitting, and their growth provides some indication of where new temporary arrays might be more easily deployed as well.

To help conceptualize this evolution in the quality and amount of seismic data available at different volcanoes, we plot the position of seismometers within 0.18° (~ 20 km) of the summit of each major edifice. We display this data on a map and a timeline for each major US Cascade volcano (Fig. 2-14). The underlying station metadata was pulled from the IRIS GMAP server (<http://ds.iris.edu/gmap/>) and the Pacific Northwest Seismic Network (PNSN) compilation (<https://pnsn.org/seismograms/map>, both updated, Sept 5th, 2022, <http://ds.iris.edu/gmap/>). We classify stations as 1 component short period (1sp), 3 component short period (3sp) or 3 component broadband (3bb). Stations considered short-period are often older, analog-telemetered with limited dynamic range and for which waveform-based measurements (such as ambient noise tomography, receiver functions, attenuation measurements) tend to be challenging. Those stations are most useful for local earthquake travel-time tomography (e.g., Moran et al., 1999). Newer broadband stations, generally installed in the mid-late 2010's, provide more imaging options.

Results

Data coverage varies widely along the Cascades (Fig. 1, Fig. 2-15). Some edifices such as Mt. St. Helens have an abundance of petrological and geophysical studies using a variety of methods (seismics, magnetotellurics, geodetics, Fig. 10), others have very few geophysical or geochemical studies (e.g., Three Sisters, Glacier Peak, Fig. 6, Fig. 13), and some are relatively well studied using one method but not the other (e.g., very little petrology at Newberry and Mt. Rainier, but moderate to good geophysical coverage, Fig. 7, Fig. 12). The variability of available data reflects a combination of the heavy focus of research efforts on certain volcanoes (particularly for petrology), quiescence or noisy geophysical signals at certain centres (Poland et al., 2017), and often-insurmountable issues associated with permitting any monitoring equipment within protected wilderness areas and parks (Moran and Benjamin, 2021). It is interesting that there is no apparent correlation between the

estimated threat level or ranking out of all US volcanoes (Ewert et al., 2018) and the availability of data. Below, we discuss the data available for each major edifice from South to North along the arc (Fig. 16).

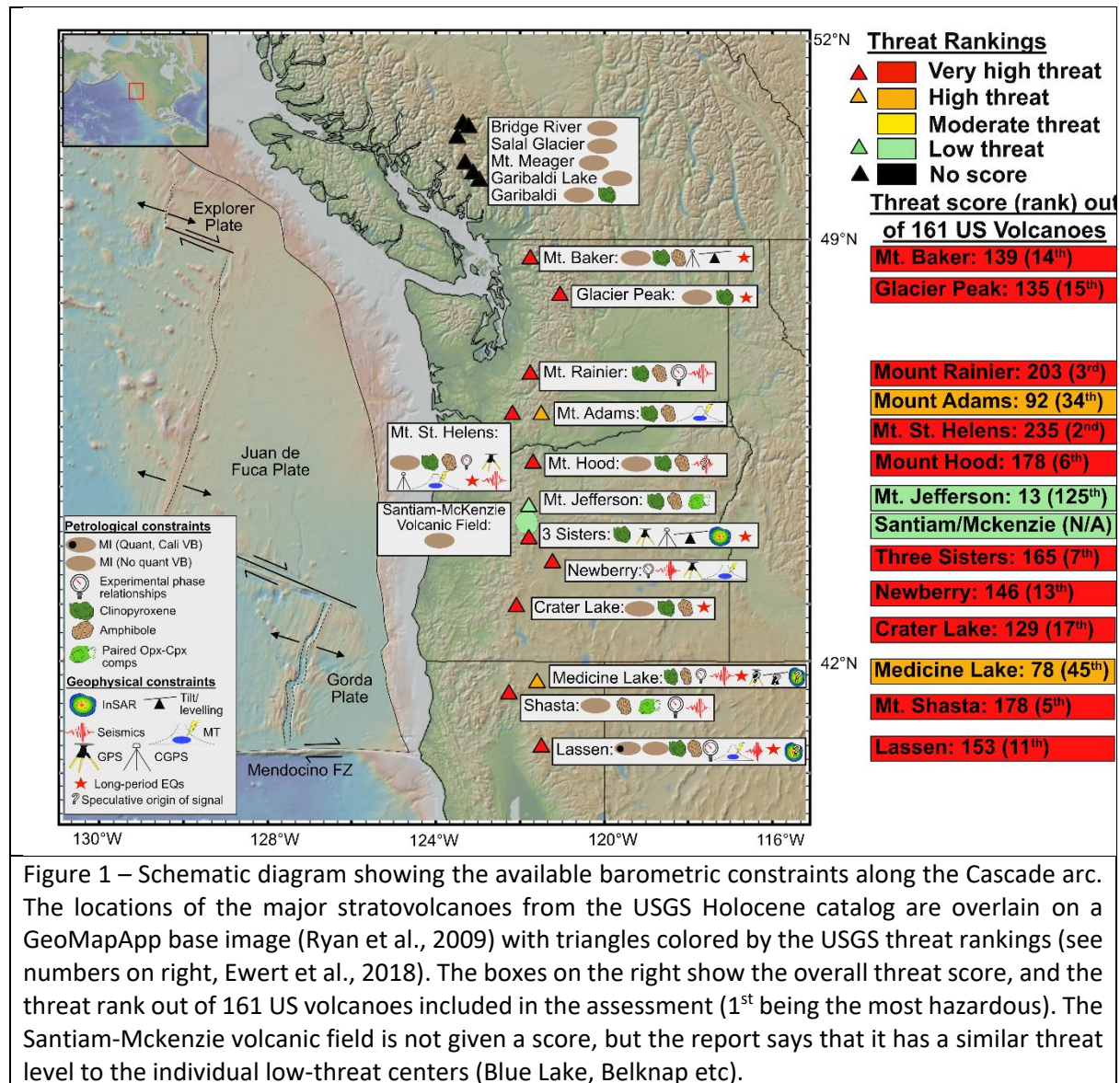


Figure 1 – Schematic diagram showing the available barometric constraints along the Cascade arc. The locations of the major stratovolcanoes from the USGS Holocene catalog are overlain on a GeoMapApp base image (Ryan et al., 2009) with triangles colored by the USGS threat rankings (see numbers on right, Ewert et al., 2018). The boxes on the right show the overall threat score, and the threat rank out of 161 US volcanoes included in the assessment (1st being the most hazardous). The Santiam-McKenzie volcanic field is not given a score, but the report says that it has a similar threat level to the individual low-threat centers (Blue Lake, Belknap etc).

Lassen Volcanic Center

Activity at Lassen Volcanic Center is subdivided into three main eruptive stages: 1) the Rockland Caldera Complex (825 – 609 ka), 2) Brokeoff Volcano (590 – 385 ka), and 3) the Lassen domefield (~300 ka to present, Clynne et al., 2008). The Lassen domefield has three dominant Holocene eruptive sequences from Chaos Craggs (~1000 AD, Clynne et al., 2008), Cinder Cone (1666 AD, Sheppard et al., 2009), and Lassen Peak (1914-1917 AD; Clynne, 1999), as well as a number of small cinder cones.

Mineral Compositions: Unpublished Cpx compositions were obtained from M. Clynne and B. Platt for samples from a range of formations from Brokeoff Volcano as described in Bullen and Clynne (1990) and Clynne et al. (2008). These include andesites from the Diller sequence (470-385 kyrs ago, e.g., Rice Creek, Mount Diller), and the Mill Canyon sequence (470-590 kyrs, Clynne and Muffler, 2010). Platt (2020) measure core-rim traverses for Cpx crystals from Brokeoff Volcano. We extract core and rim

compositions from these profiles. For the longest traverses, we extract core, intermediate and rim analyses for Cpx-only calculations.

Underwood et al. (2012) analyse Amp from the Kings Creek unit (35 ka), the dacite dome on Lassen Peak (28.3 ka), Chaos Craggs, and samples from 1914-1917 eruptions for hydrogen isotopes, water contents and ferric/ferrous ratios (all within the Lassen domefield stage). They also provide major element contents (N=316), which we use to perform Amp-only barometry calculations.

Hollyday et al., (2020) perform Cpx-Liq thermobarometry calculations on samples from a cinder cone from the basaltic-andesite of Box Canyon (middle Pleistocene age). They state that they combine N=20 core analyses with the composition of a primitive MI composition of the basalt of Big Lake (BBL) from Walowski et al. (2016), and obtain pressures of 460-700 MPa using the Cpx-Liq barometer of Neave and Putirka (2017). However, we were not able to obtain the exact liquid composition used by the authors and could not recreate these pressures. Considering all PEC-corrected MIs from BBL, and Cpx-Liq pairs in equilibrium using the tests of Neave et al., (2019), or just a K_D filter, we instead obtain pressures distributed between -0.5 to ~2.5 kbar. This discrepancy makes the inference from Hollyday et al. (2020) of lower crustal storage difficult to validate.

Overall, Cpx-only barometry using W2021 yields median pressures of ~0.6 kbar for Brokeoff volcano, and ~1.9 kbar for the Lassen domefield. Pressures using J2022 are slightly deeper for both formations (median=1.4 kbar for Brokeoff, 2.6 kbar for the domefield). These deeper pressures likely result from the fact that extra-tree regression strategies used by J2022 never yield negative numbers, skewing averages towards anomalously high values. If Amp-only pressures are calculated using just the filters of Ridolfi (2021), the median pressure is 1.2 kbar. However, if we also discard amphiboles with Al and Si cation fractions outside the range of the calibration dataset, we obtain substantially higher pressures (3.2 kbar). We favour the deeper, more extensively filtered median pressures (~3.2 kbar), as none of the experiments used to calculate the Ridolfi (2021) barometer were performed at <1.3 kbar. Overall, considering the errors on these methods, Amp- and Cpx-only barometry are broadly consistent with magma storage in the upper ~0.5 to 4 kbar of the crust, with the possibility that a small number of compositions originated deeper (but this is hard to distinguish from analytical uncertainty given the lack of metadata; Wieser et al. 2023a).

Melt inclusions: Aster et al. (2016) analyse olivine-hosted MIs from two cinder cones near Lassen (Basalt of Round Valley Butte - BRVB, and Basalt of old Railroad Grade - BORG), measuring CO₂ and H₂O in the melt phase using FTIR, and performing the first measurements of vapour bubble CO₂ in the Cascades using Raman Spectroscopy. Because of a limited number of MIs where both the bubble was measured and the MI was large enough for FTIR analyses, there are only N=9 analyses from BORG and N=4 analyses from BRVB where both phases were directly measured in the same inclusions. In addition to direct Raman measurements, Aster et al. (2016) produce a model to reconstruct vapour bubble CO₂, tracking the volume of a growing vapour bubble during post-entrapment crystallization using volume and density information from crystallization simulations in Rhyolite MELTS. They then calculate the composition of the vapour phase in the modelled bubble volume using the solubility model of Iacono-Marziano et al. (2012). While there is a broad correlation between modelled and reconstructed vapour bubble CO₂ contents when all samples are considered (Cascades, Parícutin, and Jorullo), the correlation for Lassen samples is poor ($R^2=0.01$, gradient = 0.09). Model-reconstructed values both over and underestimate the amount of CO₂ measured by Raman spectroscopy, and there is no clear association between this discrepancy and whether the bubble contained carbonates. Thus, we do not calculate pressures for their MIs where they reconstruct the bubble using their model, and only consider those where the bubble was directly measured by Raman spectroscopy. We suggest that these discrepancies may result from large uncertainties in determining the exact amount of post-

entrapment crystallization experienced by each MI (which controls the calculated bubble volume), as well as the quench rate, and the amount of H₂O loss. Their reconstructions use Petrolog3 to perform post-entrapment crystallization corrections, which requires the user to estimate the initial FeOt content of each MI. This is extremely challenging in volcanic fields/systems where there is no single liquid line of descent, so it is almost impossible to know precisely what the initial FeOt content was. This is particularly true at Lassen, where different eruptive centres have a wide range of FeOt contents at different MgO contents (Clynne, 1999), and thus is likely to be another source of uncertainty.

Walowski et al. (2016) perform FTIR measurements of olivine-hosted MIs (N=115) from a wide variety of Quaternary cinder cones in a large volcanic field surrounding Lassen Peak. They did not measure vapour bubble CO₂. Walowski et al. (2019) perform FTIR measurements of olivine-hosted MIs from the 1666 CE eruption of Cinder Cone. Again, no direct vapour bubble CO₂ measurements were made, but they did perform reconstructions using the method of Aster et al., (2016). They calculate the amount of PEC assuming an initial FeO_t content of 7 wt%. However, as described above, this method perform poorly for the Lassen samples of Aster et al., (2016), and is very sensitive to the amount of PEC, which is sensitive to the selection of the FeO_t content. Cinder Cone lavas and tephra samples have FeO_t contents ranging from 5.5-7 wt%; using Petrolog3, MI LCC-9-OL-01 has experienced 9.9 wt% PEC if reconstructed to 7 wt% FeOt, but only 2.8 % PEC if reconstructed to 5.5 wt% FeO (most MIs have differences of 6-7 % PEC). The resulting change in temperature (ΔT), and therefore the volume of the bubble (and the total mass of CO₂ in the bubble) is 2.5x less if FeOt is set at 5.5%.

Given the large uncertainties associated with these reconstructions, we only show measured H₂O-CO₂ contents for these two sets of MIs, with the caveat that they are very much minimum estimates. When all MIs are recalculated using MagmaSat (Ghiorso and Gualda, 2015), the measurements of Aster et al. (2016) yield pressures spanning 1.4-5.5 kbar. The melt-only saturation pressures from Walowski et al. (2016, 2019) are significantly shallower, as expected, and are likely not a useful constraint on magma storage.

Quinn (2014) analyse quartz (Qtz) -hosted MIs from the Chaos Craggs rhyodacite by FTIR. Discarding their MIs with <3 wt% H₂O which they suggest have undergone leakage, we calculate saturation pressures for the 34 remaining MIs. These yield pressures between around 1-2 kbar. Vapour bubbles are not mentioned in this study, so it is difficult to assess the impact of bubbles on CO₂ contents. If these vapour bubbles are CO₂-poor, these results may indicate that more evolved magmas are stored shallower than the basaltic magmas crystallizing the MIs analysed by Aster et al. (2016).

Experimental Petrology: Schwab and Castro, (2007) perform H₂O-saturated experiments to determine pre-eruptive storage conditions for the dacitic pumice erupted in 1915 from Lassen Peak. Comparison of natural and experimental products indicate that the dacitic magma equilibrated at 0.5 kbar and 800-875°C prior to mixing with an andesitic end member. Similarly, Quinn, (2014) perform H₂O-saturated experiments to assess the pre-eruptive storage conditions of the rhyodacitic magma erupted at Chaos Craggs. Based on a comparison of textures and phase assemblages in natural samples and experimental products, they infer that the most probable conditions of magma storage for these silicic magmas were 1.45±0.25 kbar and 770±10°C.

Geophysics: The first geophysical interpretation of magma storage under Lassen Volcanic Center came from Benz et al. (1992), who used teleseismic P wave arrival times to investigate lithosphere structure in northern California. They invoked a low-velocity zone (average -7.2%) beneath Lassen Volcanic Center (as well as Medicine Lake) within Layer 1 of their model, which spans 0-15 km depth (more precise estimates cannot be obtained from such teleseismic models). However, the low is displaced 30-50 km NE from Lassen, and extends to depths of 70 km, perhaps as an artifact of vertical smearing

(Thurber et al., 2009). Park and Ostos (2013) show P-wave tomography from an MSci thesis (Reeg, 2008) investigating measurements conducted using the Sierra Nevada EarthScope project (2005-2007), which imaged a 600 km x 150 km area, with Lassen National Park in the north. They identify a low velocity zone, although they cannot determine whether it is a mantle or crustal feature based on the wide station spacing (Park and Ostos, 2013). Overall, these teleseismic studies do not have sufficient resolution to reliably image relatively small crustal magma chambers beneath Lassen Peak.

Park and Ostos (2013) examine a 250-km long broadband and long period magnetotelluric line “LASS” along the 40.5°N parallel. This survey line passes 20 km north of Lassen Peak (40.488 °N). They do not image a large crustal conductor beneath Lassen Peak, supporting our assertion that the teleseismic studies described above cannot provide useful constraints on upper crustal magma storage. However, they do identify three small conductors within the Lassen Volcanic Center at ~15-30 km (rlu, presumed basl), which they suggest are basaltic reservoirs, which may be heating and melting the lower crust.

Another possible constraint comes from a compilation of the depths of earthquakes recorded from 1984 to 2016 (Fig. 6b of Taira and Brenguier, 2016). These depths show a prominent peak at between 4-6 km (rlu). Such high-frequency or volcano-tectonic earthquakes require brittle (velocity-weakening) conditions, indicating temperatures far below the solidus, and are usually seen at a few km from sites of eruption (e.g., White and McCausland, 2016). The simplest interpretation is that the main magma storage region must be deeper than this high-frequency seismicity. Pitt et al., (2002) report the depths of N=20 long-period earthquakes, ranging from ~12-27 km depth (basl). These may represent magma recharge, which may indicate that the main magma storage region is above this level. The absence of further seismic constraints at Lassen results from the fact that no high-resolution study has even been performed there, and the permanent network is very small (even today, there is only one three-component broadband station, Fig. 2f-g).

Unfortunately, geodetic measurements at Lassen Volcanic Center do not help constrain magma storage depths. Lassen Volcanic Center has experienced broad, regional subsidence since 1992, consistent with a point source at ~ 8 km depth. However, the source of this subsidence is unclear, with dominant contributions likely from regional extension, changes in the location of hydrothermal/magmatic fluids, and a possible minor influence of the cooling and crystallization of magma (Parker et al., 2016; Poland et al., 2004). Regional GPS will likely be vital to deconvolve the relative role of crustal extension compared to hydrothermal and magmatic processes. Given the ambiguity, we do not include this deformation source on Fig. 2.

Summary and future work: Cpx-only and Amp-only barometry, Qtz-hosted MI saturation pressures, and available experimental constraints indicate that the majority of magma storage surrounding Lassen is within the upper crust (<4 kbar). These depths are not inconsistent with the distribution of shallow earthquakes, but further geophysical constraints from short-term high-density arrays, or the addition of more broadband seismometers providing an opportunity for passive-source tomography, would help to confirm the location of the shallow magma reservoir. Based on the downward spread of Cpx-only and Amp-only pressures, the presence of higher saturation pressures from Aster et al. (2016), and the seismic results of Park and Ostos (2013), further work is certainly needed to investigate deeper magma storage. This could be targeted through a study focusing on vapour bubble CO₂ in a large suite of melt inclusions, experiments on relevant starting compositions, or a local high resolution seismic survey.

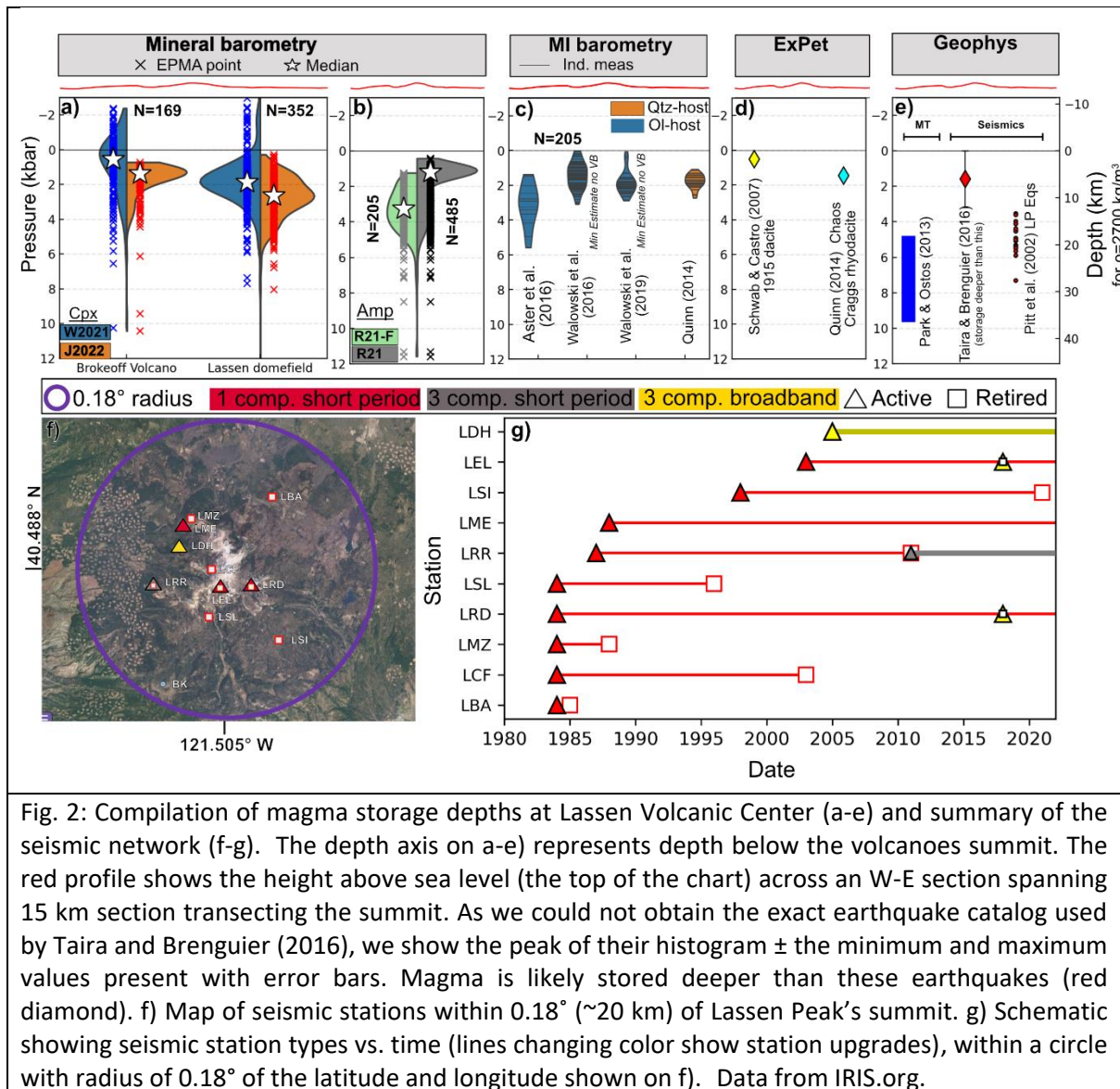


Fig. 2: Compilation of magma storage depths at Lassen Volcanic Center (a-e) and summary of the seismic network (f-g). The depth axis on a-e) represents depth below the volcanoes summit. The red profile shows the height above sea level (the top of the chart) across an W-E section spanning 15 km section transecting the summit. As we could not obtain the exact earthquake catalog used by Taira and Brenguier (2016), we show the peak of their histogram \pm the minimum and maximum values present with error bars. Magma is likely stored deeper than these earthquakes (red diamond). f) Map of seismic stations within 0.18° (~20 km) of Lassen Peak's summit. g) Schematic showing seismic station types vs. time (lines changing color show station upgrades), within a circle with radius of 0.18° of the latitude and longitude shown on f). Data from IRIS.org.

Mount Shasta

The position of Mt. Shasta west of the Cascade arc axis and only ~70 km above the subducting plate means that it could be considered a fore-arc volcano (Christiansen et al., 2017; McCrory et al., 2012). Mt. Shasta shows compositions ranging from basaltic andesite to rhyolite, with the majority of erupted products having a calc-alkaline, high-silica-andesite to low-silica-dacite composition (60-67 wt% SiO₂). Quenched mafic inclusions of more MgO-rich magma are common. The last 10 kyr of eruptive history at Mt. Shasta indicates that eruptions occur every 600-800 years, with the most likely hazards being ash, lava flows, domes, pyroclastic flows and debris flows (Christiansen et al., 2017; USGS, 2022). The USGS has suggested based on its relatively low activity over the last few thousand years and its long eruptive history that Shasta is the Cascade volcano most likely to produce a very large volume eruption (analogous to the Mazama ash from Mt. Mazama). In addition to the main volcanic edifice, Mt. Shasta is surrounded by a number of basaltic-andesite to andesitic shields (Ash Creek Butte, The Whaleback, Deer Mountain, Miller Mountain etc.), and less frequent basaltic to basaltic-andesitic cinder cones (Christiansen et al., 2017). While the majority of erupted material has a more evolved composition, small amounts of primitive magnesian andesite (PMA) and high-alumina olivine tholeiite (HAOT) with high Mg#s are found in cinder cones and on Mt. Shasta's flanks (Christiansen et al., 2013).

Mineral Compositions: Recent petrological work around Mt. Shasta has largely focused on the high-magnesian andesites (HMA) erupted at the S17 cinder cone near Whaleback Mountain, ~20 km NNE of the main edifice. The interest in this cinder cone arises from a long-standing debate regarding whether these melts represent near primary mantle melts (Baker et al., 1994; Barr et al., 2007; Grove et al., 2002) or magma mixing and crustal contamination (Streck and Leeman, 2018). Streck and Leeman (2018) display their EPMA data in an interactive tool overlain on a BSE image, allowing us to identify pairs of EPMA points on touching Opx-Cpx pairs. We assess all possible combinations of Cpx-Opx analyses for touching grains (e.g., for three EPMA spots on a Cpx, and two for a touching Opx, we obtain six pairs). This yields a total of N=122 pairs. We also manually extract N=328 Cpx analyses where the location in the crystal could be classified (Core, Rim). Phillips and Till, (2022) measure Cpx and Opx compositions from the same HMA S17 cinder cone, although from the data it is not possible to distinguish which analyses represent touching pairs. Given there is only one equilibrium test for Cpx-Opx (K_D , Fe-Mg) which shows limited success for hydrous experiments (Wieser et al. in review), we do not consider pairs when the textural context is unknown.

For the HMA samples, Cpx-only pressures are highly variable, ranging from 1-6 kbar (with very similar distributions and medians for J2022 and W2021). Cpx-Opx pressures are offset ~2-3 kbar deeper, but certainly overlap with the distribution of Cpx-only pressures.

Baker et al., (1994) perform mineral analyses on a series of lavas 20-50 km to the N and NW of Shasta's summit clustered around Highway 97 (e.g., lower than the 6000" contour on the 14,000" main edifice). They report N=3 representative Cpx compositions, however they suggest that these analyses were low precision, with the WDS background only being collected once per thin section, so the compositions should not be used for barometry (M. Baker, written coms). Grove et al. (2005) measure mineral compositions in a wide variety of lavas representing the Hotlum, Shastina, Misery and Sargents eruptive phases from on/around the main Shasta edifice. However only representative mineral composition are reported (a total of N=4 Cpx, N=2 Amp). Given the sparsity of available data, we do not perform any barometry on the main edifice, as these numbers are too small to sufficiently average out random analytical error (Wieser et al., 2023a).

Melt inclusions: Anderson (1974) perform EPMA analyses of MIs from the S17 cinder cone, calculating H₂O by volatiles by difference. Similarly, Sisson and Layne, (1993) measure glass inclusions from Copco Cone and Goosenest volcano, north of Shasta. However, because of the lack of glass (and bubble) CO₂ measurements, as well as uncertainties associated with volatile-by-difference methods (Hughes et al., 2019), we do not calculate saturation pressures for these inclusions.

Le Voyer et al. (2010) perform SIMS measurements of reheated olivine-hosted MIs from H₂O-poor, high aluminium olivine tholeiites (HAOTs) and H₂O-rich basaltic andesites from mafic flank eruptions from Mt. Shasta. Their measured basaltic-andesite H₂O contents are lower than estimated by Baker et al., (1994), which may reflect diffusive loss from the olivine (adding uncertainty to the saturation pressure). We calculate saturation pressures for the N=25 MIs with major element and volatile data.

Ruscitto et al. (2011) perform FTIR measurements of naturally quenched primitive basaltic andesite and high magnesian andesite olivine-hosted MIs from the S17 Whaleback Mountain Holocene cinder cone. We calculate saturation pressures for the N=20 MIs with major element and volatile data.

All Shasta melt inclusion studies note the presence of abundant vapour bubbles, many of which remain even after experimental homogenization (Le Voyer et al., 2010), and thus it is likely that calculated saturation pressures (clustering at 0-2 kbar) are very much minimum estimates.

Experimental phase equilibrium: Grove et al. (2005) compare Shasta whole-rock and mineral compositions to the experiments of Grove et al. (2003) to infer a period of shallow crustal differentiation of plagioclase (Plag) and pyroxene (Px) in a reservoir at 1-2 kbar (3-6 km, see also Baker et al., 1994). In the schematic model in Fig. 14 of Grove et al. (2005), two additional storage zones are invoked; a reservoir fractionating Olivine (Ol)+Px at 7-10 km, and a reservoir fractionating Ol+Amp+Px at 15-25 km (based on high amphibole Mg#s and H₂O-rich MIs). Krawczynski et al., (2012) perform additional experiments at 200, 500 and 800 MPa, and use these experiments to calibrate a barometer estimating $P_{\text{H}_2\text{O}}$ from the highest measured amphibole Mg# in a given suite of samples. By applying this equation to Shasta amphiboles, $P_{\text{H}_2\text{O}}$ values of 2.8-9.5 kbar are obtained. However, these pressures may be significant underestimates if CO₂ is present in the exsolved fluid at depth, such that $P_{\text{tot}} \neq P_{\text{H}_2\text{O}}$. Additionally, their Fig. 8 shows that the simple relationship between Mg# and P is more complex in mixed fluid experiments (and mafic melts beneath Shasta are likely in equilibrium with a mixed fluid).

Geophysics: Poland et al. (2017) summarize available geodetic constraints, indicating that no detectable deformation has occurred at least since the 1980s. Thurber et al. (2009) present a regional 3D tomographic model of P wave velocity for all of Northern California using a double-difference tomography algorithm (Zhang et al., 2004) with nodes 15-20 km apart. They image a low velocity zone (~5.5 km/s, 5% reduction) beneath Mt. Shasta centred at ~12 km depth (bsl). However, the 40-km horizontal extent of this body makes it impossible to distinguish thermal from magmatic contributions to the local velocity low. The lack of high resolution, local seismic inversions reflects the fact that no high density temporary deployments have ever been deployed around Shasta to our knowledge (unlike Mt. St Helens). Additionally, Shasta also shows relatively few earthquakes (Weaver et al., 1990), despite a long-lived short-period monitoring network. This network has been recently upgraded with four three component broadband seismometers (Fig. 3g). Meaningful inversions on this new network will be reliant on collecting sufficient earthquakes. To our knowledge, there are no other geophysical constraints on magma storage beneath Shasta.

Summary and Future work: Despite the clear hazard potential of the main edifice of Mt. Shasta (ranked as the 5th most hazardous US volcano), we have remarkably few constraints on the magmatic plumbing system under the main edifice. While the S17 high magnesian andesite cinder cone is academically interesting from the perspective of the generation of arc magma compositions, this cone has little relevance to future eruptions at Mt. Shasta given the relative paucity of these high-magnesian andesite compositions in this volcanic field and its age pre-dating construction of the modern edifice (see Phillips and Till, 2022). We suggest that further work targeting MIs, mineral compositions and phase equilibration experiments in the presence of mixed fluids from the main edifice is desperately needed. From a geophysical perspective, a high-density temporary deployment of seismometers using active sources would help, although permitting would be non-trivial. Soon, we expect sufficient earthquakes to be collected on the upgraded seismic network for a first-order seismicity assessment.

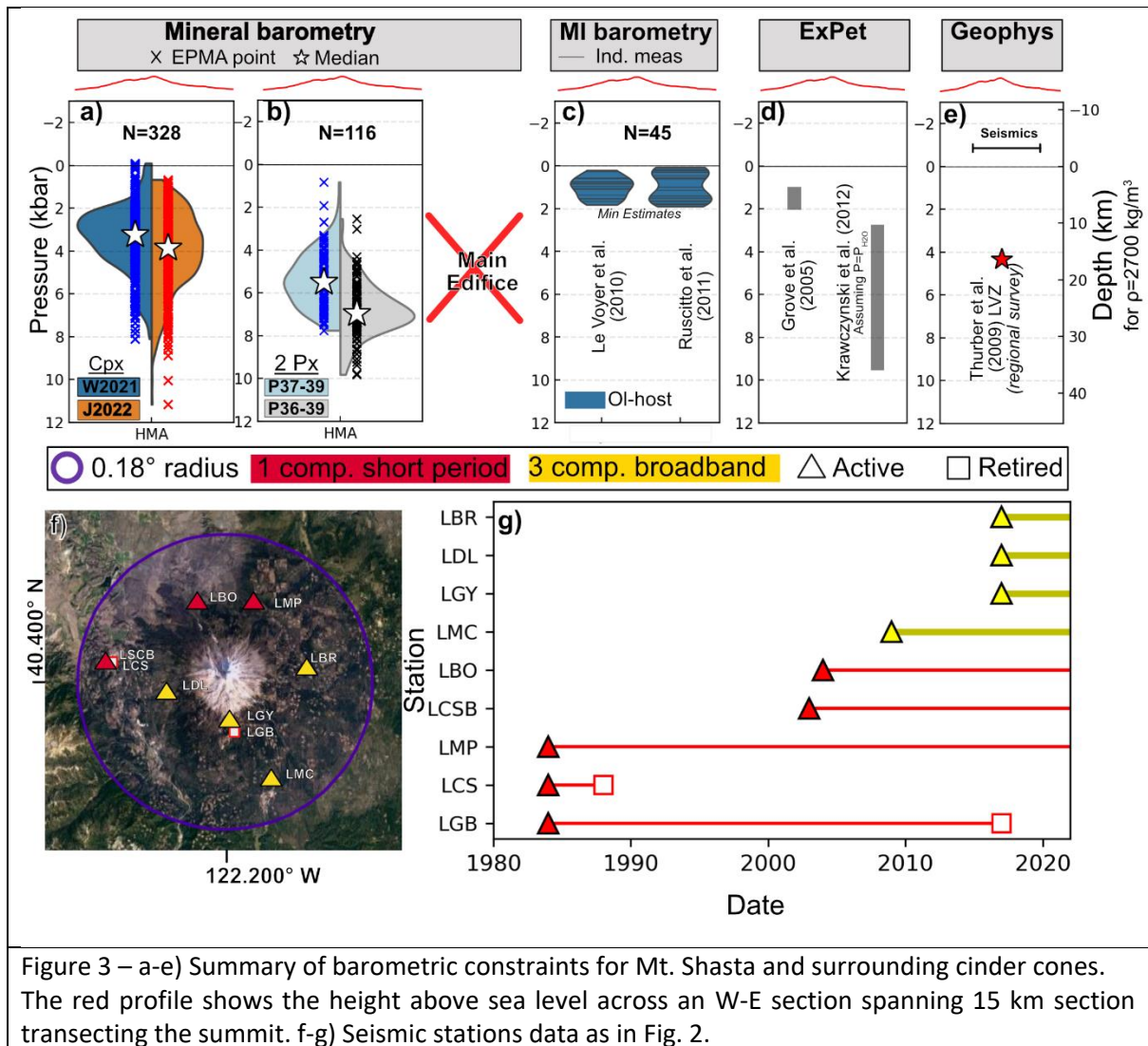


Figure 3 – a-e) Summary of barometric constraints for Mt. Shasta and surrounding cinder cones. The red profile shows the height above sea level across an W-E section spanning 15 km section transecting the summit. f-g) Seismic stations data as in Fig. 2.

Medicine Lake

Medicine Lake Volcano is located ~50 km E-NE of Mt. Shasta and the main Cascade front, on the western edge of the Basin and Range extensional province. It has erupted a wide variety of magma compositions, ranging from hydrous calc-alkaline magmas (basalt to rhyolite), to relatively anhydrous, high-aluminium olivine tholeiites. In general, basalts and andesites form the flank of the volcano, with rhyolites and small volumes of dacites occurring at the summit (Donnelly-Nolan, 1988). It is the volcano with the largest volume in the Cascades.

Mineral Compositions: Despite a number of detailed petrological studies, there is a notable paucity of published mineral data as most papers only provide representative analyses (N=12 Cpx, N=6 Amp remain after filtering for quality). For example, Gerlach and Grove, (1982) report N=8 Cpx, Grove and Donnelly-Nolan, (1986) report only N=4 Cpx and N=3 Amp from three types of magmatic inclusions, Grove et al., (1997) present data from N=1 Cpx and N=3 Amp from Glass Mountain, and Kinzler et al. (2000) report the composition of a N=1 Cpx from the Callahan lavas, as well as N=1 Cpx within a MI (not included here).

Melt Inclusions: Sisson and Layne, (1993) perform EPMA analyses of MIs from Black Crater, using volatile-by-difference methods to infer a H₂O content of ~0.2 wt%. Kinzler et al. (2000) report an Amp-

bearing MI within an Mg-rich olivine with ~3 wt% H₂O. In addition to significant uncertainties associated with volatile-by-difference methods, no CO₂ data exists for either the melt phase or the bubble. Thus, we do not calculate saturation pressures for these inclusions. MI work analysing the melt and vapour phase for H₂O and CO₂ in the Paint Pot basaltic deposit is currently in progress (see Couperthwaite et al., 2022)

Experimental phase equilibrium: Grove et al., (1982) conducted experiments investigating the origin of the calc-alkaline series at Medicine Lake. However, other than demonstrating that P_{H₂O} must be greater than 1 kbar to generate calc-alkaline compositions, no further constraints are placed on magma storage depths. One possible constraint appears in Bartels et al., (1991) perform experiments at 1 atm, 10 and 15 kbar on high-aluminium basalts from Medicine Lake, demonstrating that these liquid compositions are close to equilibrium with a mantle lherzolite source. However, the high-pressure nature of these experiments mean they do not provide insights into the depth at which magma is stored in the crust beneath Medicine Lake. Finally, Grove et al., (1997) perform experiments at 1, 1.5, and 2 kbar to investigate the origin of the Rhyolite of Glass Mountain. They suggest that the presence of Amp in more mafic inclusions indicates crystallization at >2 kbar, while Ol-Plag and Ol-Plag-Cpx inclusions indicate crystallization at near H₂O-saturated conditions at ≤1 kbar.

Geophysics: Evans and Zucca (1988) and Chiarabba et al. (1995) use active source seismic topography (the NeHT experiment of 1985) and seismic refraction studies in 1982 and 1984 to image P-wave velocity and attenuation beneath Medicine Lake. Evans and Zucca, (1988) obtain ~1-2 km depth resolution in the upper 5-7 km of the crust, and image a low Q (high attenuation), low velocity region in their layer 3 (1.2-3.25 km depth bsl, 3.6-5.6 km below ground level) beneath the east central caldera with a volume of a few 10s of km³. Chiarabba et al., (1995) experiment with alternative inversion strategies and find that the low-velocity body is well resolved at 3 - 5 km depth (bgl), although some less-stable inversion strategies suggest that the low velocity zone is deeper (>6.8 km). Overall, they conclude that the low velocity zone likely occurs at 3-4 km depth (bgl), but may be as great as 7 km depth. The small size of the low velocity anomaly identified in these two seismic studies, roughly 10 km wide horizontally, can account for the fact it is not seen in teleseismic studies (e.g., Ritter and Evans, 1997).

Pitt et al. (2002) report 1 LP EQ beneath Medicine Lake in Dec 1989 (15 km basl). The notable paucity of seismometers (particularly three component broadband) means that there have not been any more recent investigations of magma storage using passive source techniques since the flurry of geothermal exploration activity in the 1980's (Fig. 4g).

Interpreting geodetic data at Medicine Lake is complicated by the fact that this volcano impinges on the western edge of the Basin and Range, such that it is subject to regional extension. Additionally, Medicine Lake's large volume, and therefore mass, means that it loads and deforms the surrounding crust. These "background" signals make it difficult to distinguish the smaller signals resulting from inflation, deflation, or crystallization of crustal magma chambers (Dzurisin et al., 1991; Poland et al., 2006). Dzurisin et al. (1991) and Dzurisin et al., (2002) examine levelling surveys from 1954-1989, and a small summit survey in 1988, as well as seismicity in 1978, 1981, and 1988. They infer that there is possibly a minor role for crystallization and magma withdrawal, but this is overwhelmed by regional/loading signals.

Poland et al. (2006) investigate campaign GPS data and InSAR data from Medicine Lake Volcano. InSAR identifies ~10mm/yr of approximately radially symmetric subsidence centred on the caldera region (consistent with GPS and levelling data). However, they show that the GPS horizontal displacements are not consistent with the model of Dzurisin et al. (2002) suggesting volume is being lost at 10-11 km

depth, as this should produce radially-inward horizontal deformation up to 40 km radius. Instead, they invert for a Mogi point source at shallower depths (~6 km) to explain the fact only GPS stations within ~10 km of the summit show inward deformation. This deformation source can also be fitted as a deflating sill at 5 km depth (with higher misfit). However, this deflating sill source does not effectively recreate the vertical deformation of the 1954-1989 levelling survey of Dzurisin et al. (1991). They suggest the dominant signal is edifice loading and extension of a hot weak crust, rather than magma withdrawal.

Parker et al. (2014) examine additional InSAR data (up to 2011), and also suggest that deformation is caused by tectonic extension and gravitational loading, with a possible role for cooling and crystallization of an intrusive body at depth (rather than an active magma chamber). Given this substantial uncertainty, we do not include geodetic constraints in our compilation.

Summary and future directions: We suggest that the most precise constraints on magma storage beneath Medicine Lake could be obtained by performing detailed MI studies on rapidly quenched material where available. For slower-cooled lava flows, detailed analysis of minerals and any fresh glasses could help provide barometric constraints to supplement the small amounts of publicly-available mineral data. Without densification of the seismic network with three component broadband seismometers, or targeted local studies, additional geophysical constraints are unlikely to be obtained in the near future.

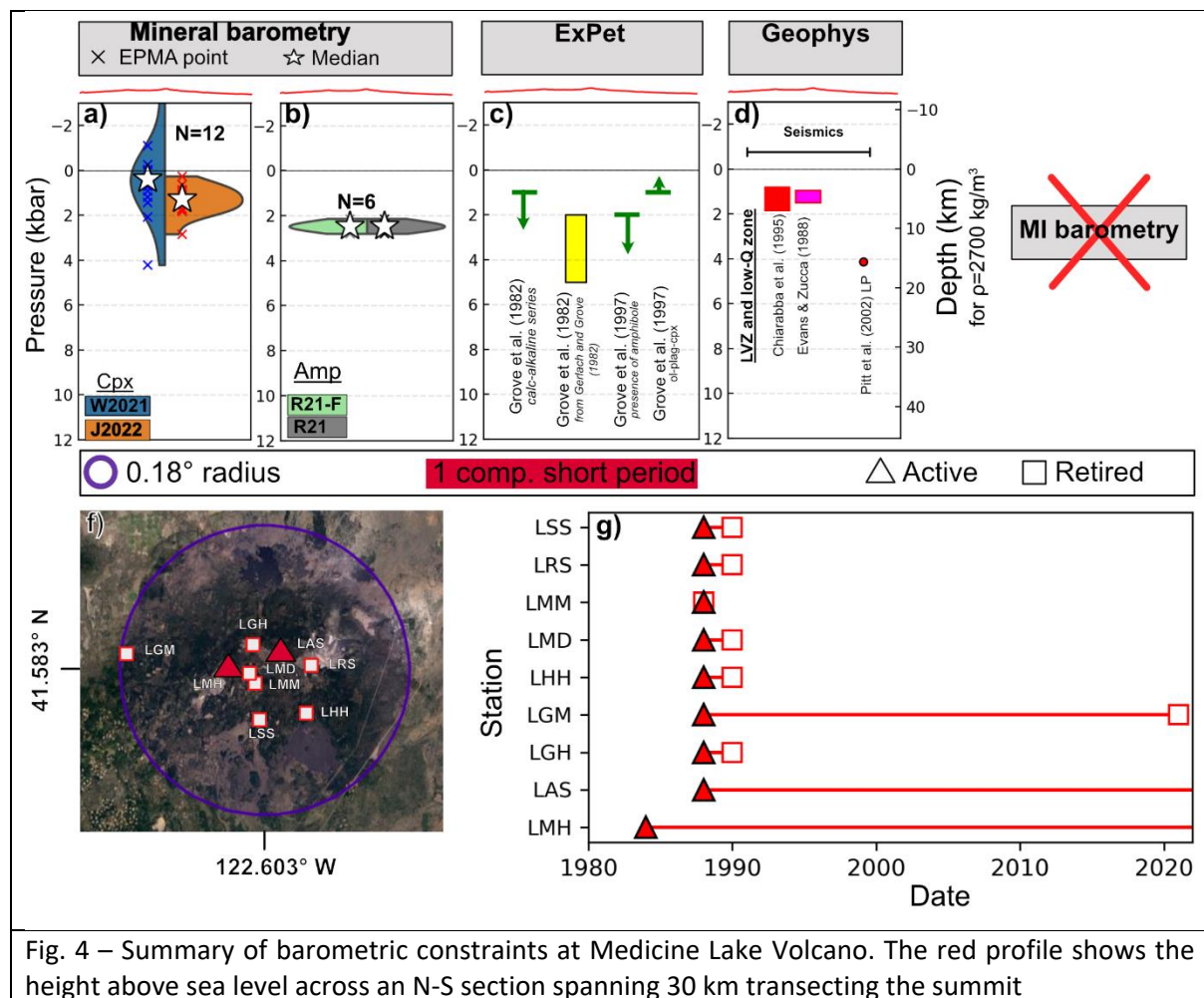


Fig. 4 – Summary of barometric constraints at Medicine Lake Volcano. The red profile shows the height above sea level across an N-S section spanning 30 km transecting the summit

Crater Lake/ Mount Mazama

The climatic eruption of Mt. Mazama at ~ 7.7 ka produced the modern-day caldera known as Crater Lake. Activity at Mt. Mazama began around ~ 420 ka, producing basaltic andesite, medium-K andesites and dacites. The first preclimatic rhyodacites erupted at ~ 27 ka. The evolution of this silicic reservoir was terminated by the massive climatic eruption of ~ 50 km³ at 7.7 ka (Bacon and Lanphere, 2006). Post-caldera volcanism was dominated by andesite for 200-500 yrs after the climatic event, followed by an eruption of a rhyodacite at 4.8 kyrs.

Mineral Compositions: We compile N=16 Cpx from preclimatic rhyodacites from Nakada et al. (1994), and N=126 Cpx analyses from the 8 dacitic-rhyodacitic deposits spanning 71-7.7 ka samples described in Wright et al. (2012) from the authors. Additionally, we digitized N=194 Cpx and N=245 Amp from the original handwritten datasheets of EPMA analyses for samples described in Druitt and Bacon (1989). Finally, we obtain N=7 Cpx analyses from Prueher and McBirney, (1988).

The dacitic-rhyodacitic deposits at Crater Lake are outside the calibration range of the W2021 barometer, which could explain why calculated pressures are so shallow (median= -0.2 kbar). That said, in the dataset of arc experiments from Wieser et al. (2023b), there was no clear correlation between melt SiO₂ content and discrepancy between the calculated and experimental pressures, unlike for temperature. The median pressure for the J2022 barometer is ~ 1.2 kbar, with a skewed distribution to higher pressures (as this barometer does not return very shallow pressures). Si-Al filtered Amp pressures are very similar to those unfiltered, with median pressures of ~ 3 kbar. There is also a small cluster of Amp-only pressures at ~ 7 kbar, from samples 80c444 (Ol-Px rich scoria from top of the climatic ignimbrite), 82C882 (high-Sr scoria from top of climatic ignimbrite), 82C938 (high-Sr enclave from Liao rock) and 1290 (low-Sr scoria from the top of the climatic ignimbrite), all from Druitt and Bacon (1989). This population of high-Mg# Amp yield H₂O-only pressures from the Mg# barometer of Krawczynski et al., (2012) of ~ 1.8 - 3.8 kbar for Δ NNO=0-1. Assuming CO₂ was present in the relatively mafic melts crystallizing these high-Mg# Amp (resulting in a higher pressure than indicated by H₂O-only pressures), both barometers indicate a possible region of high pressure crystallization of more mafic magmas. It is difficult to interpret the single Cpx measurement from Wright et al., (2012) yielding a pressures in this range, without detailed information on the analytical uncertainty associated with these measurements (see Wieser et al. 2023a).

Melt Inclusions: Bacon et al. (1992) analyse plagioclase-hosted MIs from three rhyodacitic Holocene eruptions (~ 7 kyrs-6.8 yrs BP) from Crater Lake by FTIR (Liao Rock, Cleetwood, and the climatic event). CO₂ concentrations in these MIs are < 25 ppm, and often undetectable by FTIR. We remove MIs with low H₂O contents (< 3.1 wt%) which the authors suggest may have a connection to the outside (leaving N=10 MIs). Mandeville et al. (2009) analyse plagioclase and pyroxene-hosted MIs from the same three eruptive episodes as Bacon et al. (1992), also using FTIR. None of the reported N=48 MIs have visible connections to the outside or cracks, and CO₂ concentrations are below the FTIR detection limit. Wright et al. (2012) analyse N=127 plagioclase and pyroxene-hosted MIs from 8 dacitic-rhyodacitic deposits spanning 71-7.7 ka using SIMS (along with a subset by FTIR). They identify high H₂O (3-4.6 wt%) and low H₂O (< 2.4 wt%) populations of MIs. They suggest that the low-H₂O population likely reflects leakage, and diffusive re-equilibration. Thus, for consistency with Bacon et al. (1992), we do not calculate saturation pressures for inclusions with < 3.1 wt% H₂O. Wright et al. (2012) only detect CO₂ noticeably above detection limit in deposits from the 71 ka Pumice Castle. All these MI saturation pressures cluster at ~ 1 kbar depth. To our knowledge, no vapour bubbles have been measured in these more silicic MIs, although this doesn't mean they are CO₂-free.

Experimental Petrology: We are not aware of any experimental petrology studies placing constraints on magma storage depths beneath Crater Lake.

Geophysics: Poland et al., (2017) summarize available geodetic constraints at Crater Lake, which show no deformation resolvable above survey noise since the 1980s. The only seismic constraints we are aware of is a single LP at ~32 km depth (Nichols et al., 2011), and a brief mention of a low velocity zone in the lower crust below Crater Lake in the regional teleseismic study by Harris et al, (1991). However, Harris et al. (1991) do not provide a depth or place any quantitative constraints on the size of this body, so we do not include this in our compilation. The lack of seismic constraints on magma storage is not surprising; the seismic network at Crater Lake has only been upgraded very recently with three component broadband seismometers, and the network was non-existent for more than 20 years (Fig. 5g). Once sufficient earthquakes have been measured on this new network, additional constraints on magma storage may be possible.

Summary and Future work: We suggest that further petrological and experimental work examining the resurgent materials erupted at Wizard Island could provide useful insights into the likely storage depths of the next eruption at Crater Lake. Examination of CO₂ within more silicic MI vapour bubbles would also be a worthy target. Although permitting would certainly be a challenge, a higher resolution array with active sources could help provide additional geophysical constraints.

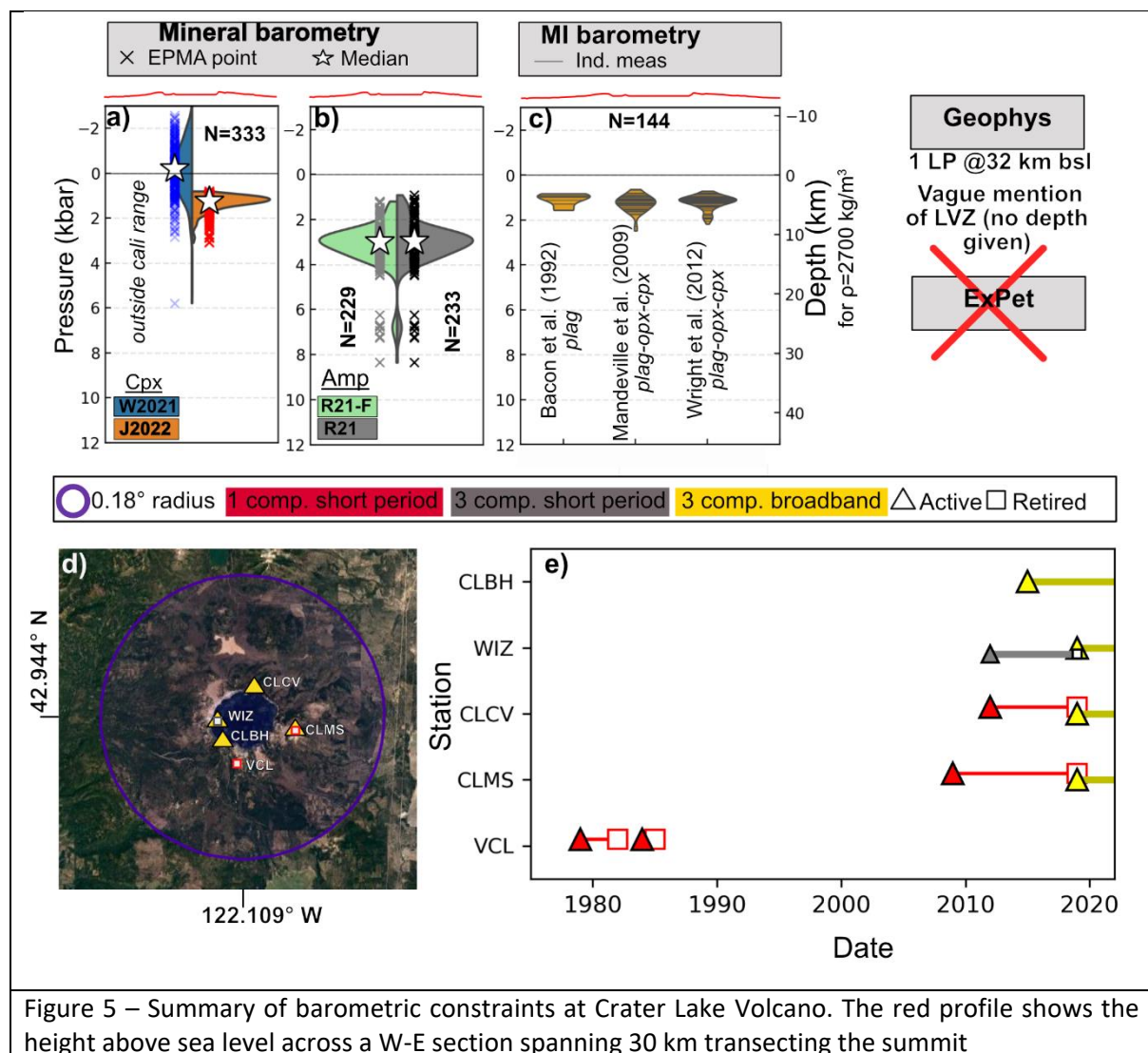


Figure 5 – Summary of barometric constraints at Crater Lake Volcano. The red profile shows the height above sea level across a W-E section spanning 30 km transecting the summit

Three Sisters

The Three Sisters volcanic field consists of three prominent summits (North, Middle and South Sister), as well as a number of distributed vents. North Sister has a very monotonous basaltic composition, with activity between ~120-50 ka, including a small shield (Little Brother), and a string of fissures (Matthieu Lakes fissure, Fierstein et al., 2011; Schmidt and Grunder, 2011). Activity at Middle and South Sister has been largely contemporaneous, with Middle Sister erupting basalt, andesite and dacite, while South Sister erupts only intermediate to more felsic compositions. In general, relatively little petrological work has been done on this area.

Mineral Compositions: We were only able to compile N=6 Cpx from the Matthieu Lakes Fissure transecting North Sister from Schmidt and Grunder, (2011), and N=12 Cpx from South Sister dacites from Waters et al. (2021).

Melt Inclusions: To our knowledge, there are no published MI analyses from South or Middle Sister. Mordensky and Wallace, (2018) analyse olivine-hosted MIs from North Sister using FTIR. Nine out of 15 of these MIs have vapour bubbles. They find that minimal PEC has occurred (0-2.3%, representing $\Delta T \sim 20^\circ\text{C}$). They perform a bubble correction similar to that of Aster et al. (2016), and infer ~48-78% of CO_2 is within the bubble. However, for such small amounts of PEC, where the vast majority of the bubble grows during syn-eruptive cooling, bubble reconstructions assuming re-equilibration between vapour bubble and melt can greatly overestimate bubble CO_2 contents (Wieser et al., 2021). Additionally, with such low amounts of PEC, the correction is heavily affected by the choice of FeO_t content, which shows scatter in local whole-rock compositions. Mordensky and Wallace, (2018) report PEC-corrected major element data for N=8 North Sister MIs, six of which have CO_2 below-detection limit. Given the low N, low CO_2 contents in the glass, lack of published major element contents for many MIs, and lack of bubble CO_2 data, we do not perform saturation pressure calculations for these MIs. Mercer and Johnston, (2008) cite unpublished MI data from North Sister, which we were not able to obtain for this study.

Experimental Petrology: Mercer and Johnston, (2008) perform experiments using a North Sister melt composition, mostly to constrain the lower crustal mineralogy the melt last equilibrated with. They propose based on phase relationships and the absence of garnet or amphibole signatures that mantle-derived melts likely stall at ~12 kbar in a deep crustal hot zone, and then ascent to ~1 km where observed phases such as Ol, Plag and Cpx crystallize. We do not include these depths in our compilation, as they are not precise constraints on magma storage locations, but instead constrain the likely ascent path based more on inference of crustal structure than precise experimental constraints on phase stability.

Geophysics: The lightly vegetated flanks around the Three Sisters makes it an attractive location for satellite-based geodetics (Poland et al., 2017). InSAR acquisitions between 1992-2000 reveal inflation over a broad area (10 x 20 km) centred ~6 km west of the South Sister summit (Wicks, 2002). This inflation can be modelled with a Mogi point source at 6.5 ± 0.4 km depth (rlu), with a volume increase of 0.0023 ± 0.003 km³. Wicks (2002) suggest that this source could result from the injection of new magma, or pressurization of a hydrothermal system, with the former being more likely as hydrothermal activity is often accompanied with seismic activity (and this episode was relatively aseismic).

InSAR was vital to identify this period of deformation, as it was offset to the west of the electro-optical distance meter (EDM) and tilt-levelling methods installed at the summit between 1985-1986. Dzurisin et al. (2006) supplement InSAR observations with tilt surveys in 1985, 1986 and 2001, and EDM surveys in 1985-1986, and Campaign GPS from 2001-2002, and levelling in 2002-2003 along survey lines

intersecting the deformation centre. By inverting these three datasets, they investigate Mogi point sources, as well as elliptical and dislocation sources. The best fit uses a shallowly-dipping sill at 6.5 ± 2.5 km depth bgl. Dzurisin et al., (2009) further supplement this data with InSAR, GPS, and levelling data collected up to 2006. This reveals that the inflation rate has been decreasing exponentially. They suggest that the best fit to a shallowly-dipping sill proposed by Dzurisin et al., (2006) results from combining early InSAR data with later GPS data during this change in deformation, skewing the relative proportions of horizontal motion (which GPS is most sensitive to) and vertical deformation (which InSAR is most sensitive to). They propose two vertical prolate sources, which provide better fits to the data once these temporal changes are accounted for. One of their sources sits at 4.4 km depth bgl with an aspect ratio of 0.9 if network translation is ignored, (5.4 km with an aspect ratio of 0.86 accounting for network translation). They also conclude based on spring chemistry that an intrusion of magma is a more likely cause of deformation than a hydrothermal system perturbation. Riddick and Schmidt, (2011) examine C-band InSAR from two satellites (ERS and ENVISAT), and suggest that deformation tails off following two separate linear trends (1998-2003, 2004-2010). Using a Mogi sill source, they obtain depths of 4-5.5 km bgl, and 7 km bgl.

We are not aware of any seismic constraints on magma storage at Three Sisters, and the PNSN only locates 0-3 earthquakes within 10 km per year. Seismic constraints are not helped by the fact that there are relatively few seismometers within a very broad area, and these were only upgraded to broadband seismometers relatively recently (Fig. 6g).

Summary and Future work: Given recent renewed uplift ~ 5 km W of South Sister (Jan 2022) in addition to the deformation discussed above, more detailed petrological work on this edifice is warranted. In particular, MI constraints could help determine whether the depth identified in geodetic data is similar to that of magma reservoirs feeding past eruptive episodes, and experimental constraints could be used to investigate the relationship between mafic and silicic magmas. The extreme paucity of reported mineral compositions could also be addressed to develop a more coherent model of the magmatic plumbing system. In order to investigate the storage depths of the more mafic fissures and cinder cones of North Sister and the surrounding area (e.g. Collier Cone), a detailed study of vapour bubble CO_2 in MIs is required.

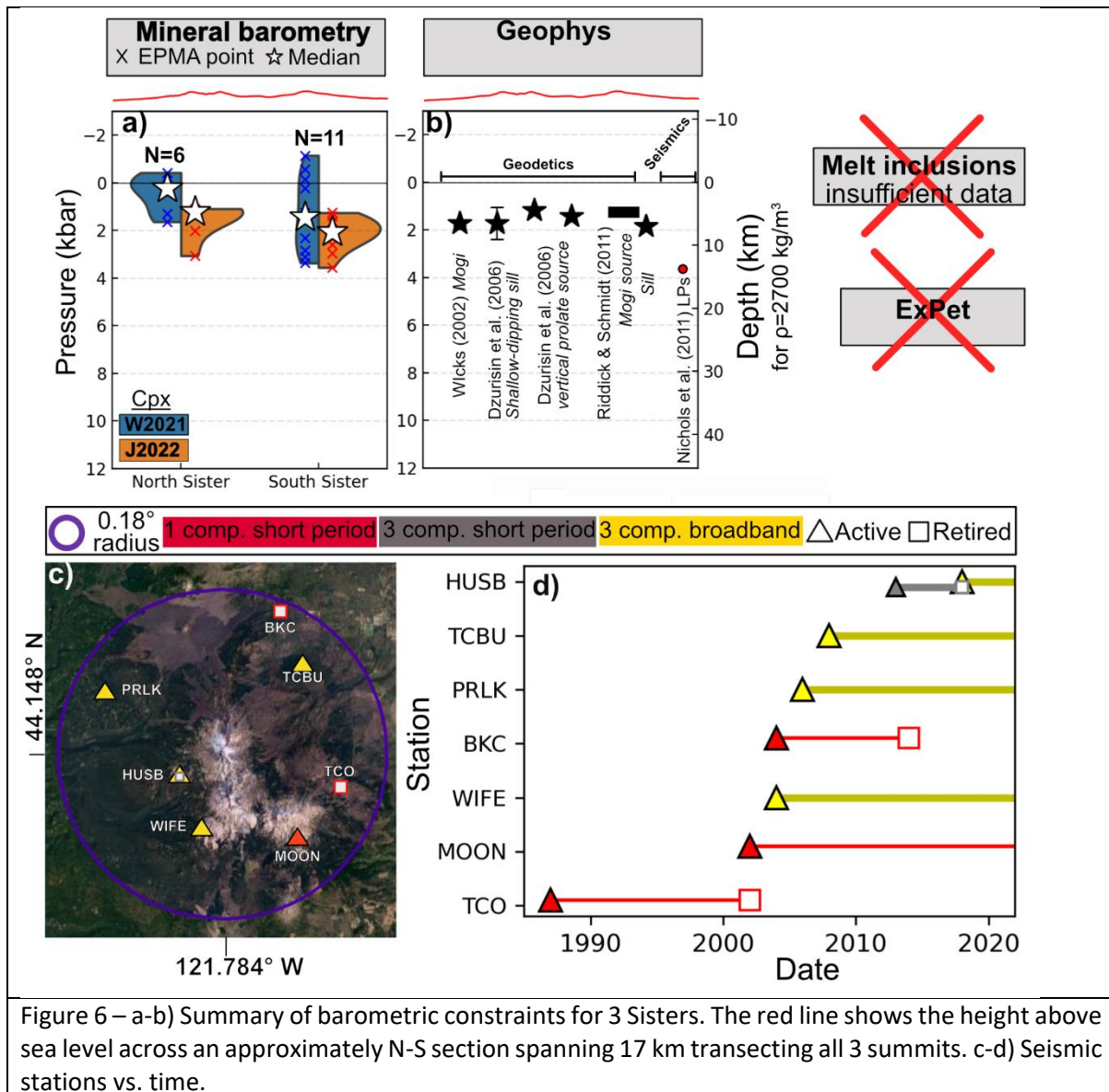


Figure 6 – a-b) Summary of barometric constraints for 3 Sisters. The red line shows the height above sea level across an approximately N-S section spanning 17 km transecting all 3 summits. c-d) Seismic stations vs. time.

Newberry Volcano

Newberry Volcano lies ~50-60 km east of the main arc front and has the largest area of all Cascade volcanoes (second in volume to Medicine Lake). Newberry exhibits predominantly bimodal volcanism; intracaldera eruptions are rhyolitic, while its north-west trending rift zone hosts basaltic-andesite fissures and cinder cones. Newberry caldera was formed at ~75 ka with the eruption of a compositionally-zoned basaltic-andesite to rhyolite tuff (Donnelly-Nolan et al., 2011).

Mineral Compositions/Melt inclusions: We were unable to find any published mineral compositions or MIs from Newberry Volcano.

Experimental Petrology: Mandler et al. (2014) perform 1 bar (anhydrous) and H₂O-saturated 1-2 kbar experiments on the ~75 ka caldera-forming tuff from Newberry Volcano. They find that the 1 kbar experiments best reproduce the samples from the caldera-forming tuff, but that these experiments are still too H₂O-rich (e.g., differentiation was H₂O-undersaturated). It is difficult to constrain the exact pressure, as the effect of pressure on phase equilibria in undersaturated magmas are small at crustal conditions. Overall, they conclude they can constrain that differentiation occurred in the upper crust.

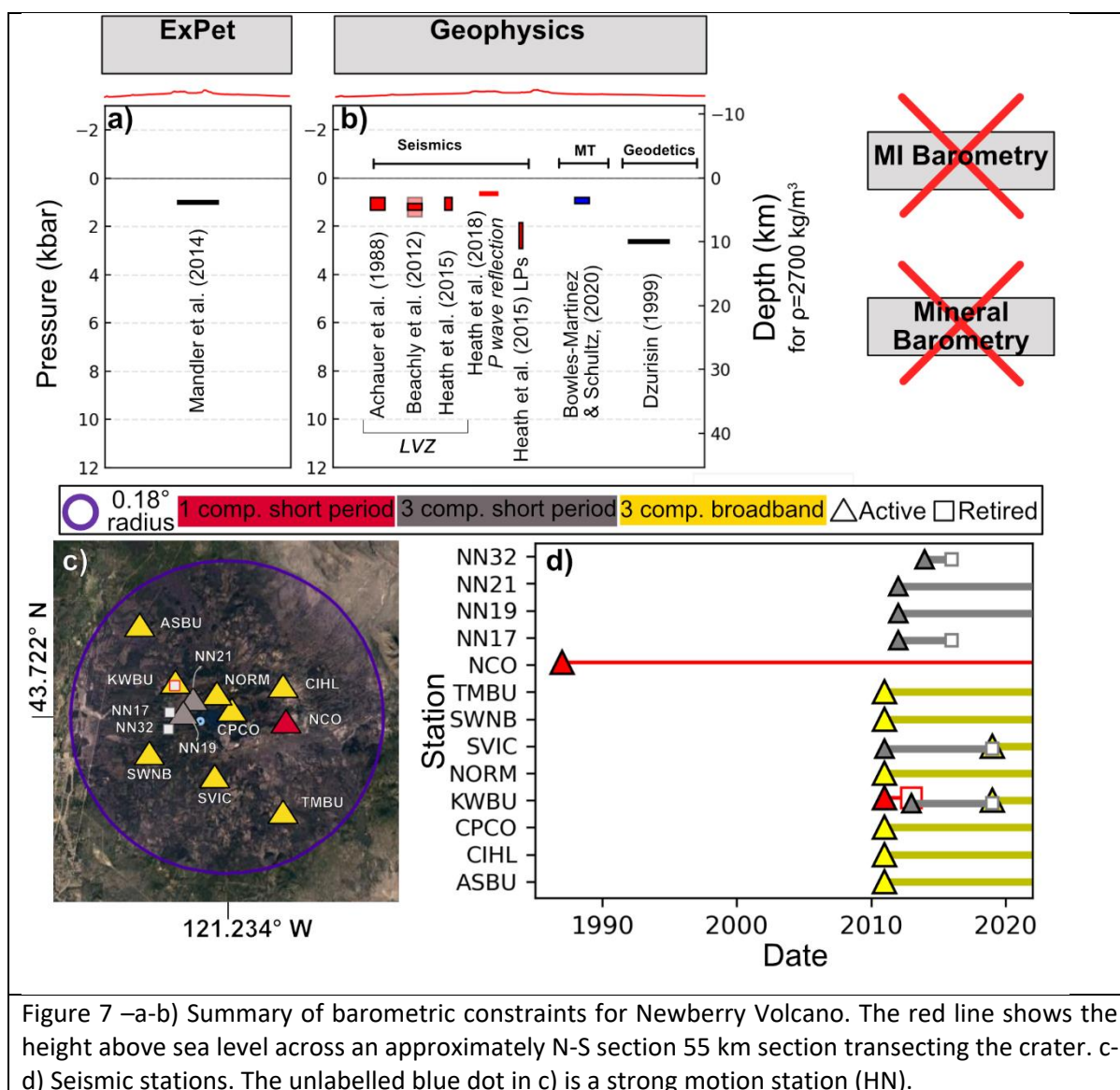
Geophysics: Extensive geophysical work has been performed at Newberry as a result of its geothermal potential. The teleseismic study of Stauber et al. (1988) indicates that no magma chamber is resolvable within the resolution of their study (e.g., ~5 km width). Using active source tomography with higher resolution, Achauer et al. (1988) identify a low velocity body at 3-5 km depth bgl, which they interpret to be a small silicic or stratified magma body (although the lower end of this body is difficult to resolve in their inversion). Zucca and Evans (1992) investigate P-wave attenuation using the same seismic data investigated by Achauer et al. (1988). If the low velocity zone is partial melt, it should also be characterized by high attenuation. They find that the low velocity zone in their layer 3 has average attenuation, such that it may reflect a recently solidified, hot cracked pluton, rather than actual melt. More recently, Beachly et al. (2012) use travel time tomography and forward modelling of arrival times and seismic amplitudes from an active-source seismic experiment in 2008 consisting of 75 three component seismometers. They identify a central low velocity anomaly at 3-6 km below the caldera floor. They find the best fit is a molten sill with a thin mush region at the bottom (in their schematic the melt body is located at ~4-5 km depth beneath the caldera).

The seismic network at Newberry was densified with three component broadbands in ~2010, increasing the opportunity for passive source techniques if supplemented by data from the active source campaigns. Heath et al. (2015) combine active and passive source seismic data collected on the 2008 array to better constrain seismic velocity, with increased resolution at depths >6 km (the limit of the Beachly et al. 2012 study). They identify the main low velocity volume at 3-5 km depth below the crater floor, with horizontal dimensions of 5 x 3 km, and a vertical thickness of 2 km. They suggest that the location of this body is consistent with it hosting the rhyolitic magmas erupted in the caldera. Their model requires ~10% melt with a minimum volume of 2.5 km³ in this region. They also report LPs from PNSN seismometers between 2012 and 2015 at 7-11 km depth (rlu). Finally, Heath et al. (2018) use seismic autocorrelation, and find a coherent P-wave reflection at 2.5 km depth beneath the caldera, which they infer to arise from the top of the magma body.

Bowles-Martinez and Schultz, (2020) use 3D magnetotellurics to identify a relatively resistive magma chamber beneath Newberry Volcano at 3-4 km depth below the crater floor. The relatively high resistivity of this body does not require melt and could be a fractured pluton. However, for consistency with the seismic studies described above, they show that this body could be melt, as long as that melt is relatively water-poor (they estimate ~1.5% H₂O). They indicate that such a low H₂O content is reasonable if the rhyolitic melt differentiated from a dryer basalt. However, given that differentiation of a basalt with ~0.3 wt% H₂O to a dacite at Kilauea Volcano raises H₂O contents to 2 wt% at even shallower depths (Wieser et al., 2022c), it seems unlikely fractional crystallization alone at 3-5 km depth to a rhyolite could produce such a dry magma (substantial melting of very anhydrous crustal material would be required).

Dzurisin, (1999) examine levelling data over a period of uplift between 1931-1994. They suggest that one possible mechanism for this uplift is the intrusion of 0.06 km³ of magma ~10 km below the crater floor. No further volcanic deformation has occurred at Newberry since the 1980s, making it hard to investigate this deformation source further (Poland et al. 2017).

Summary and Future work: Overall, Newberry has been subjective to extensive geophysical investigation. However, it is clear that substantially more petrological work involving mineral and MI compositions is required. In particular, MI work constraining pre-eruptive H₂O contents will help inform geophysical inversions (e.g., determining whether rhyolitic melts are as dry as suggested by Bowles-Martinez and Schultz, 2020).



Mt. Jefferson

Mt. Jefferson has a complex history over 4-8 Myrs, with 160 separate units from monogenetic and composite cones, shields, and domes spread over 150 km² (Conrey, 1991). Compositions span from basalts to rhyodacites, with heterogenous crystal cargoes (Ustunisik et al., 2016)

Mineral Compositions: We obtain N=87 Amp analyses from Conrey (1991), N=224 from DiGuilio, (2015), and N=32 from Ustunisik et al., (2016). While Conrey (1991) present a large number of Cpx analyses, they do not report Na₂O data, so these measurements cannot be used with the J2022 and W2021 barometers. DiGuilio, (2015) report N=25 Cpx and Ustunisik et al. (2016) N=11 Cpx analyses. DiGuilio, (2015) also report 25 Opx-Cpx pairs, although only N=3 of these are in high-T K_D equilibrium following Putirka (2008).

The median Cpx-only pressure is ~2.5 kbar using W2021, and ~1.9 kbar using J2022. Amp-only median pressures are reasonably similar (~3 kbar). In contrast, median Cpx-Opx pressures are 6.7 kbar using Eq37-39, and 5.7 kbar using Eq36-39 from Putirka (2008). Given the relatively poor performance of Cpx-Opx barometers in arc magmas (Wieser et al. in review) and the relatively small number of analyses, we suggest that more substantial evidence is needed to infer a deeper magma storage zone.

Melt Inclusions: The only MI measurements from Mt. Jefferson to our knowledge are from Ustunisik et al. (2016). However, they do not measure MI H₂O or CO₂, so no barometric constraints can be obtained from these samples.

Experimental Petrology: To our knowledge, there are no experimental constraints on magma storage at Mt. Jefferson.

Geophysics: No-ground based geodetic studies have been performed at Mount Jefferson. InSAR from the 1990s-2000s shows coherence, but no deformation (Poland et al., 2017). We are not aware of literature describing seismic or magnetotelluric evidence of magma storage zones. Given there is only a single one component short-period seismometer at considerable distance from the summit (>10 km), and on average the PNSN locates an average of 0 earthquakes per decade, the absence of seismic constraints on magma storage is unsurprising.

Summary and Future work: Further petrological work would help to further investigate the plumbing system, particularly MI or experimental petrology. However, given its relative inactivity, this work is perhaps not as urgent as similar data gaps at higher threat volcanoes (Fig. 1).

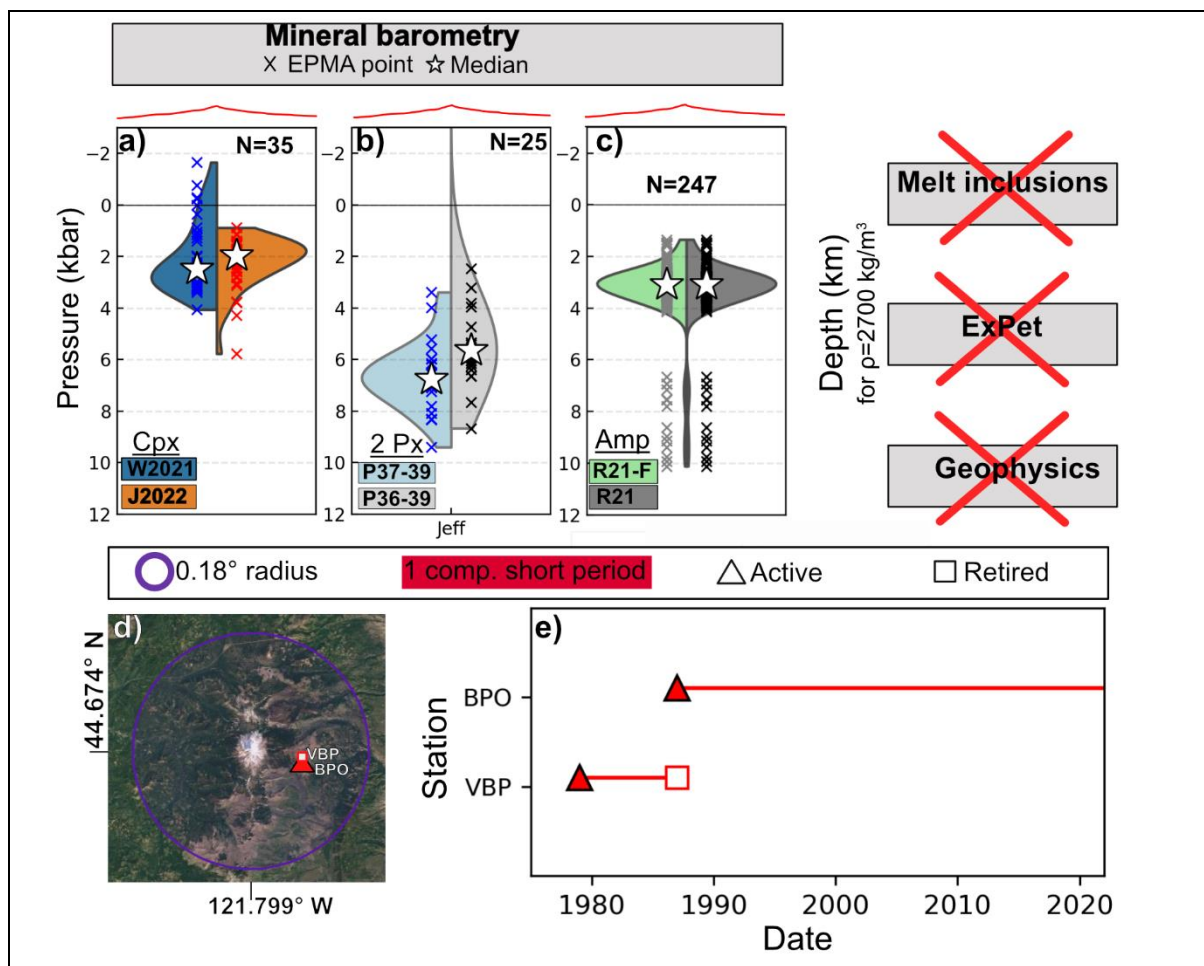


Figure 8 – Summary of barometric constraints for Mt. Jefferson Volcano. The red line shows the height above sea level across an approximately W-E section spanning 10 km transecting the summit.

Regional mid crustal anomalies around Mt. Hood, Mt. St. Helens, Mt. Adams and Mt. Rainier

To avoid repetition in the following sections, we discuss the regional anomalies in the mid to lower crust in the region around Mt. Hood, Mt. St. Helens, Mt. Adams and Mt. Rainier here in a single section.

Stanley (1984) perform a regional magnetotelluric (MT) study, identifying a conductive zone in the region between Mt. St. Helens, Mt. Adam and Mt. Rainier termed the Southern Washington Cascades Conductor (SWCC). He suggests that this feature reflects a band of conductive sediments and volcanic rocks of approximately Tertiary age. Hill et al. (2009) perform a higher-resolution MT study over a 35 km² area near Mt. St. Helens, and a 2D line stretching from Mt. St. Helens to just north of Mt. Adams across the southern portion of the SWCC. They identify a conductor stretching beneath the summit of Mt. St. Helens, merging with a thick conductive region at ~15 km depth, and stretching across to Mt. Adams, where it has some weak upper crustal features. They interpret the shallow zone beneath Mt. St. Helens as a magma conduit supplying the volcano, which showed unrest during the survey. By extension, they suggest that the connected mid crustal feature also represents 2-12% interconnected melt, which feeds the dacitic magmas erupted at Mt. St. Helens and Mt. Adams. Bedrosian et al. (2018) further investigate the magma vs. sediments hypothesis, using a larger dataset and 3D inversion across the entire SWCC. They note that the conductor beneath MSH imaged by Hill et al. (2009) extends 10's of km away from the volcano, extending into a metasedimentary belt. They believe the conductivity of dacite partial melt would be dwarfed by the ~10x higher conductivity of these metasediments, and as a result conclude MT cannot unambiguously distinguish magma storage vs. sedimentary deposits.

Flinders and Shen, (2017) use 3D ambient-noise tomography to investigate the velocity structure of the SWCC, with a particular focus around Mt. Rainier. They find a large low velocity zone in approximately the same region as the MT-defined SWCC, with its top at depths of ~10 km bsl towards the northern extent closer to Mt. Rainier, and ~15 km depth closer to Mt. St. Helens and Mt. Adams. They suggest that the base is likely unconstrained in the model, but may extend to ~27 km bsl. They also suggest that portions of the SWCC have seismic velocities most consistent with the presence of ~6% melt, particularly in the context of the large number of Quaternary volcanic vents over this feature (>100).

In addition to local anomalies at Mt. St. Helens, Ulberg et al. (2020) identify a broad region with low P-wave velocity at >10 km depth around Mt. Rainier to Mt. Adams. They speculate that this may indicate fluid or melt present, or high crustal temperatures.

Jiang et al. (2023) use ambient noise interferometry on a regional seismic network to further investigate the origin of these crustal anomalies. Crucially, their approach uses EarthScope array data in addition to regional seismic networks, which helps to mitigate edge effects, allowing them to expand their reconstruction to cover the area around Mt. Hood. They identify two subparallel low Vs zones stretching from Mt. Rainier to Mt. Adams, and Mt. St. Helens to Mt Hood at 15-30 km depth bsl. They interpret these as deep crustal magma sills with ~2.5-6% melt.

Overall, there seems to be consensus from seismic and magnetotelluric signals that there is a region of mid-lower crustal melt around these four Cascade volcanoes. What is less clear is how this region of partial melt is associated with the anomalies resulting from shallower crustal storage discussed below for each volcano.

Mount Hood

Construction of the modern edifice at Mt. Hood began at ~500 ka. Activity has since been dominated by remarkably homogenous andesitic (and sometimes dacitic) lava flows and domes, with no evidence for explosive eruptions in the tephra record. The three most recent eruptive episodes are Polallie (13-20 kyrs), Timberline (1.5 kyrs), and Old Maid (~200 yrs, Koleszar et al., 2012), with the Main Stage preceding this (>29 kyrs, Scott et al., 1997).

Mineral Compositions: Darr (2006) present N=15 Cpx analyses from the Main Stage (>29kyrs) and Parkdale Flow (7.5-7.7 kyrs, Scott et al., 1997). Cribb, (1997) present N=123 Cpx from the Main Stage Cloud Cap (400-600 kyr, Keith et al., 1985), Main Stage, and Polallie. We also obtain N=109 Amp compositions from Koleszar, (2011), Koleszar et al., (2012) and Loewen, (2012). The median Cpx-only pressure is ~1.4 kbar for W2021, and ~1.6 kbar for J2022, with W2021 extending as a tail to much shallower pressures (while J2022 shows the absence of very shallow pressures typical of this barometer). The median Amp-only pressure regardless of filtering is ~1.6 kbar, which is remarkably similar to the Cpx-only pressure estimates.

Melt Inclusions: Koleszar et al. (2012) present N=38 Plag, Opx, Cpx hosted MIs from the Old Maid, Timberline, and Polallie Stages. A subset of MIs that were large enough for double polishing (N=12) were measured using FTIR and yielded no CO₂ above the detection limit. The remaining MIs (<60-80 µm diameter, N=28) were measured by SIMS. These inclusions contain CO₂ contents up to 2400 ppm, although they note that the lack of standards with >540 ppm CO₂ required their calibration line to be extrapolated for these measurements. These high CO₂ contents are unusual in such evolved materials, so Koleszar et al., (2012) suggest they may result from the presence of undetected microcracks with CO₂ contamination during sample preparation. They also note that many MIs contain vapour bubbles, which may contain additional CO₂. Their FTIR H₂O measurements range from 0.8-3.6 wt%, while SIMS measurements range from 0.9-5.4 wt%. The higher SIMS H₂O contents may reflect the superior ability of smaller MIs to retain high volatile contents (e.g., less resistant to cracking/rupturing), although it is possible this also reflects calibration issues. They note that there is a general trend towards lower H₂O contents with increasing SiO₂, indicating MI entrapment during degassing induced-crystallization, which makes it hard to apply a filter based on H₂O contents. Thus, considering the poorly-constrained nature of CO₂, and the probable influence of degassing on H₂O, saturation pressure from these MIs are not a rigorous constraint on magma storage. That being said, the MI and Amp-only pressures overlap, although the MI pressures show a peak slightly shallower than the mineral-only barometers (perhaps preferentially recording ascent processes).

Experimental Petrology: While Mt. Hood andesite has been used widely as an experimental starting material, we are not aware of any experimental studies directly relating to magma storage conditions beneath Mt. Hood. Additionally, erupted Mt Hood andesites are mixed magmas and are thus not representative of a single multiply-saturated liquid (Kent et al., 2010).

Geophysics: Weaver et al. (1982) report the results from a 16-station seismic network established in 1977 at Mt. Hood. They find no significant velocity anomalies beneath Mt. Hood indicative of magma reservoirs.

Use of earthquakes directly, rather than through inversions for crustal structure, has been hindered at Mt. Hood by the fact that low frequency earthquakes and tremor are exceedingly rare (if present at all). Jones and Malone, (2005) summarize that most earthquakes picked up on the Mt. Hood seismic network have characteristics of tectonic earthquakes, likely reflecting the northern edge of regional Basin and Range seismicity. Following a M4.5 earthquake in June 2002 ~4.6 km South of Mt. Hood, there was a swarm of >200 aftershocks, which Jones and Malone (2005) subdivide into four groups. A small subset of these earthquakes (Group D) occurred at very shallow depths. They suggest that these may reflect volcanic processes beneath Mt. Hood (although they do not speculate further as to whether these represent magma or fluid movement). Other than the regional mid-crustal anomalies discussed above, there are no further seismic constraints on upper crustal storage to our knowledge, likely in part due to the fact that a local high-resolution study has not been conducted using modern instrumentation.

Poland et al., (2017) summarize available geodetic constraints at Mt. Hood, which show no consistent deformation patterns that can be associated with volcanic activity since the 1980s.

Summary and Future work: Future work remeasuring CO₂ and H₂O in MIs and their vapour bubbles using more robust SIMS or FTIR calibrations would help resolve whether the high pressure MIs of Koleszar et al. (2012) represent a deeper magma storage region or an analytical artefact. Hints of higher-pressure storage (2-4 kbar) are perhaps seen in the Cpx and Amp pressures as well. Coupled measurements of mineral chemistry and MIs within a single crystal would help to investigate this further. Like many of the volcanoes discussed so far, Mt. Hood's seismic network has been recently densified with three-component broadband seismometers (Fig. 9e). Once sufficient earthquakes have been recorded on this network, local, passive-source inversions should provide additional constraints on the presence/absence of magma storage regions and low velocity zones, and a greater understanding of the origin of earthquakes at Mt. Hood (Jones and Malone, 2005).

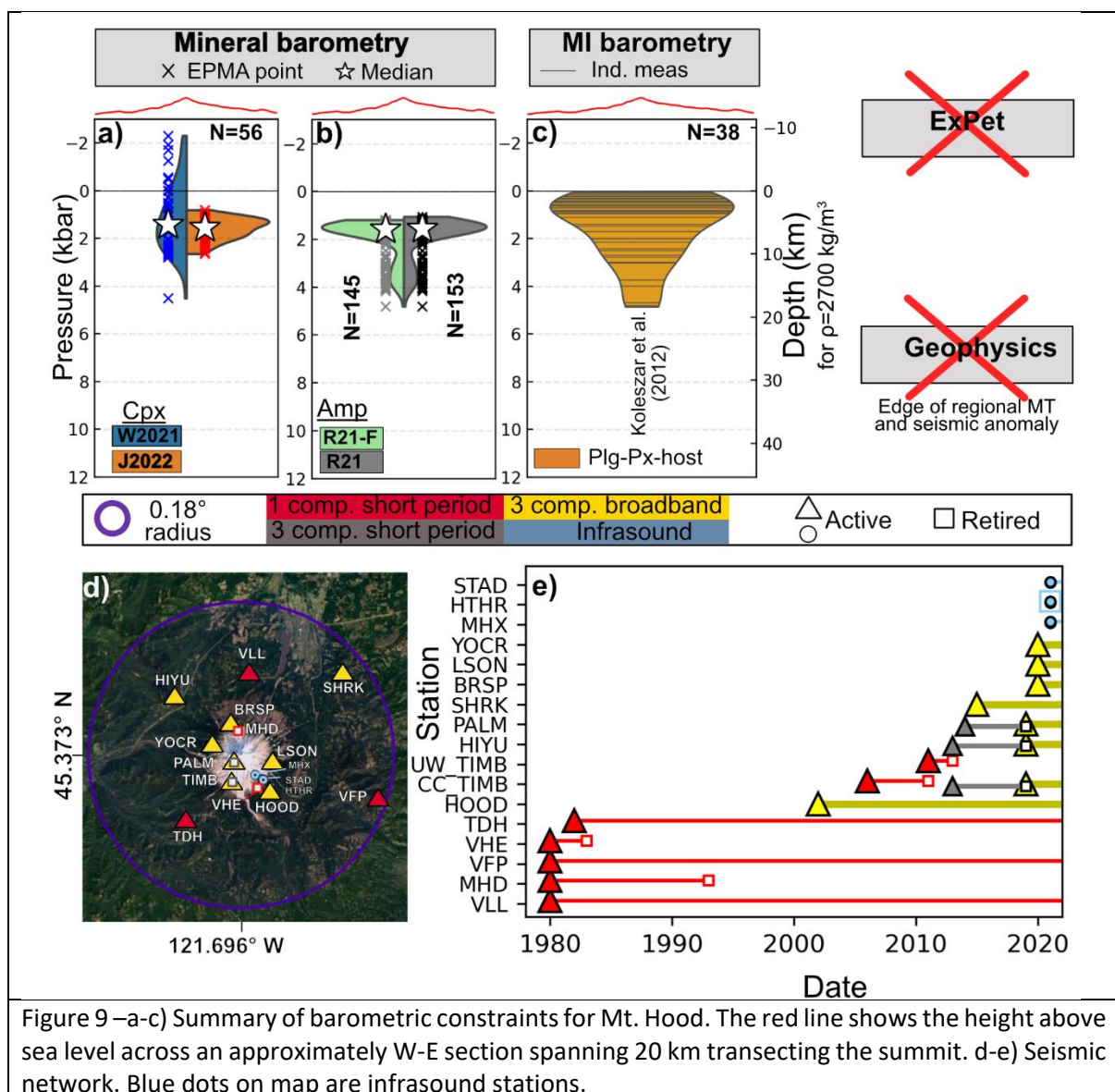


Figure 9—a-c) Summary of barometric constraints for Mt. Hood. The red line shows the height above sea level across an approximately W-E section spanning 20 km transecting the summit. d-e) Seismic network. Blue dots on map are infrasonic stations.

Mount St. Helens

Mt. St. Helens is located 53 km west of Mount Adams and 35-50 km W of the main arc front, so can be classified as a fore-arc volcano. It erupts primarily dacitic compositions with plagioclase, pyroxene and amphibole phenocrysts (with more minor rhyodacites; Hildreth, 2007). It is one of the most active, and youngest volcanoes in the Cascades, erupting more than half its 75 km³ magma volume in the last 28 kyrs. Following its Plinian eruption in 1980, and re-awakening in 2004-2008, it represents one of the best-studied Cascade volcanoes both in terms of petrology and geophysics.

Mineral Compositions: We compile N=57 Cpx compositions from the Kalama (~1480 AD) and Castle Creek andesites (1.9-1.7 kyr BP) from Cooper and Reid (2003), N=21 Cpx from the 2004-2005 eruption from Rowe et al. (2008), and N=4 Cpx from the Castle Creek andesite from Smith and Leeman (1993). Significantly more Amp analyses are available; N=77 and N=49 from the 2004-2005 episode from Rowe et al. (2008), N=171 from the May-80 cryptodome and pumice fall, the June-12th 1980 airfall, and the July 1980 pyroclastic flow from Humphreys et al. (2019), N=171 from the 1980 eruption from Loewen (2012), N=446 from 2004-1980 samples from Thornber et al. (2008), and N=54 from mafic Castle Creek samples from Wanke et al. (2019).

The median Cpx-only pressure is 2.3 kbar using W2021, and 1.8 kbar using J2022, with relatively similar distributions (although W2021 shows a deeper tail). Filtered and unfiltered Amp-only pressures are 3.1 and 3.2 kbar respectively, although, as for Cpx, the distributions are quite broad. In general, Amp pressures are offset ~ 1 kbar deeper than Cpx, which is well within the uncertainty of these methods.

Melt Inclusions: Rutherford et al., (1985) measure 57 MIs using EPMA, calculating H₂O using volatiles-by-difference techniques (~4.6 wt%). Blundy and Cashman (2005) measure H₂O in mostly Plag-hosted MIs (some Amp- and Opx-hosted) using SIMS. Texturally, many of these MIs show evidence for connection to the outside of the crystal, and there is a correlation between H₂O and SiO₂. These textural and chemical trends are indicating decompression-induced degassing accompanying MI entrapment, meaning that MIs saturation pressures may be weighted towards recording processes occurring during magma ascent. Blundy and Cashman (2005) state that their preliminary FTIR measurements show that CO₂ contents are very low, so calculate H₂O-only saturation pressures. However, Blundy et al. (2010) supplement these analyses with new SIMS analyses of CO₂ in N=77 MIs, finding CO₂ above the FTIR detection limit. We only use these later measurements. This is intriguingly similar to the scenario at Mt. Hood where Koleszar et al. (2012) find no CO₂ using FTIR, but abundant CO₂ using SIMS. The SIMS analyses of Blundy et al. (2010) for MIs from the 1980 plinian episode have relatively low CO₂ (<400 ppm) and high H₂O (~4-6 wt%), while the later subplinian to vulcanian and effusive events have higher CO₂ and lower H₂O. They attribute these differences to CO₂-flushing. Four MIs have 0.4-1.7 wt% CO₂, which Blundy et al. (2010) link to deeper magma storage, but carbon contamination should also be considered a possibility.

Experimental phase equilibrium: Rutherford et al. (1985) perform experiments on a bulk sample of MSH dacitic pumice at 1-3.2 kbar, varying the fluid composition and oxygen fugacity. They show that the observed phase assemblage and crystallinity of the May 18th 1980 magma can only be produced if $P_{\text{H}_2\text{O}} \neq P_{\text{Total}}$, requiring either water-undersaturation, or a relatively CO₂-rich melt. They conclude that the upper part of the MSH magma reservoir was at a pressure of 2.2 ± 0.3 kbar, $P_{\text{H}_2\text{O}}$ was 0.5 to 0.7, and T was $930 \pm 10^\circ\text{C}$. However, they note that the exact storage pressure is not rigorously defined, because these conditions were not simultaneously satisfied in different experiments. Rutherford and Devine (1988) perform additional experiments at 920°C and 2.2 and 3.2 kbar, with variable f_{O_2} and $X_{\text{H}_2\text{O}}$ with a particular focus on Amp stability. They find that the phase assemblage of the 1980 eruption

including Amp is reproduced at $P=2.2$ kbar, $T=920$ °C, and $X_{H_2O} \geq 0.67$. They suggest that a surge of Plag crystallization occurred when X_{H_2O} decreased just before eruption.

Rutherford and Devine, (2008) perform experiments on the 2004-2006 dacite, indicating that the Fe and Al-rich Amp cores formed at 2-3 kbar, and 900°C, as Amp forming in experiments at <2 kbar had lower Al than observed products. They suggest the observed An_{68-40} Plag compositions form when pressure drops to 2 kbar at 900°C, and the outer rims of some Amp phenocrysts may have formed at 1-2 kbar.

Geophysics: Scandone and Malone, (1985) use subsidence recorded by electronic tiltmeters in June-November 1980 to make a first estimate of the reservoir depth supplying the 1980 eruption (~7-9 km, rlu). They also analyse earthquake hypocenters accompanying each explosive event, identifying an aseismic zone at ~ 7 km depth (rlu) extending vertically for 6+ km which they suggest is a magma reservoir connected to the surface by a ~50 m wide conduit. Barker and Malone (1991) use earthquake focal mechanisms to identify an aseismic zone at 7-11 km bsl associated with magma storage. Musumeci et al. (2002) relocate 447 earthquakes from the late 90s to produce a 1D velocity structure beneath Mount Saint Helens, and identify a magma reservoir at ~5.5-10 km depth (bsl), and a thin vertical conduit similar to that invoked by Scandone and Malone (1985). More recently, Waite and Moran, (2009) present a P-wave travel time velocity model using earthquake data recorded on the local network over 25 yrs, supplemented by 19 temporary broadband seismometers from 2005-2006. They identify a low-velocity zone at ~2-3.5 km bsl which they attribute to a shallow magma storage zone. Their model has limited resolution beneath 6 km, but they identify low velocities at ~5.5-8 km bsl in an aseismic zone, which approximately aligns with the older estimates described above.

The numerous geophysical studies described above mostly imaged the upper crust, as travel time tomography struggles to produce high resolution images at >6 km depth. Kiser et al. (2016) present results from the active source portion of the iMUSH (imaging Magma Under St. Helens) project. They identify a high V_p/V_s anomaly at 4-13 km bsl which they attribute to magma storage, and a low V_p column extending from 15 km to the Moho to the southeast of Mt. St. Helens. Kiser et al. (2018) build on this study, using a finite-frequency tomographic method to place more detailed constraints on the geometry of the magma storage region. They identify a number of low V_p anomalies forming a near continuous body spanning 3.5-14 km bsl, with the highest amplitude V_p anomalies at 4-6 km bsl.

Ulberg et al. (2020) use local source V_s and V_p tomography as part of the iMUSH broadband array of 70 broadband seismometers to image the upper 20 km of the crust beneath Mount St. Helens. They identify a low P- and S-wave anomaly at 6-15 km depth bsl, with a diameter of 5-7 km, which they interpret to represent a magma storage region with ~3% partial melt over ~15-20 km³. They also image the broader low P-wave velocity region discussed above. Ambient noise imaging from the same array showed low-velocity lower-crustal anomalies between Mount St. Helens and Mount Adams (Crosbie et al., 2019).

Interestingly, neither Kiser et al. (2016, 2018), Ulberg et al. (2020), nor Crosbie et al. (2019) image the low velocity region at 2-3 km bsl identified by Waite and Moran (2009). Ulberg et al. (2020) suggest that the difference between the inversion techniques in the two studies may explain this discrepancy, while Kiser et al. (2018) suggest that the low velocity zone may have been a temporary anomaly related dome-forming activity between 2004-2008. The magma body may be too small to be resolved at the relatively long wavelengths of microseismic noise used in ambient noise imaging (Crosbie et al., 2019).

Lisowski et al. (2008) examine GPS deformation associated with the onset of unrest in 2004. They model the deformation in an elastic half space model as arising from a vertically-elongate magma reservoir centred at ~7-8 km (basl). Mastin et al., (2008) model geodetic data from 8 continuous GPS stations as an ellipsoidal source with its top at 5 ± 1 km (basl). While the base is less well constrained, they place it somewhere below 10 km (likely 10-20 km basl). They note that the source lies 1.3-1.6 km east of the crater centre.

In general, the shallower geophysical anomalies cluster at ~2-4 kbar, which is reasonably consistent with the median pressures from mineral barometry, while MIs appear to record shallower processes, perhaps during ascent towards the surface.

Summary and Future work: Relative to the rest of the Cascade arc, magma storage depths are well constrained at Mt. St. Helens. However, given experimental and MI evidence for the importance of CO₂, it would be worthwhile re-evaluating the CO₂ budget of Mt. St. Helens MIs to account for any CO₂ which has partitioned into the vapor bubble of MI. Further MI work on more mafic cones in the general area may provide petrological evidence for the geophysically imaged mid-crustal anomaly. The recent densification of three component broadband stations will greatly increase the potential for local, passive-source inversions. The biggest unanswered question revolves around whether the shallow low velocity anomaly of Waite and Moran (2009) was an ephemeral feature, difficult to resolve by other methods, or an imaging artefact.

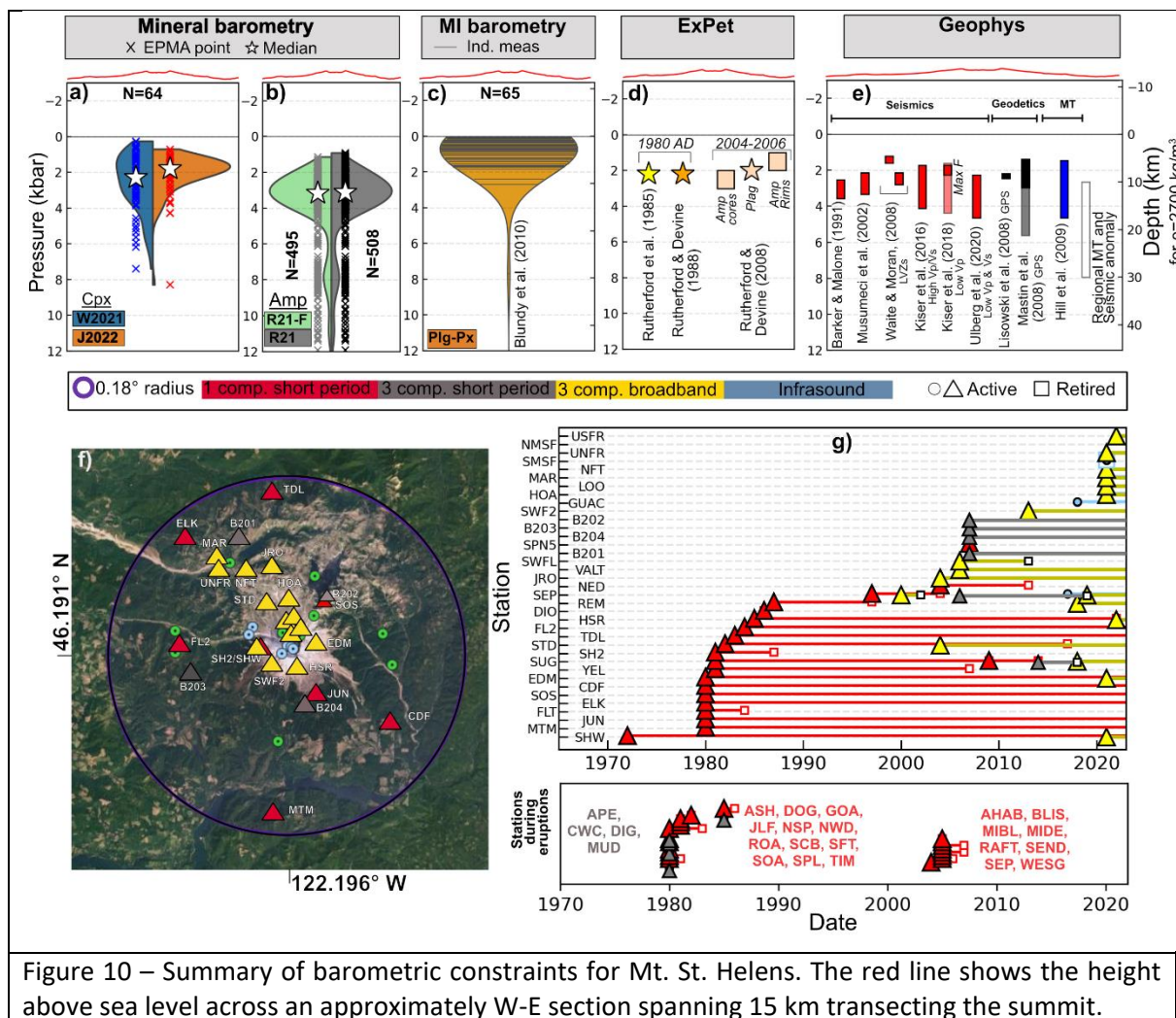


Figure 10 – Summary of barometric constraints for Mt. St. Helens. The red line shows the height above sea level across an approximately W-E section spanning 15 km transecting the summit.

Mount Adams

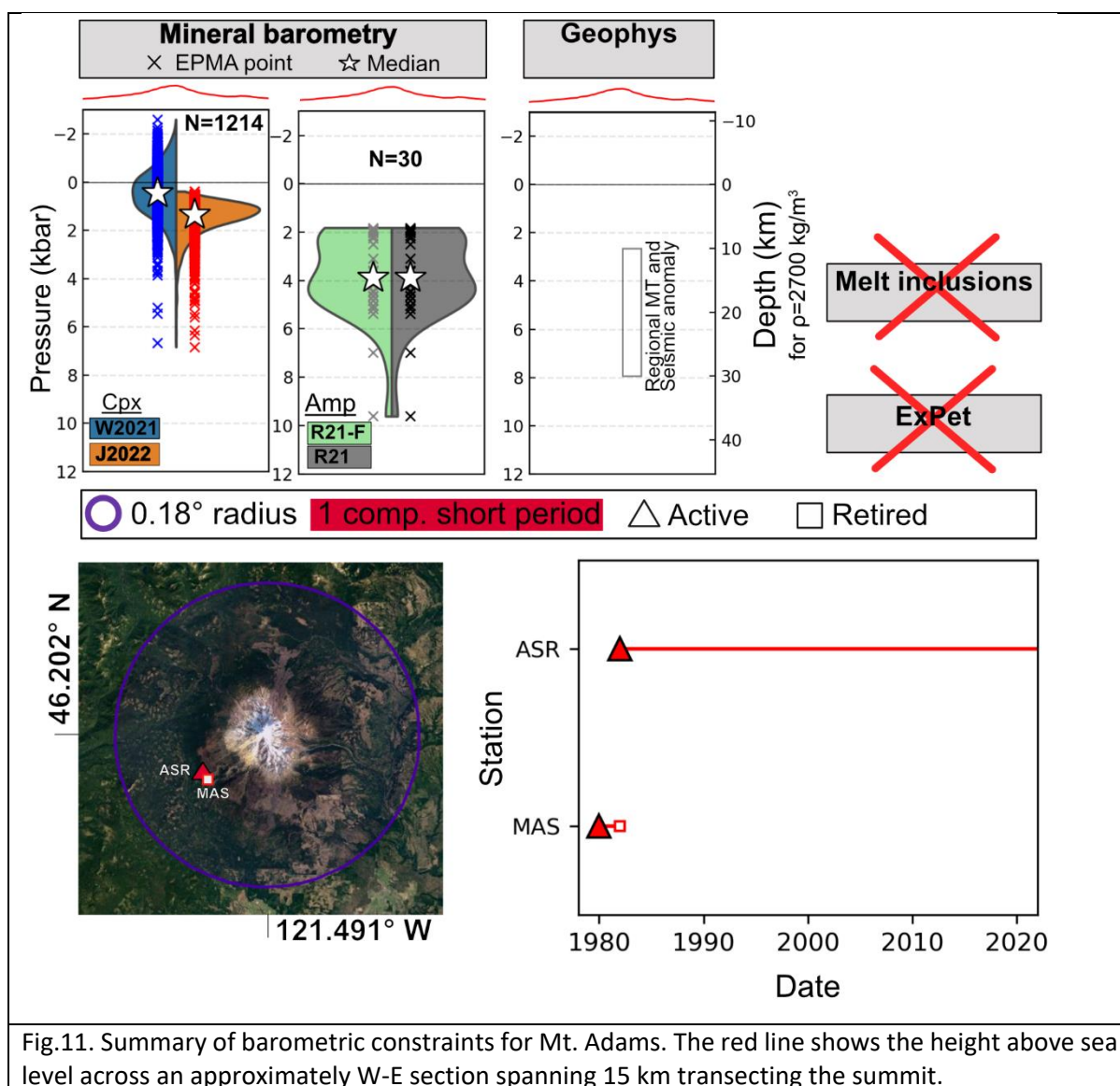
Mt. Adams is an andesitic-dacitic stratovolcano, located east of Mt. St. Helens along the main arc-axis. The large edifice lies in the centre of a larger volcanic field with ~120 spatter, scoria cones, and shield volcanoes. Vents within ~6 km of the summit are classified as flank vents because of compositional similarity to summit lavas, while those further away are mostly exhibit basaltic or basaltic-andesitic compositions (Hildreth, 2007).

Mineral Compositions: J. Fierstein supplied N=45 Amp and N=1219 Cpx analyses from the post-glacial (0-15 kyr) period of Mt. Adams (samples discussed in Hildreth and Fierstein, 1997). The median Cpx-only pressure is ~0.4 kbar for W2021 and ~1.3 kbar for J2022 (similar offset to that seen between these barometers at other edifices). In contrast, Amp-only pressures span a significantly greater range, from ~2-6 kbar, with a median pressure of 3.9 kbar.

Experimental phase equilibrium & Melt Inclusions: We are not aware of any phase-equilibrium constraints for Mt. Adams or MI studies.

Geophysics: Apart the regional mid crustal anomalies discussed above, there are no seismic constraints for magma storage at Mt. Adams, reflecting the fact there is only a single 1 component short period seismometer installed in the area (Fig. 11d), and no detailed local studies have been performed. The iMUSH array extends to the western flanks of Mt. Adams, and does indicate potential for melt storage in the lower crust west of Adams (Kiser et al., 2016; Crosbie et al., 2019; Ulberg et al., 2020). However, the lack of stations on or east of the summit, due to permitting constraints, makes it difficult to image a proximal magma system. In addition, no ground based geodetic studies have been performed at Mount Adams, and while InSAR shows coherence, there were no obvious signals of deformation in the 1990s to early 2000s (Poland et al., 2017).

Summary and Future work: The absence of upper crustal geophysical constraints, MIs and experimental petrology is very concerning, particularly given Mt. Adams is classified as high threat, and ranked the 34th most hazardous US volcano. While the difference in Cpx-only and Amp-only pressures may reflect different storage regions with different crystallizing phases, these barometers are too imprecise to be sure without other proxies for magma storage. A densified seismic network would be an important next step, along with more focused petrological studies specifically targeting magma storage depths (e.g., MIs).



Mount Rainier

Mt. Rainier is a voluminous stratocone and the highest elevation Cascade peak. It is made predominantly of pyroxene andesites-dacites with minor amphibole (59–66 wt% SiO₂; Hildreth, 2007). Unlike other Cascade volcanoes with numerous peripheral vents, Rainier's activity primarily occurs on the main edifice. While lava flows dominate, two large pumice falls >10 km³ from ~190 ka and ~380 ka have been identified (Sisson and Lanphere, 2000) and ~10 post-glacial pumices.

Mineral Compositions: We obtain N=12 Cpx and N=5 Amp analyses from the large andesitic Burroughs Mountain lava flow, which is thought to have been emplaced at ~496 kyr at the beginning of activity at the modern edifice of Mt. Rainier (Stockstill, 1999). We also obtain representative compositions from Venezky and Rutherford, (1997, N=5 Cpx, N=4 Amp). T. Sisson supplied additional EPMA analyses (N=13 Amp, N=35 Cpx) from the Sunset Amphitheatre dacite (~85 ka) examined by Sisson et al. (2019) and some cognate plutonic blocks from other Rainier lava flows (T. Sisson, Pers. Comms). We also obtain analyses of Cpx (N=27) and Amp (N=9) from K-rich spessartite samples, which occurs in small eruptions on the flank and vent, and are thought to bypass the main plumbing system (Sisson et al., 2014).

Considering all formations together, the median Cpx-only pressure is ~2.7 kbar using W2021 and ~2 kbar using J2022. While the number of analyses is relatively small for each formation, Cpx-only pressures from the spessartite samples are deeper than the mafic sunset amphitheatre samples (median of 4.4 vs 2.2 kbar using W2021, 2.9 kbar vs. 1.4 kbar using J2022, Supporting Fig. S3). This is consistent with the hypotheses that these spessartine melts bypass the main plumbing system. Burroughs mountain shows a very broad distribution of pressures, overlapping with both groups.

For Amp-only barometry, the median pressure for all samples is 3.1 kbar. Only 2 spessartine-hosted Amp pass the quality checks of Ridolfi (2021), although these are offset to deeper pressure by ~1-2 kbar from the Sunset mafic Amp (~1-3 kbar). Far more analyses per formation than could be obtained from the literature are required to accurately resolve any differences in magma storage using mineral compositions.

Experimental phase equilibrium: Venezky and Rutherford, (1997) investigate natural products from the 2.2 ka tephra layer C from Mt. Rainier, and conduct experiments at 0.25-2.5 kbar. They interpret the products of this eruption to form during mixing of an andesitic and dacitic magma. Their experiments on a powdered Rainier dacite show that the matrix glass composition is produced at H₂O-saturated conditions at <0.5 kbar (~2.4 km). Determining the storage conditions of the andesitic melt is harder (see discussion in MI section below), although they suggest that the presence of Amp indicates storage at >7 km depth (reasonably consistent with the Amp-only pressures we obtain).

Melt Inclusions: We are not aware of any published MI work measuring both CO₂ and H₂O. Venezky and Rutherford, (1997) describe an “exhaustive” attempt to find suitable MIs, noting that most inclusions were either too small to analyse, or were partially crystallized. They analyse 20 Plag- and Pyroxene-hosted MIs in the dacitic magma, obtaining H₂O contents of 2.4-3.3 wt% by volatiles by difference. For the andesitic magma, they obtain 4-6 wt% (although they acknowledge possible issues due to post-entrapment crystallization). They use these H₂O contents to infer entrapment depths of ~2.4 km for the dacite, and >7 km for the andesite. However, volatile-by-difference methods are associated with large uncertainties (Hughes et al., 2019), and H₂O can easily be driven up by post-entrapment crystallization (which it is noted these MIs show textural evidence for). Additionally, ongoing MI work indicates that Rainier melts are relatively CO₂-rich and H₂O-poor (T. Sisson, Pers. Comms), so we do not believe it is insightful to calculate H₂O-only saturation pressures based on volatile-by-difference methods.

Geophysics: Moran et al. (1999) investigate P-wave velocities using a local earthquake tomography imaging experiment. They identify a ~10-15 km wide low velocity zone at 1-14 km bsl. Based on the P-wave speeds (6 km s⁻¹), and the absence of earthquakes within this cylindrical anomaly, they suggest that this anomaly consists of hot fractured rock with the possible presence of small amounts of melt and fluid. The absence of significant S-wave attenuation indicates that no large, continuous bodies of melt or fluid exist in this volume.

McGary et al. (2014) use data from the CAFE (Cascade Array for Earthscope) experiment, which collocated seismic and magnetotelluric data in a E-W transect passing near Mt. Rainier. While they mostly image the deeper structure down to the subducting slab, they do image a crustal conductor they infer to represent a magma reservoir. However, this feature is offset 6-10 miles from the volcano's summit, so further investigation of this feature is warranted to determine whether it is magma, or another source of conductivity (Bonner, 2015). Obrebski et al. (2015) jointly inverted receiver functions and ambient-noise-derived phase-velocity dispersion curves. They did not detect any unambiguous low-velocity bodies in the upper crust, although signals were complicated and

station spacing of > 10 km probably cannot resolve a magma body the size of that imaged by Moran et al. (1999). There are also 18 LP earthquakes located by Nichols et al. (2011).

From a geodetic perspective, no deformation has been detected at Mt. Rainier since at least the 1980s, despite numerous levelling and GPS surveys, CGPS sites and InSAR acquisitions (Poland et al., 2017). Overall, these geophysical constraints are reasonably consistent with petrological methods, with no concrete evidence for magma storage below ~6 kbar (or 20 km).

Summary and Future work: Further petrological and geophysical work is desperately needed at Mt. Rainier, the 3rd most hazardous volcano in the US (Ewert et al. 2018). Specifically, MI studies could provide insights into the storage conditions of the andesitic melt. The recent densification of the seismic network (Fig. 12f) should help to further constrain the origin of seismic anomalies beneath Mt. Rainier, and determine whether these reflect melt (and how much is present).

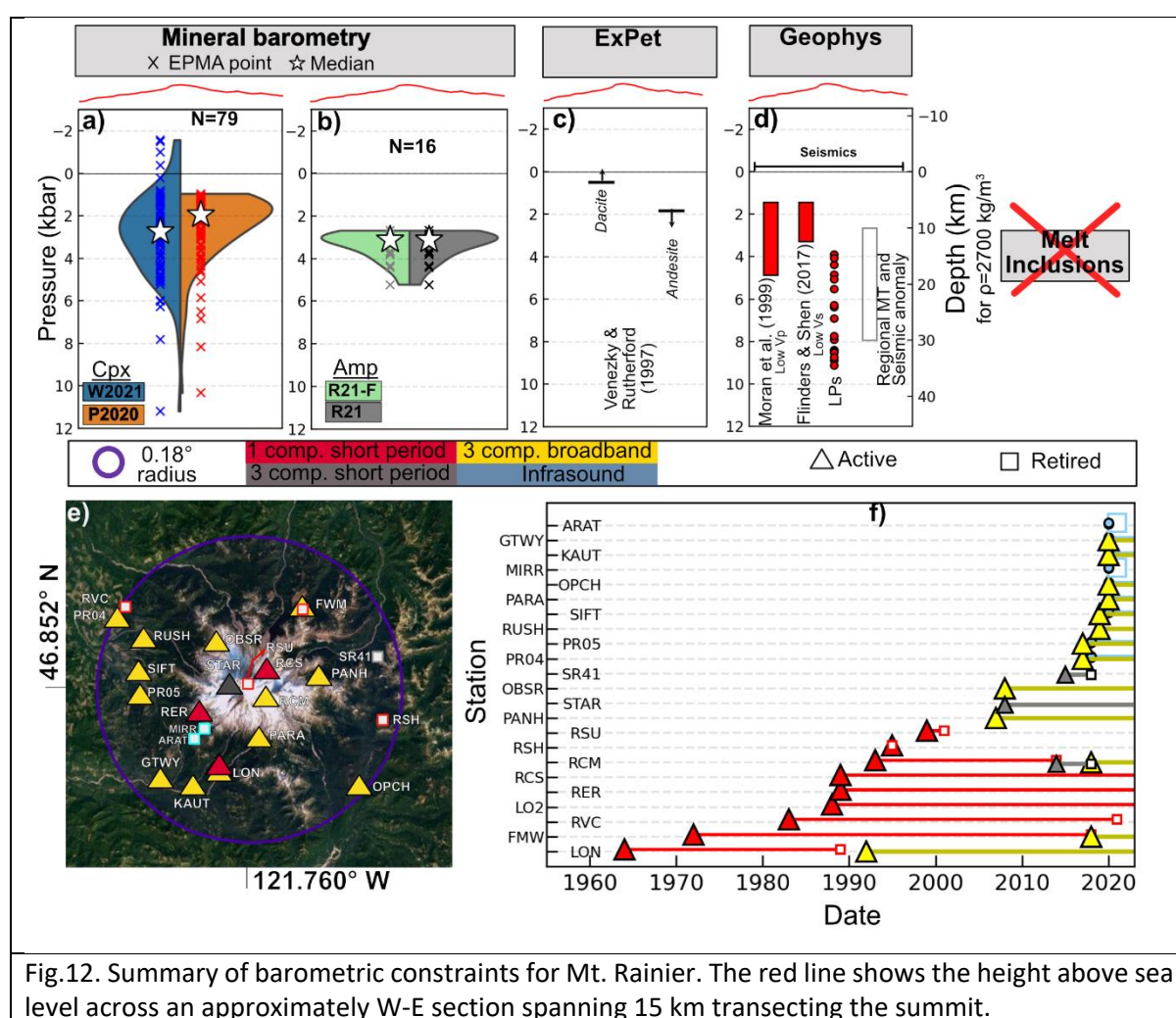


Fig.12. Summary of barometric constraints for Mt. Rainier. The red line shows the height above sea level across an approximately W-E section spanning 15 km transecting the summit.

Glacier Peak

Glacier Peak is a predominantly dacitic edifice that has substantially less topographic prominence above neighbouring peaks than many Cascade volcanoes (Fig. 13d). The early history of Glacier Peak was eroded during the last major glaciation. Subsequently, since glacial retreat ca. ~15 ka (Waite et al., 1995), Glacier Peak produced at least 9 pumice layers indicative of large explosive eruptions and

past eruptions have been characterised by numerous lahars. Thus, its activity more closely resembles Mt. St. Helens rather than the many other effusion-dominated Cascade volcanoes.

Mineral Compositions: We were only able to obtain N=19 Cpx compositions from the Lightning Creek high magnesian basaltic andesite from Sas et al., (2017). The median Cpx-only pressures is ~2.2 kbar for both W2021 and J2022.

Melt Inclusions: Shaw (2011) measure 16 olivine-hosted MIs from a primitive calc-alkaline basalt and a primitive low-potassium olivine tholeiite cinder cone (data reported in Venugopal et al., 2020). However, Shaw (2011) did not measure CO₂ in MI vapour bubbles. Venugopal et al., (2020) make a prediction of the amount of bubble CO₂ by assuming the same proportion of melt-vapour partitioning as at their measurements at Mt. Meager. However, given the partitioning of CO₂ into a vapour bubble is very dependent on the amount of PEC, which can vary to a large extent even within a single eruption let alone between different volcanoes (Wieser et al. 2021), we favour stating minimum estimates rather than using these reconstructions.

Experimental phase equilibrium: We are not aware of any phase equilibrium experiments relevant to Glacier Peak.

Geophysics: We are not aware of any geophysical constraints on magma storage, other than identification of 8 LP earthquakes (Nichols et al., 2011). No ground-based geodetic studies have been attempted, and InSAR hasn't detected any deformation (although the ice-covered summit and heavily vegetated flanks make coherence challenging; Poland et al., 2006). There is only a single one-component short-period seismometer, so the lack of seismic constraints other than LPs is not surprising (Fig. 13).

Summary and Future work: Glacier Peak is ranked as very high threat, and the 15th most hazardous US volcano. The absence of petrological or geophysical constraints on magma storage is a very clear data gap to address with future work.

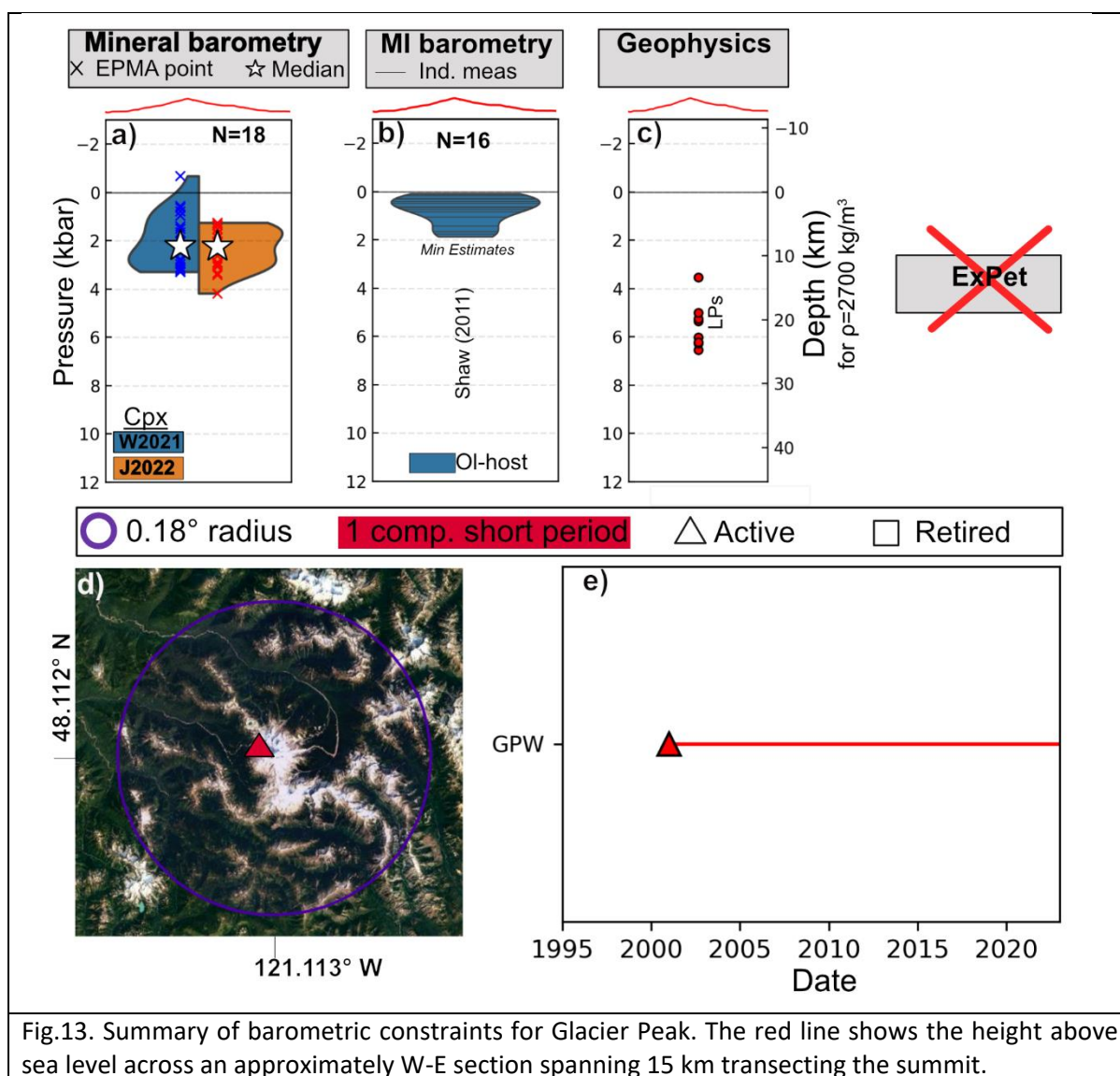


Fig.13. Summary of barometric constraints for Glacier Peak. The red line shows the height above sea level across an approximately W-E section spanning 15 km transecting the summit.

Mount Baker

Mt. Baker is a stratocone situated within a larger multi-vent volcanic field active since 1.3 Ma. It is one of the youngest volcanoes in the Cascades, with most of the modern edifice built over the last 40 ka (Hildreth et al., 2003). The larger volcanic field is predominantly andesitic and rhyodacitic in composition, with basalt and dacite making up only ~1-3% of the total volume. Mt Baker itself comprises of andesites, two pyroxene dacites, with some olivine-bearing andesites (Hildreth et al., 2003)

Mineral Compositions: We obtained N=12 Amp and N=133 Cpx from Gross, (2012), N=17 Cpx from Baggerman and DeBari, (2011), N=32 Cpx from Sas et al., (2017), N=28 Cpx from Mullen and McCallum, (2014), and N=26 Cpx from Moore and DeBari, (2012). The median Cpx-only pressure is 2.4 kbar for W2021 and 1.8 kbar for J2022, while the median Amp-only pressure is ~2.9 kbar.

Melt Inclusions: Shaw, (2011) measure 8 olivine-hosted MIs from Mt. Baker (reported by Venugopal et al., 2020), with the same caveats regarding CO₂ as described for Glacier Peak. These MIs return pressures between 0-2 kbar, which are likely anomalously shallow as bubble CO₂ is not properly quantified.

Experimental phase equilibrium: We are not aware of any phase equilibrium experiments relevant to Mt. Baker.

Geophysics: Seismically, Mt. Baker is relatively quiescent, with most shallow (<3 km) events thought to reflect activity of the glacier. Nichols et al., (2011) report 31 LPs earthquakes from Mt. Baker, the most of any Cascade volcano. We find one abstract describing a local seismic survey conducted at Mt. Baker, but no clear link to magma storage (Rohay and Malone, 1977). The lack of seismic data is unsurprising given the sparse coverage of the seismic network (even today, only a single three component broadband seismometer is present).

Hodge and Crider, (2010) investigate edifice deflation between 1981 to 2007 recorded by continuous GPS and EDM at Mt. Baker. This deflation is best recreated by a source at ~5.8 km depth (basl, ~2000 m), located 1.5 km to the E-NE of the summit. This aligns reasonably well with Cpx-only and Amp-only pressures.

Mt. Baker also experienced a period of thermal unrest in 1975, investigated retrospectively by Crider et al. (2011). At the time, a large area of snow-free ground was created in the crater, with high magmatic gas emissions, and an accompanying increase in gravity in the 30 yrs following this period (in addition to the inflationary period described above), but was interpreted not to have magmatic origins due to the lack of seismicity. However, Crider et al. (2011) note the presence of recent aseismic intrusions at other arc volcanoes worldwide (e.g., Lu et al., 2000), and that an absence of seismicity doesn't necessary mean an intrusion didn't happen. Unfortunately, there was insufficient monitoring data to place detailed constraints on this episode beyond the speculation that it was likely caused by intrusion into the mid crust.

Summary and Future work: The paucity of data for the 14th most hazardous very high threat US volcano is a concern. Mt. Baker is an obvious target for MI work, given the presence of tephra layers. Experimental phase equilibrium would also help to place constrains on storage conditions. Without a concerted geophysical campaign, it is unlikely that meaningful magma storage information will be gleamed from the current seismic network without further densification.

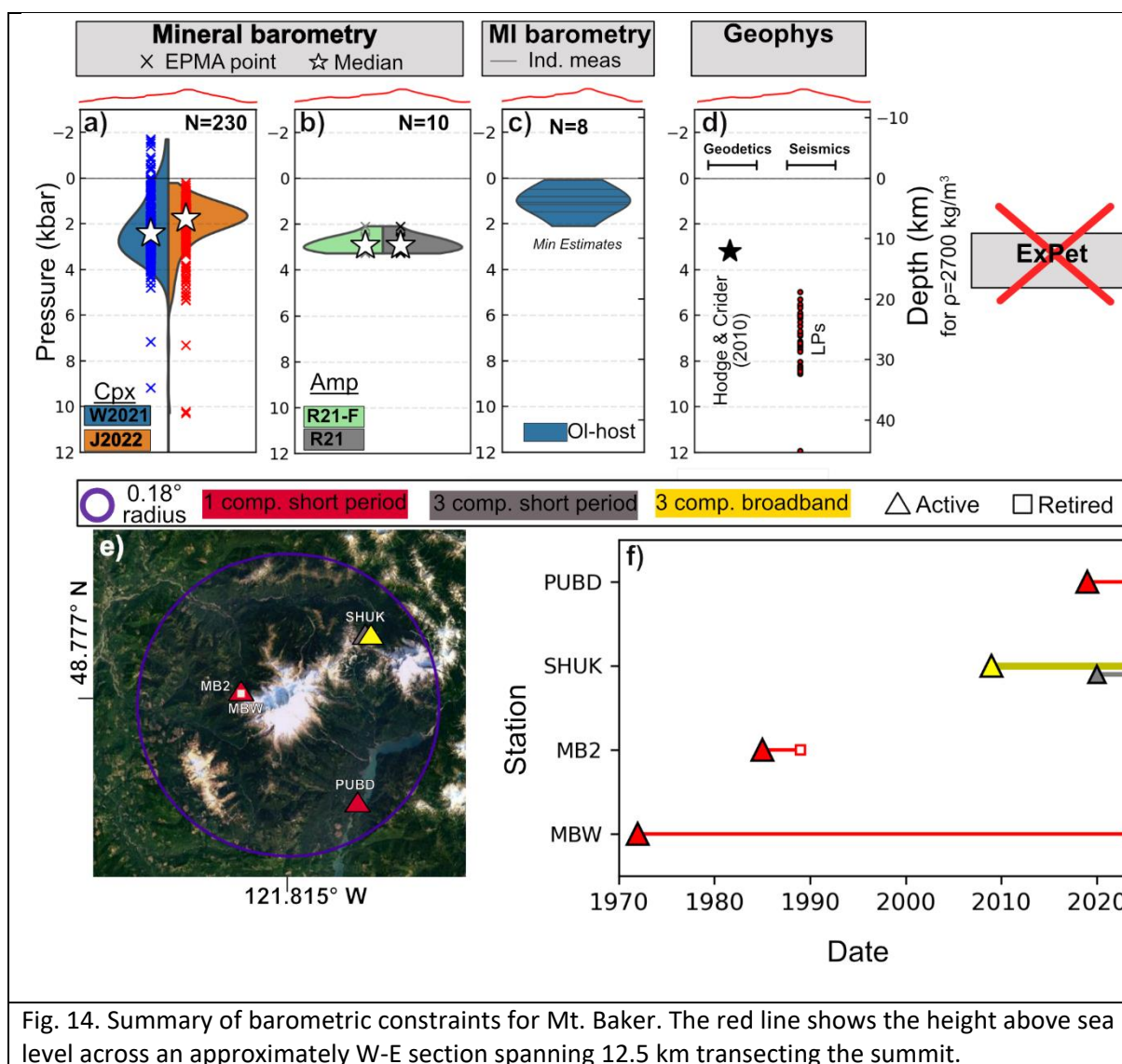


Fig. 14. Summary of barometric constraints for Mt. Baker. The red line shows the height above sea level across an approximately W-E section spanning 12.5 km transecting the summit.

Canadian Garibaldi Volcanic Belt:

The Garibaldi Volcanic Belt consists of 2300 distinct vents, and 22 major edifices, including Glacier Peak and Mt. Baker (Hildreth, 2007). Within Canada, some of the major edifices include Mt. Garibaldi, Garibaldi Lake, Mt. Meager, Salal Glacier, Bridge River. A wide variety of compositions are present in the Canadian segment, ranging from dacites and rhyodacites at Garibaldi and Cayley, high Si rhyolites at Mt. Garibaldi (Hildreth, 2007). These Canadian centres also erupt olivine-bearing basalts and basaltic-andesites (Venugopal et al., 2020).

Mineral Compositions: We compile N=15 Cpx compositions from the Garibaldi Volcanic Complex from Fillmore, (2014). We were unable to find any other mineral data. W2021 yields median pressures of 0.19 kbar, and 1.8 kbar for J2022.

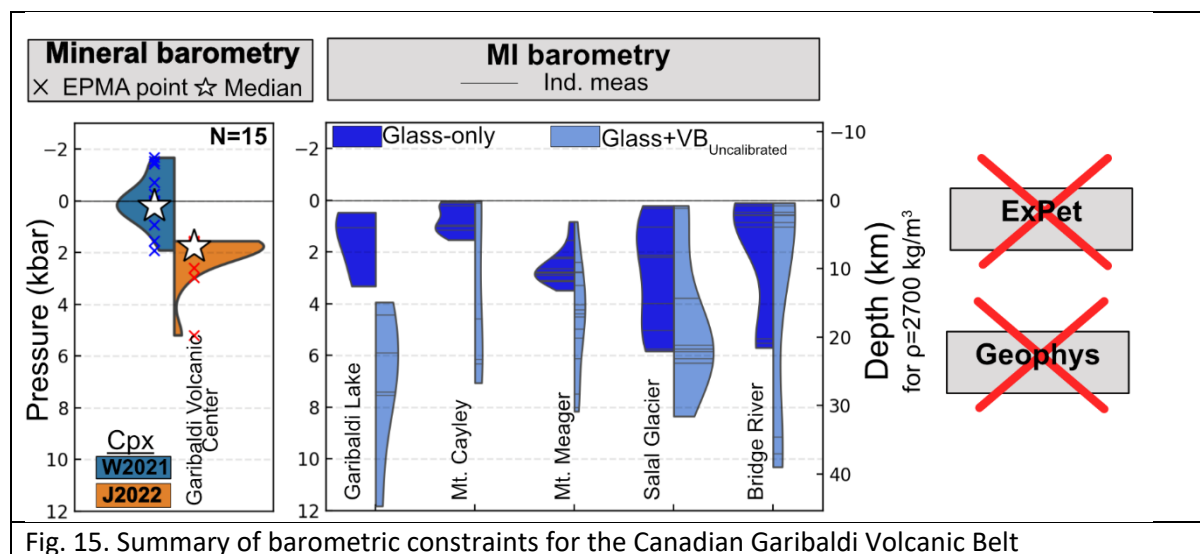
Experimental phase equilibrium: We are not aware of any experimental phase constraints on magma storage conditions in the Garibaldi Volcanic Belt

Melt Inclusions: As mentioned in the introduction, Venugopal et al., (2020) perform glass and vapour bubble measurements, but do not perform an instrument specific Raman calibration. Given that their high CO₂ densities are thermodynamically impossible at room temperatures, it seems highly likely the

amount of CO₂ in the vapour bubble was overestimated. We show their vapour-bubble reconstructed CO₂ alongside glass-only saturation pressures for completeness.

Geophysics: There are no geodetic constraints on magma storage in the Garibaldi Volcanic belt. No-ground based geodetic studies have been performed, and while C-band InSAR obtains some coherent images on the volcanoes flank, InSAR is generally hindered by the large amounts of vegetation on its slopes, and its ice-covered summit (Poland et al., 2017). We do not find any direct seismic constraints on magma storage beneath these volcanoes. Querying the IRIS database for the Canadian networks yields 4 seismometer stations in the general vicinity of the Garibaldi volcanic Belt (the broader distribution of vents and less well defined summits relative to the US Cascades makes it harder to define clear query criteria). There is a 3bb station close to Whistler which is ~28km due E of Mt. Cayley, and ~30 km north of Mt. Garibaldi (2013-present) There is a second 3bb station near Squamish which is ~27 km south of Mt. Garibaldi (1bb, 1996-2018, 3bb 2018-present). There was a 3bb station ~8km W of Mt. Meager and 10-15 km SW of Salal Glacier between 2016-2019, and a 3bb station about ~20km ESE along the same river valley from 1993-1998. Lu and Bostock, (2022) use the record from these 4 stations to identify 48 deep long period earthquakes (DLPs) at ~4-45 km depth in the region near Mt. Meager.

Summary and Future work: The paucity of work on the Garibaldi Volcanic Belt likely reflects its relative inaccessibility, snow and ice cover, and the lower hazard compared to the more active, US-based volcanoes.



Arc-Scale trends

Data Availability

Our compilation shows the presence of many concerning data gaps affecting our knowledge of magma storage depths along the Cascade Arc. The quantity of data available along the arc is highly variable, and is also poorly correlated with the USGS threat index for individual volcanoes (Fig. 16; Ewert et al., 2018). Some systems are relatively well covered, but many high threat volcanoes show a disturbing paucity of geochemical and geophysical data that constrains the nature of crustal magma storage. For example, at the second highest threat volcano in the Cascades (Mt. Rainier, 3rd highest threat volcano in the US) we have no magma storage depth constraints from MIs, very few reported Amp and Cpx compositions, one experimental pressure constraint, and only two seismic constraints. Recent

deployment of 13 broad band seismometers (Fig. 12f) does provide potential for better seismological imaging in future (e.g. receiver functions, P and S wave topography). Mt. Hood (6th highest threat in US) and Three Sisters (7th highest threat in US) are also very understudied. Available melt inclusions from Mt. Hood are limited and potentially unreliable due to issues relating to SIMS calibration, and there are no detailed geophysical or experimental constraints on magma storage depths. Similarly, the Three Sisters have no usable melt inclusion data (due to issues relating to data reporting, and lack of Raman measurements), no seismic studies, and no experimental studies placing precise constraints on magma storage reservoir depths. The only real depth constraints at Three Sisters come from a geodetic inversion of the 1998 inflation episode. However, it has been suggested based on spring chemistry and the lack of surface volcanism <10 ka that numerous intrusions likely occur in the deforming area with a very low probability of eruption (Evans et al., 2004). Thus, it is unclear if these geodetic estimates are providing useful information on the storage depths of melts. In addition, Mt. Baker and Glacier Peak, which are both ranked as very high threat (#14 and #15 highest threat in US) have also been greatly understudied from a petrological and geophysical perspective.

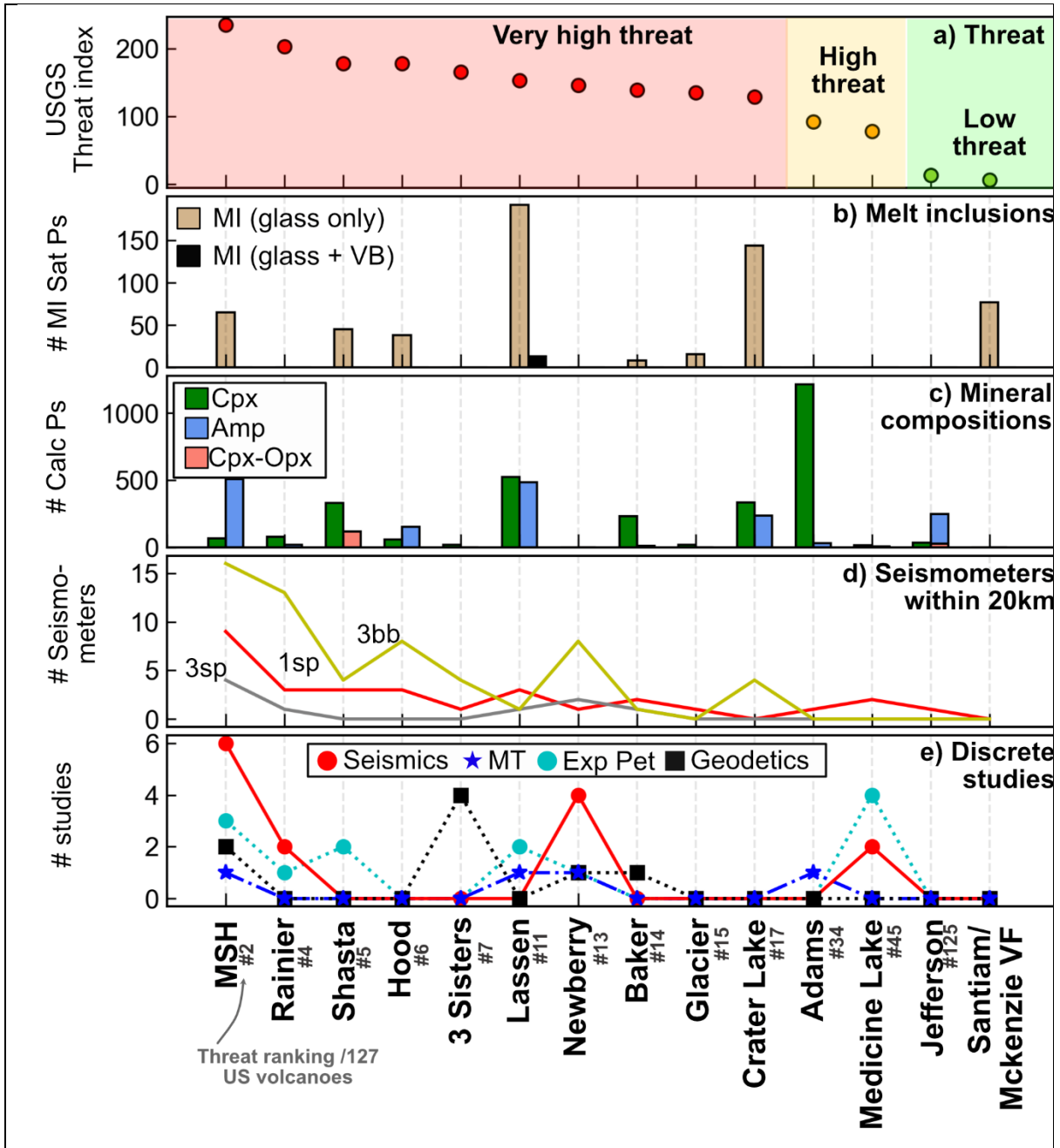


Figure 16: Visualization of number of available data, published studies and seismometers for each Cascade volcano in the U.S. ordered by the USGS threat index (highest threat to the left, lowest to the right). We only include seismic and MT studies which provide direct constraints beneath a specific volcano (rather than regional anomalies).

Probable trends

With the caveat of the relatively sparse and variable data coverage, we compile the available geophysical (Fig. 17a) and mineral (Fig. 17b) constraints on magma storage depth as a function of latitude to investigate along-arc trends in magma storage.

From a geophysical perspective, the vast majority of constraints on proximal magma chambers (rather than regional anomalies) are clustered at depths corresponding to ~1-5 kbar, with only magnetotelluric anomalies, LP earthquakes and regional seismic surveys returning higher pressures.

Considering the high imprecision of mineral-only barometers, Cpx-only pressures from P2020 and Amp-only pressures from R2021 are remarkably constant along the arc although the Amp-only pressures show slightly more scatter. In general, the median pressures from these mineral-only barometers suggest the vast majority of magma storage occurs in the upper 4 kbar (15 km) of the crust. The general agreement within the ± 2 -3 kbar uncertainty of Amp and Cpx-based barometers gives us confidence in this result, along with the fact that geodetic and seismic constraints on magma storage generally have depths equivalent to ~ 0 -5 kbar. It is hard to interpret whether the spread of individual calculated pressures to shallower and deeper pressures represents true transcrustal storage or analytical uncertainty based on reported information (Wieser et al. 2023b).

The general confinement of magma storage estimates at pressures less than 4 kbar has been noted in a recent global compilation of geophysical estimates of magma storage depths in volcanic arcs, cyan histogram, Fig. 17b). Rasmussen et al. (2022) find a strong correlation between water contents in melt inclusions from arcs and geophysically-determined magma storage depths, with the relationship between pressure and H₂O plotting along the water-saturation curve. They suggest two options: 1) H₂O controls magma storage depth through an increase in viscosity accompanying water exsolution (which they refer to as a 'mantle control') or 2) Water contents diffusively reset at a depth determined by a 'crustal control'. The authors infer that a crustal control would cause correlations between ratios such as Nb/Ce and Ba/La to be lost, while a mantle control would preserve these relationships. Based on the preservation of strong H₂O-incompatible element ratios in the Aleutians, Rasmussen et al. (2022) favour a mantle control, with primary magmatic water contents controlling magma storage depths.

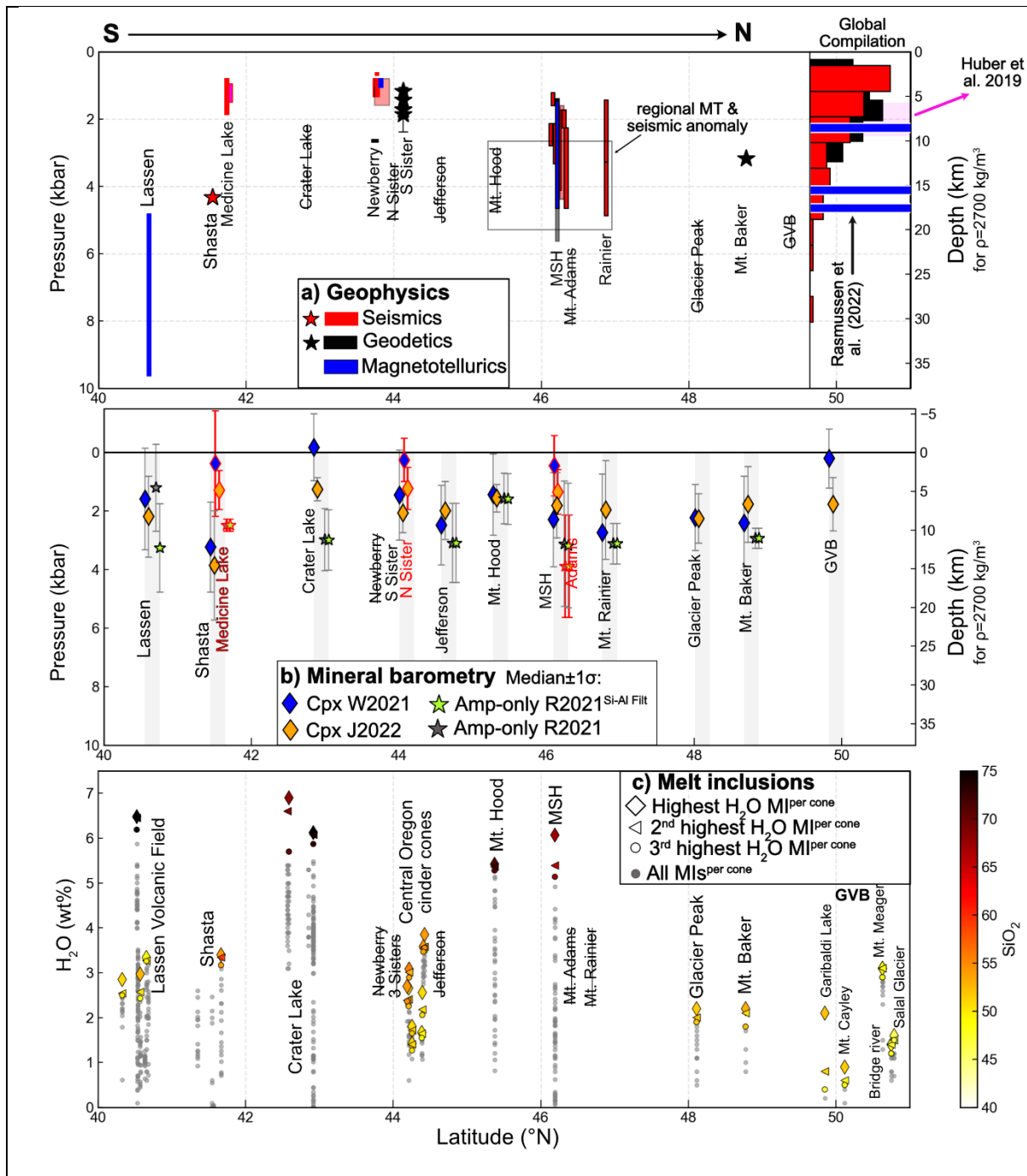


Figure 17: Summary of magma storage depths along the Cascades, with the x axis showing approximate latitude (Medicine Lake and Mt. Adams are shifted slightly from true latitude to avoid overlap with Shasta and MSH respectively). a) Compilation of geophysics for each center. The histogram shows a global compilation from Rasmussen et al. (2022) using the same color scheme as for the Cascades, and the ± 0.5 kbar from the compilation of Huber et al. (2019). b) Compilation of mineral barometry. Red outlines on symbols are used for Medicine Lake and MSH because of overlaps in latitude with Shasta and Mt. Adams. c) H₂O contents from melt inclusions, with the 3 most H₂O-rich melt inclusions from each volcano/cinder cone colored based on the melt inclusion SiO₂ content. Tephra samples collected at different locations but from the same source (E.g. the S17 cone, Mt. Shasta) are grouped as one. Volcanoes with no constraints are indicated with crossed out text.

To further test this interpretation we consider trends in H₂O with latitude along the Cascades, selecting the three most H₂O-rich MIs from each volcanic center (colored diamonds, triangles and circles, Fig 17c) as representative of the H₂O contents most resistant to degassing and diffusive re-equilibration. Unlike compiled magma storage depths, H₂O contents show considerable variation along strike. There is also a strong positive correlation between MI SiO₂ content and H₂O (Supporting Fig. S3). This may be indicative of differentiation in the presence of a relatively CO₂-rich mixed fluid, where CO₂ initially dominates the vapour phase, so H₂O can behave relatively incompatibly during fractional crystallization (Wieser et al., 2022b). This is not consistent with the model inferred by Rasmussen et al. (2022), which assumes the volatile system is dominated by a H₂O-rich vapour phase. However, these trends in H₂O are not reflected in available data for magma storage depths. The best way to test this hypothesis in the Cascades would be to compare MI H₂O and saturation pressure directly in inclusions where the amount of CO₂ in the VB has been precisely determined.

Thus, we suggest based on our compilation that it is more likely that a crustal process operating along the entire arc (whether due to a rheological boundary, or density-controlled) is restricting storage of all but the most mafic magmas to the upper 0-5 kbar of the crust (Chaussard and Amelung, 2014; Huber et al., 2019). Our compilation does show hints of deeper crustal magma storage, likely of more mafic magmas. However, due to the very nature of magma differentiation itself, crystals from the mafic predecessors to the more evolved erupted liquids are poorly preserved, meaning deeper magma storage is easily obscured. This preservation bias is particularly hard to see through given the small number of published mineral compositions at many Cascade volcanoes (e.g., N=18 Cpx from Glacier Peak, N=16 Amp from Mt. Rainier, N=11 Cpx from 3 sisters). If we imagine that 1% of deeper crystals are erupted, we would need thousands of analyses to get a cluster of deeper pressures that would be interpretable, rather than appearing as outliers. Petrologic experiments on predecessor mafic magmas erupted at the periphery of Mt. Shasta and Mt. Rainier do support a period of mid- to lower-crustal storage that results in crystallization (e.g., Krawczynski et al., 2012) and/or crustal melting (e.g., Blatter et al., 2013; 2017) that are likely important to evolve mantle-derived magmas to the intermediate and silicic compositions characteristic of those stored in the upper crust. Future MI work measuring the MI melts and vapour bubbles, petrologic experiments, and substantially more mineral analyses are thus required to further investigate the prevalence of deeper storage of mafic melts in the Cascades arc relative to the ubiquitous upper crustal reservoirs recorded by the compiled geophysical studies and available mineral data.

Conclusions

A detailed review of available petrological, geochemical and geophysical constraints on the depth of magma storage beneath Cascade arc volcanoes suggest that the majority of subvolcanic magma storage is restricted to the upper 0-5 kbar (0-20 km) of the crust, and it appears magma storage is remarkably uniform along strike. However, further consideration of magma storage at higher resolution, and evaluation of latitudinal variations is limited by issues with accuracy and by high uncertainties of techniques used for estimating storage pressure, and by numerous data gaps that exist along the arc. Considering the number of high-threat volcanoes in the Cascades, the paucity of data to constrain magma storage from geochemical and geophysical perspectives is highly concerning, and a stark contrast to other high-threat volcanoes in the US (e.g., Kilauea, Poland et al., 2014).

Gaps in geophysical datasets result from: 1) difficult access because of terrain, snow and ice cover, 2) the fact many Cascade volcanoes have been relatively quiescent in the last few decades, 3) dense geophysical imaging campaigns are costly and uncommon, and 4) permitting issues in wilderness areas hindering the establishment of dense monitoring networks (Moran and Benjamin, 2021; Poland et al.,

2017). Gaps in the geochemical and petrological datasets reflect a lack of study of many important systems, specific technique limitations (e.g. neglecting CO₂ vapour bubbles, poor quality EPMA analyses of mineral compositions, Wieser et al., 2023b), and poor data reporting (e.g., publishing only representative mineral analyses). We therefore recommend targeted melt inclusion, petrologic, and where possible geophysical studies of the understudied high threat volcanoes in the Cascades arc to determine their depths of magma storage, which are critical for interpreting future monitoring signals and will influence the style, size, and frequency of future eruptions.

Acknowledgements

The authors acknowledge support from a National Science Foundation Grants 1948862 and 1850779 (to AJRK), 1949173 (to CBT), and 1948834 (to GAA). We also acknowledge support from the National Science Foundation ICER-20-26904 granted to OFM Research (PI. Ghiorso) for maintaining the ENKI server used to perform saturation pressure calculations using VESlcal. This study relies heavily on data provided by corresponding authors, many of whom went to considerable effort to track down decade-old data. We thank Martin Streck for help extracting mineral compositions from his online textural tool, Judy Fierstein for sharing a large quantity of mineral data from Mt. Adams, Nicole Moore for sharing mineral data from Mt Baker, Allison Koleszar for sharing amphibole data from Mt Hood, Warner Cribb for sharing pdf tables of mineral data from his thesis on Mt. Hood, Heather Wright for sharing mineral data from Crater Lake, Thomas Sisson for sharing data from Rainier, Kristina Walowski and Melissa Scruggs for help reconstructing their Cpx-Liq datasets, Michael Clynne and Bryan Platt for sharing large amounts of data from Brokeoff Volcano, and Tim Druitt and Charlie Bacon for posting large quantities of handwritten EPMA data from Crater Lake. We thank Ellen Aster for help interpreting her vapour bubble data from Lassen. We thank Matthew Gleeson for sending many journal pdfs which were behind paywalls. We thank Nick Barber for his VMSG QGIS course, which we used to help extract topographic profiles of the Cascades. Throughout this paper, the post-colonial names are used for Cascade volcanic centres. We acknowledge that Indigenous cultures of the region have names for these volcanoes, and we hope that one day the official names of these volcanoes reflect these names.

Open Research

A compiled dataset of mineral compositions, melt inclusions and seismic stations, along with the Jupyter Notebooks used to compile, filter and plot data are available on Penny Wieser's GitHub (https://github.com/PennyWieser/Cascade_data_Compilation/tree/main). Upon article acceptance, this will be archived on Zenodo.

References

- Achauer, U., Evans, J.R., Stauber, D.A., 1988. High-resolution seismic tomography of compressional wave velocity structure at Newberry Volcano, Oregon Cascade Range. *J. Geophys. Res.* 93, 10135–10147. <https://doi.org/10.1029/JB093iB09p10135>
- Anderson, A.T., 1974. Evidence for a Picritic, Volatile-rich Magma beneath Mt. Shasta, California. *Journal of Petrology* 15, 243–267.
- Aster, E.M., Wallace, P.J., Moore, L.R., Watkins, J., Gazel, E., Bodnar, R.J., 2016. Reconstructing CO₂ concentrations in basaltic melt inclusions using Raman analysis of vapor bubbles. *Journal of Volcanology and Geothermal Research* 323, 148–162. <https://doi.org/10.1016/j.jvolgeores.2016.04.028>
- Bacon, C.R., Lanphere, M.A., 2006. Eruptive history and geochronology of Mount Mazama and the Crater Lake region, Oregon. *Geological Society of America Bulletin* 118, 1331–1359. <https://doi.org/10.1130/B25906.1>

- Bacon, C.R., Newman, S., Stolper, E., 1992. Water, CO₂, Cl, and F in melt inclusions in phenocrysts from three Holocene explosive eruptions, Crater Lake, Oregon 10.
- Baggerman, T.D., DeBari, S.M., 2011. The generation of a diverse suite of Late Pleistocene and Holocene basalt through dacite lavas from the northern Cascade arc at Mount Baker, Washington. *Contrib Mineral Petrol* 161, 75–99. <https://doi.org/10.1007/s00410-010-0522-2>
- Baker, M.B., Grove, T.L., Price, R., 1994. Primitive basalts and andesites from the Mt. Shasta region, N. California: products of varying melt fraction and water content. *Contr. Mineral. and Petrol.* 118, 111–129. <https://doi.org/10.1007/BF01052863>
- Barr, J., Grove, T.L., Elkins-Tanton, L., 2007. High-magnesian andesite from Mount Shasta: A product of magma mixing and contamination, not a primitive melt: Comment and Reply: Comment. *Geology* 35, e147–e147.
- Bartels, K.S., Kinzler, R.J., Grove, T.L., 1991. High pressure phase relations of primitive high-alumina basalts from Medicine Lake volcano, northern California. *Contr. Mineral. and Petrol.* 108, 253–270. <https://doi.org/10.1007/BF00285935>
- Beachly, M.W., Hooft, E.E.E., Toomey, D.R., Waite, G.P., 2012. Upper crustal structure of Newberry Volcano from P-wave tomography and finite difference waveform modeling: NEWBERRY FINITE DIFFERENCE MODELING. *J. Geophys. Res.* 117. <https://doi.org/10.1029/2012JB009458>
- Bedrosian, P.A., Peacock, J.R., Bowles-Martinez, E., Schultz, A., Hill, G.J., 2018. Crustal inheritance and a top-down control on arc magmatism at Mount St Helens. *Nature Geosci* 11, 865–870. <https://doi.org/10.1038/s41561-018-0217-2>
- Benz, H.M., Zandt, G., Oppenheimer, D.H., 1992. Lithospheric structure of northern California from teleseismic images of the upper mantle. *J. Geophys. Res.* 97, 4791. <https://doi.org/10.1029/92JB00067>
- Blundy, J., Cashman, K., 2005. Rapid decompression-driven crystallization recorded by melt inclusions from Mount St. Helens volcano. *Geol* 33, 793. <https://doi.org/10.1130/G21668.1>
- Blundy, J., Cashman, K.V., Rust, A., Witham, F., 2010. A case for CO₂-rich arc magmas. *Earth and Planetary Science Letters* 290, 289–301. <https://doi.org/10.1016/j.epsl.2009.12.013>
- Bonner, R., 2015. A magnetotelluric investigation of shallow conductivity sources beneath the Cascadia Volcanic Arc. Honors Thesis, Oregon State University.
- Bowles-Martinez, E., Schultz, A., 2020. Composition of Magma and Characteristics of the Hydrothermal System of Newberry Volcano, Oregon, From Magnetotellurics. *Geochem. Geophys. Geosyst.* 21. <https://doi.org/10.1029/2019GC008831>
- Bullen, T.D., Clynne, M.A., 1990. Trace element and isotopic constraints on magmatic evolution at Lassen Volcanic Center. *J. Geophys. Res.* 95, 19671. <https://doi.org/10.1029/JB095iB12p19671>
- Cashman, K.V., Sparks, R.S.J., Blundy, J.D., 2017. Vertically extensive and unstable magmatic systems: A unified view of igneous processes. *Science* 355, eaag3055. <https://doi.org/10.1126/science.aag3055>
- Chaussard, E., Amelung, F., 2014. Regional controls on magma ascent and storage in volcanic arcs. *Geochem. Geophys. Geosyst.* 15, 1407–1418. <https://doi.org/10.1002/2013GC005216>
- Chiarabba, C., Amato, A., Evans, J., 1995. Variations on the NeHT high-resolution tomography method: A test of technique and results for Medicine Lake Volcano, northern California. *Journal of Geophysical Research* B3, 4035–4052.
- Christiansen, R., Calvert, A., Champion, D., 2013. Voluminous tholeiitic basalts near Mount Shasta, California, as regional strain markers. Presented at the AGU Fall Meeting Abstracts, pp. V11D-03.
- Christiansen, R.L., Calvert, A.T., Grove, T.L., 2017. Geologic Field-Trip Guide to Mount Shasta Volcano, Northern California.
- Clynne, M.A., 1999. A Complex Magma Mixing Origin for Rocks Erupted in 1915, Lassen Peak, California. *Journal of Petrology* 40, 105–132. <https://doi.org/10.1093/petroj/40.1.105>

- Clynne, M.A., Christiansen, R.L., Trimble, D.A., McGeehin, J.P., 2008. Radiocarbon dates from volcanic deposits of the Chaos Crags and Cinder Cone eruptive sequences and other deposits, Lassen Volcanic National Park and vicinity, California.
- Clynne, M.A., Muffler, L., 2010. Geologic Map of Lassen Volcanic National Park and Vicinity, California.
- Conrey, R., 1991. Geology and petrology of the Mt. Jefferson area, High Cascade range, Oregon.
- Cooper, K.M., Reid, M.R., 2003. Re-examination of crystal ages in recent Mount St. Helens lavas: implications for magma reservoir processes. *Earth and Planetary Science Letters* 213, 149–167. [https://doi.org/10.1016/S0012-821X\(03\)00262-0](https://doi.org/10.1016/S0012-821X(03)00262-0)
- Couperthwaite, F.K., Wieser, P.E., Kent, A.J.R., Ruth, D.C.S., Gazel, E., DeVitre, C.L., 2022. Combining Fe-Mg diffusion in olivine and volatile concentrations from olivine-hosted melt inclusions to constrain eruption timescales and magma storage depths beneath Paint Pot Crater, Medicine Lake. Presented at the Chapman Conference on Distributed Volcanism.
- Cribb, J.W., 1997. A Petrologic and Geochemical Investigation of the Evolutionary History of Calc-alkaline Magmas, Mount Hood, Oregon. Ohio State University PhD thesis.
- Crider, J.G., Frank, D., Malone, S.D., Poland, M.P., Werner, C., Caplan-Auerbach, J., 2011. Magma at depth: a retrospective analysis of the 1975 unrest at Mount Baker, Washington, USA. *Bull Volcanol* 73, 175–189. <https://doi.org/10.1007/s00445-010-0441-0>
- Crosbie, K.J., Abers, G.A., Mann, M.E., Janiszewski, H.A., Creager, K.C., Ulberg, C.W., Moran, S.C., 2019. Shear Velocity Structure From Ambient Noise and Teleseismic Surface Wave Tomography in the Cascades Around Mount St. Helens. *J. Geophys. Res. Solid Earth* 124, 8358–8375. <https://doi.org/10.1029/2019JB017836>
- Danyushevsky, L.V., Plechov, P., 2011. Petrolog3: Integrated software for modeling crystallization processes. *Geochemistry, Geophysics, Geosystems* 12, n/a-n/a. <https://doi.org/10.1029/2011GC003516>
- Darr, C., 2006. Magma Chamber Processes Over the Past 475,000 Years at Mount Hood, Oregon: Insights From Crystal Zoning and Crystal Size Distribution Studies. Oregon State University Masters Thesis.
- Das, T., Nolet, G., 1998. Crustal thickness map of the western United States by partitioned waveform inversion. *J. Geophys. Res.* 103, 30021–30038. <https://doi.org/10.1029/98JB01119>
- DeVitre, C.L., Allison, C.M., Gazel, E., 2021. A high-precision CO₂ densimeter for Raman spectroscopy using a Fluid Density Calibration Apparatus. *Chemical Geology* 584, 120522. <https://doi.org/10.1016/j.chemgeo.2021.120522>
- DiGuilio, J., 2015. Reconstructing the Physical Record of a Four-Million-Year Volcanic System: Geochemistry, Thermobarometry, and Geologic Map of the Mount Jefferson Area, Oregon. Oregon State University Masters Thesis.
- Dixon, J.E., 1997. Degassing of alkalic basalts. *American Mineralogist* 82, 368–378. <https://doi.org/10.2138/am-1997-3-415>
- Donnelly-Nolan, J.M., 1988. A magmatic model of Medicine Lake volcano, California. *Journal of Geophysical Research* 93, 4412–4420.
- Donnelly-Nolan, J.M., Grove, T.L., Lanphere, M.A., Champion, D.E., Ramsey, D.W., 2008. Eruptive history and tectonic setting of Medicine Lake Volcano, a large rear-arc volcano in the southern Cascades. *Journal of Volcanology and Geothermal Research* 177, 313–328. <https://doi.org/10.1016/j.jvolgeores.2008.04.023>
- Donnelly-Nolan, Stovall, W.K., Ramsey, D.W., Ewert, J., Jensen, R., 2011. Newberry Volcano—central Oregon’s sleeping giant.
- Druitt, T.H., Bacon, C.R., 1989. Petrology of the zoned calcalkaline magma chamber of Mount Mazama, Crater Lake, Oregon. *Contr. Mineral. and Petrol.* 101, 245–259. <https://doi.org/10.1007/BF00375310>

- Ducea, M.N., Saleeby, J.B., Bergantz, G., 2015. The Architecture, Chemistry, and Evolution of Continental Magmatic Arcs. *Annu. Rev. Earth Planet. Sci.* 43, 299–331. <https://doi.org/10.1146/annurev-earth-060614-105049>
- Dufek, J., Cashman, K., Hooft, E., Bedrosian, P., 2022. The Nature of Active Magma Reservoirs and Storage Underneath Cascade Volcanoes. *Elements* 18, 239–245. <https://doi.org/10.2138/gselements.18.4.239>
- Dzurisin, D., 1999. Results of repeated leveling surveys at Newberry Volcano, Oregon, and near Lassen Peak Volcano, California. *Bulletin of Volcanology* 61, 83–91. <https://doi.org/10.1007/s004450050264>
- Dzurisin, D., Donnelly-Nolan, J.M., Evans, J.R., Walter, S.R., 1991. Crustal subsidence, seismicity, and structure near Medicine Lake Volcano, California. *J. Geophys. Res.* 96, 16319. <https://doi.org/10.1029/91JB01452>
- Dzurisin, D., Lisowski, M., Wicks, C.W., 2009. Continuing inflation at Three Sisters volcanic center, central Oregon Cascade Range, USA, from GPS, leveling, and InSAR observations. *Bull Volcanol* 71, 1091–1110. <https://doi.org/10.1007/s00445-009-0296-4>
- Dzurisin, D., Lisowski, M., Wicks, C.W., Poland, M.P., Endo, E.T., 2006. Geodetic observations and modeling of magmatic inflation at the Three Sisters volcanic center, central Oregon Cascade Range, USA. *Journal of Volcanology and Geothermal Research* 150, 35–54. <https://doi.org/10.1016/j.jvolgeores.2005.07.011>
- Dzurisin, D., Poland, M.P., Bürgmann, R., 2002. Steady subsidence of Medicine Lake volcano, northern California, revealed by repeated leveling surveys: SUBSIDENCE OF MEDICINE LAKE VOLCANO. *J. Geophys. Res.* 107, ECV 8-1-ECV 8-16. <https://doi.org/10.1029/2001JB000893>
- Evans, J.R., Zucca, J.J., 1988. Active high-resolution seismic tomography of compressional wave velocity and attenuation structure at Medicine Lake Volcano, Northern California Cascade Range. *J. Geophys. Res.* 93, 15016–15036. <https://doi.org/10.1029/JB093iB12p15016>
- Evans, W.C., van Soest, M.C., Mariner, R.H., Hurwitz, S., Ingebritsen, S.E., Wicks, C.W., Schmidt, M.E., 2004. Magmatic intrusion west of Three Sisters, central Oregon, USA: The perspective from spring geochemistry. *Geol* 32, 69. <https://doi.org/10.1130/G19974.1>
- Ewert, J., Diefenbach, A.K., Ramsey, D.W., 2018. 2018 update to the U.S. Geological Survey national volcanic threat assessment (Scientific Investigations Report 2018-5140), Scientific Investigations Report.
- Fierstein, J., Hildreth, W., Calvert, A.T., 2011. Eruptive history of South Sister, Oregon Cascades. *Journal of Volcanology and Geothermal Research* 207, 145–179. <https://doi.org/10.1016/j.jvolgeores.2011.06.003>
- Fillmore, J.A., 2014. The Origin of Adakites in the Garibaldi Volcanic Complex, southwestern British Columbia, Canada. Master of Science, University of Regina.
- Flinders, A.F., Shen, Y., 2017. Seismic evidence for a possible deep crustal hot zone beneath Southwest Washington. *Sci Rep* 7, 7400. <https://doi.org/10.1038/s41598-017-07123-w>
- Gerlach, D.C., Grove, T.L., 1982. Petrology of Medicine Lake Highland volcanics: Characterization of endmembers of magma mixing. *Contr. Mineral. and Petrol.* 80, 147–159. <https://doi.org/10.1007/BF00374892>
- Ghiorso, M.S., Gualda, G.A.R., 2015. An H₂O–CO₂ mixed fluid saturation model compatible with rhyolite-MELTS. *Contrib Mineral Petrol* 169, 53. <https://doi.org/10.1007/s00410-015-1141-8>
- Gleeson, M.L.M., Gibson, S.A., Stock, M.J., 2021. Upper Mantle Mush Zones beneath Low Melt Flux Ocean Island Volcanoes: Insights from Isla Floreana, Galápagos. *Journal of Petrology* 61, egaa094. <https://doi.org/10.1093/petrology/egaa094>
- Gross, J., 2012. Felsic magmas from Mt. Baker in the northern Cascade arc: Origin and role in andesite production, Western Washington University Masters Thesis, <https://cedar.wvu.edu/wwuet/239/>. ed.
- Grove, T., Parman, S., Bowring, S., Price, R., Baker, M., 2002. The role of an H₂O-rich fluid component in the generation of primitive basaltic andesites and andesites from the Mt.

- Shasta region, N California. *Contrib Mineral Petrol* 142, 375–396.
<https://doi.org/10.1007/s004100100299>
- Grove, T.L., Baker, M.B., Price, R.C., Parman, S.W., Elkins-Tanton, L.T., Chatterjee, N., Montener, O., 2005. Magnesian andesite and dacite lavas from Mt. Shasta, northern California: products of fractional crystallization of H₂O-rich mantle melts. *Contrib Mineral Petrol* 148, 542–565.
<https://doi.org/10.1007/s00410-004-0619-6>
- Grove, T.L., Donnelly-Nolan, J.M., 1986. The evolution of young silicic lavas at Medicine Lake Volcano, California: Implications for the origin of compositional gaps in calc-alkaline series lavas. *Contr. Mineral. and Petrol.* 92, 281–302. <https://doi.org/10.1007/BF00572157>
- Grove, T.L., Donnelly-Nolan, J.M., Housh, T., 1997. Magmatic processes that generated the rhyolite of Glass Mountain, Medicine Lake volcano, N. California. *Contributions to Mineralogy and Petrology* 127, 205–223. <https://doi.org/10.1007/s004100050276>
- Grove, T.L., Elkins-Tanton, L.T., Parman, S.W., Chatterjee, N., Montener, O., Gaetani, G.A., 2003. Fractional crystallization and mantle-melting controls on calc-alkaline differentiation trends. *Contributions to Mineralogy and Petrology* 145, 515–533. <https://doi.org/10.1007/s00410-003-0448-z>
- Grove, T.L., Gerlach, D.C., Sando, T.W., 1982. Origin of calc-alkaline series lavas at Medicine Lake Volcano by fractionation, assimilation and mixing. *Contr. Mineral. and Petrol.* 80, 160–182. <https://doi.org/10.1007/BF00374893>
- Guffanti, M., Weaver, C.S., 1988. Distribution of Late Cenozoic volcanic vents in the Cascade range: Volcanic arc segmentation and regional tectonic considerations. *J. Geophys. Res.* 93, 6513. <https://doi.org/10.1029/JB093iB06p06513>
- Harris, R.A., Iyer, H.M., Dawson, P.B., 1991. Imaging the Juan de Fuca Plate beneath southern Oregon using teleseismic *P* wave residuals. *J. Geophys. Res.* 96, 19879–19889. <https://doi.org/10.1029/91JB02046>
- Heath, B.A., Hooft, E.E.E., Toomey, D.R., 2018. Autocorrelation of the Seismic Wavefield at Newberry Volcano: Reflections From the Magmatic and Geothermal Systems. *Geophys. Res. Lett.* 45, 2311–2318. <https://doi.org/10.1002/2017GL076706>
- Heath, B.A., Hooft, E.E.E., Toomey, D.R., Bezada, M.J., 2015. Imaging the magmatic system of Newberry Volcano using joint active source and teleseismic tomography. *Geochem. Geophys. Geosyst.* 16, 4433–4448. <https://doi.org/10.1002/2015GC006129>
- Hildreth, W., 2007. Quaternary magmatism in the Cascades- Geological Perspectives, USGS Professional paper 1744.
- Hildreth, W., Fierstein, J., 2015. Geologic map of the Simcoe Mountains Volcanic Field, main central segment, Yakama Nation, Washington (Scientific Investigations Map 3315), Scientific Investigations Map.
- Hildreth, W., Fierstein, J., 1997. Recent eruptions of Mount Adams, Washington Cascades, USA. *Bulletin of Volcanology* 58, 472–490. <https://doi.org/10.1007/s004450050156>
- Hildreth, W., Fierstein, J., Lanphere, M., 2003. Eruptive history and geochronology of the Mount Baker volcanic field, Washington. *Geological Society of America Bulletin* 115, 729–764. [https://doi.org/10.1130/0016-7606\(2003\)115<0729:EHAGOT>2.0.CO;2](https://doi.org/10.1130/0016-7606(2003)115<0729:EHAGOT>2.0.CO;2)
- Hill, G.J., Caldwell, T.G., Heise, W., Chertkoff, D.G., Bibby, H.M., Burgess, M.K., Cull, J.P., Cas, R.A.F., 2009. Distribution of melt beneath Mount St Helens and Mount Adams inferred from magnetotelluric data. *Nature Geosci* 2, 785–789. <https://doi.org/10.1038/ngeo661>
- Hilley, G., Brodsky, E., Roman, D., Shillington, D., Tobin, H., 2022. SZ4D Implementation Plan. Stanford Digital Repository. <https://doi.org/10.25740/HY589FC7561>
- Hodge, B.E., Crider, J.G., 2010. Investigating mechanisms of edifice deflation, 1981–2007, at Mount Baker volcano, Washington, United States. *J. Geophys. Res.* 115, B04401. <https://doi.org/10.1029/2009JB006730>

- Hollyday, A.E., Leiter, S.H., Walowski, K.J., 2020. Pre-eruptive storage, evolution, and ascent timescales of a high-Mg basaltic andesite in the southern Cascade Arc. *Contrib Mineral Petrol* 175, 88. <https://doi.org/10.1007/s00410-020-01730-z>
- Huber, C., Townsend, M., Degruyter, W., Bachmann, O., 2019. Optimal depth of subvolcanic magma chamber growth controlled by volatiles and crust rheology. *Nat. Geosci.* 12, 762–768. <https://doi.org/10.1038/s41561-019-0415-6>
- Hughes, E.C., Buse, B., Kearns, S.L., Blundy, J.D., Kilgour, G., Mader, H.M., 2019. Low analytical totals in EPMA of hydrous silicate glass due to sub-surface charging: Obtaining accurate volatiles by difference. *Chemical Geology* 505, 48–56. <https://doi.org/10.1016/j.chemgeo.2018.11.015>
- Humphreys, M.C.S., Cooper, G.F., Zhang, J., Loewen, M., Kent, A.J.R., Macpherson, C.G., Davidson, J.P., 2019. Unravelling the complexity of magma plumbing at Mount St. Helens: a new trace element partitioning scheme for amphibole. *Contrib Mineral Petrol* 174, 9. <https://doi.org/10.1007/s00410-018-1543-5>
- Iacono-Marziano, G., Morizet, Y., Le Trong, E., Gaillard, F., 2012. New experimental data and semi-empirical parameterization of H₂O–CO₂ solubility in mafic melts. *Geochimica et Cosmochimica Acta* 97, 1–23. <https://doi.org/10.1016/j.gca.2012.08.035>
- Iacovino, K., Matthews, S., Wieser, P.E., Moore, G., Begue, F., 2021. VESical Part I: An open-source thermodynamic model engine for mixed volatile (H₂O–CO₂) solubility in silicate melt. *Earth and Space Science*. <https://doi.org/10.1029/2020EA001584>
- Jiang, C., Schmandt, B., Abers, G.A., Kiser, E., Miller, M.S., 2023. Segmentation and radial anisotropy of the deep crustal magmatic system beneath the Cascades arc. *Geochemistry, Geophysics, Geosystems*. <https://doi.org/10.1002/essoar.10512621.1>
- Johnson, E.R., Cashman, K.V., 2020. Understanding the storage conditions and fluctuating eruption style of a young monogenetic volcano: Blue Lake crater (<3 ka), High Cascades, Oregon. *Journal of Volcanology and Geothermal Research* 408, 107103. <https://doi.org/10.1016/j.jvolgeores.2020.107103>
- Jones, J., Malone, S.D., 2005. Mount Hood Earthquake Activity: Volcanic or Tectonic Origins? *Bulletin of the Seismological Society of America* 95, 818–832. <https://doi.org/10.1785/0120040019>
- Jorgenson, C., Higgins, O., Petrelli, M., Bégué, F., Caricchi, L., 2022. A Machine Learning-Based Approach to Clinopyroxene Thermobarometry: Model Optimization and Distribution for Use in Earth Sciences. *JGR Solid Earth* 127. <https://doi.org/10.1029/2021JB022904>
- Keith, T.E., Donnelly-Nolan, J., Markman, J., Beeson, M., 1985. K–Ar ages of rocks in the Mount Hood area, Oregon. *Isotopes* 42, 12–17.
- Kent, A.J.R., Darr, C., Koleszar, A.M., Salisbury, M.J., Cooper, K.M., 2010. Preferential eruption of andesitic magmas through recharge filtering. *Nature Geosci* 3, 631–636. <https://doi.org/10.1038/ngeo924>
- Kinzler, R.J., Donnelly-Nolan, J.M., Grove, T.L., 2000. Late Holocene hydrous mafic magmatism at the Paint Pot Crater and Callahan flows, Medicine Lake Volcano, N. California and the influence of H₂O in the generation of silicic magmas. *Contrib Mineral Petrol* 138, 1–16. <https://doi.org/10.1007/PL00007657>
- Kiser, E., Levander, A., Zelt, C., Schmandt, B., Hansen, S., 2018. Focusing of melt near the top of the Mount St. Helens (USA) magma reservoir and its relationship to major volcanic eruptions. *Geology* 46, 775–778. <https://doi.org/10.1130/G45140.1>
- Kiser, E., Palomeras, I., Levander, A., Zelt, C., Harder, S., Schmandt, B., Hansen, S., Creager, K., Ulberg, C., 2016. Magma reservoirs from the upper crust to the Moho inferred from high-resolution V_p and V_s models beneath Mount St. Helens, Washington State, USA. *Geology* 44, 411–414. <https://doi.org/10.1130/G37591.1>
- Koleszar, A.M., 2011. Controls on Eruption Style and Magma Compositions at Mount Hood, Oregon. Oregon State University PhD thesis.

- Koleszar, A.M., Kent, A.J.R., Wallace, P.J., Scott, W.E., 2012. Controls on long-term low explosivity at andesitic arc volcanoes: Insights from Mount Hood, Oregon. *Journal of Volcanology and Geothermal Research* 219–220, 1–14. <https://doi.org/10.1016/j.jvolgeores.2012.01.003>
- Krawczynski, M.J., Grove, T.L., Behrens, H., 2012. Amphibole stability in primitive arc magmas: effects of temperature, H₂O content, and oxygen fugacity. *Contrib Mineral Petrol* 164, 317–339. <https://doi.org/10.1007/s00410-012-0740-x>
- Lamadrid, H.M., Moore, L.R., Moncada, D., Rimstidt, J.D., Burruss, R.C., Bodnar, R.J., 2017. Reassessment of the Raman CO₂ densimeter. *Chemical Geology* 450, 210–222. <https://doi.org/10.1016/j.chemgeo.2016.12.034>
- Le Voyer, M., Rose-Koga, E.F., Shimizu, N., Grove, T.L., Schiano, P., 2010. Two Contrasting H₂O-rich Components in Primary Melt Inclusions from Mount Shasta. *Journal of Petrology* 51, 1571–1595. <https://doi.org/10.1093/petrology/egq030>
- Lee, C.-T.A., Anderson, D.L., 2015. Continental crust formation at arcs, the arclogite “delamination” cycle, and one origin for fertile melting anomalies in the mantle. *Science Bulletin* 60, 1141–1156. <https://doi.org/10.1007/s11434-015-0828-6>
- Lerner, A.H., O’Hara, D., Karlstrom, L., Ebmeier, S.K., Anderson, K.R., Hurwitz, S., 2020. The Prevalence and Significance of Offset Magma Reservoirs at Arc Volcanoes. *Geophys. Res. Lett.* 47. <https://doi.org/10.1029/2020GL087856>
- Lisowski, M., Dzurisin, D., Denlinger, R.P., Iwatsubo, E., 2008. Analysis of GPS-Measured Deformation Associated with the 2004–2006 Dome-Building Eruption of Mount St. Helens, Washington, in: *A Volcano Rekindled: The Renewed Eruption of Mount St. Helens, 2004–2006*, USGS Professional Paper 1750.
- Loewen, M.W., 2012. Volatile Mobility of Trace Metals in Volcanic Systems. PhD dissertation, Oregon State University. 237.
- Lu, L., Bostock, M.G., 2022. Deep long-period earthquakes near Mount Meager, British Columbia. *Canadian Journal of Earth Sciences* 59, 407–417.
- Lu, Z., Wicks, C., Dzurisin, D., Thatcher, W., Freymueller, J.T., McNutt, S.R., Mann, D., 2000. Aseismic inflation of Westdahl volcano, Alaska, revealed by satellite radar interferometry. *Geophysical Research Letters* 27, 1567–1570.
- Mandeville, C.W., Webster, J.D., Tappen, C., Taylor, B.E., Timbal, A., Sasaki, A., Hauri, E., Bacon, C.R., 2009. Stable isotope and petrologic evidence for open-system degassing during the climactic and pre-climactic eruptions of Mt. Mazama, Crater Lake, Oregon. *Geochimica et Cosmochimica Acta* 73, 2978–3012. <https://doi.org/10.1016/j.gca.2009.01.019>
- Mandler, B.E., Donnelly-Nolan, J.M., Grove, T.L., 2014. Straddling the tholeiitic/calc-alkaline transition: the effects of modest amounts of water on magmatic differentiation at Newberry Volcano, Oregon. *Contrib Mineral Petrol* 168, 1066. <https://doi.org/10.1007/s00410-014-1066-7>
- Mastin, L.G., Roeloffs, E., Beeler, N.M., Quick, J.E., 2008. Constraints on the Size, Overpressure, and Volatile Content of the Mount St. Helens Magma System from Geodetic and Dome-Growth Measurements During the 2004–2006+ Eruption. *A Volcano Rekindled: The Renewed Eruption of Mount St. Helens, 2004–2006*. U.S. Geological Survey Professional Paper 1750 28.
- McCrary, P.A., Blair, J.L., Waldhauser, F., Oppenheimer, D.H., 2012. Juan de Fuca slab geometry and its relation to Wadati-Benioff zone seismicity: JDF SLAB GEOMETRY AND WBZ SEISMICITY. *J. Geophys. Res.* 117. <https://doi.org/10.1029/2012JB009407>
- McGary, R.S., Evans, R.L., Wannamaker, P.E., Elsenbeck, J., Rondenay, S., 2014. Pathway from subducting slab to surface for melt and fluids beneath Mount Rainier. *Nature* 511, 338–340. <https://doi.org/10.1038/nature13493>
- Mercer, C.N., Johnston, A.D., 2008. Experimental studies of the P–T–H₂O near-liquidus phase relations of basaltic andesite from North Sister Volcano, High Oregon Cascades: constraints

- on lower-crustal mineral assemblages. *Contrib Mineral Petrol* 155, 571–592.
<https://doi.org/10.1007/s00410-007-0259-8>
- Mironov, N.L., Tobelko, D.P., Smirnov, S.Z., Portnyagin, M.V., Krasheninnikov, S.P., 2020. Estimation of CO₂ Content in the Gas Phase of Melt Inclusions Using Raman Spectroscopy: Case Study of Inclusions in Olivine from the Karymsky Volcano (Kamchatka). *Russian Geology and Geophysics* 61, 600–610. <https://doi.org/10.15372/RGG2019169>
- Moore, L.R., Gazel, E., Tuohy, R., Lloyd, A.S., Esposito, R., Steele-MacInnis, M., Hauri, E.H., Wallace, P.J., Plank, T., Bodnar, R.J., 2015. Bubbles matter: An assessment of the contribution of vapor bubbles to melt inclusion volatile budgets. *American Mineralogist* 100, 806–823. <https://doi.org/10.2138/am-2015-5036>
- Moore, L.R., Mironov, N., Portnyagin, M., Gazel, E., Bodnar, R.J., 2018. Volatile contents of primitive bubble-bearing melt inclusions from Klyuchevskoy volcano, Kamchatka: Comparison of volatile contents determined by mass-balance versus experimental homogenization. *Journal of Volcanology and Geothermal Research* 358, 124–131. <https://doi.org/10.1016/j.jvolgeores.2018.03.007>
- Moore, N.E., DeBari, S.M., 2012. Mafic magmas from Mount Baker in the northern Cascade arc, Washington: probes into mantle and crustal processes. *Contrib Mineral Petrol* 163, 521–546. <https://doi.org/10.1007/s00410-011-0686-4>
- Moran, S., Benjamin, P., 2021. Permitting Volcano Monitoring Stations in Wilderness/Restricted Areas: A Case Study From Mount Hood, Oregon, in: D138. Presented at the GSA Meeting, Portland.
- Moran, S.C., Lees, J.M., Malone, S.D., 1999. *P* wave crustal velocity structure in the greater Mount Rainier area from local earthquake tomography. *J. Geophys. Res.* 104, 10775–10786. <https://doi.org/10.1029/1999JB900036>
- Mordensky, S.P., Wallace, P.J., 2018. Magma storage below Cascades shield volcanoes as inferred from melt inclusion data: A comparison of long-lived and short-lived magma plumbing systems. *Journal of Volcanology and Geothermal Research* 368, 1–12. <https://doi.org/10.1016/j.jvolgeores.2018.10.011>
- Mullen, E.K., McCallum, I.S., 2014. Origin of Basalts in a Hot Subduction Setting: Petrological and Geochemical Insights from Mt. Baker, Northern Cascade Arc. *Journal of Petrology* 55, 241–281. <https://doi.org/10.1093/petrology/egt064>
- Musumeci, C., Gresta, S., Malone, S.D., 2002. Magma system recharge of Mount St. Helens from precise relative hypocenter location of microearthquakes: MAGMA RECHARGE OF ST. HELENS FROM HYPOCENTERS. *J. Geophys. Res.* 107, ESE 16-1-ESE 16-9. <https://doi.org/10.1029/2001JB000629>
- Nakada, S., Bacon, C.R., Gartner, A.E., 1994. Origin of Phenocrysts and Compositional Diversity in Pre-Mazama Rhyodacite Lavas, Crater Lake, Oregon. *Journal of Petrology* 35, 127–162. <https://doi.org/10.1093/petrology/35.1.127>
- NASA/METI/AIST/Japan Spacesystems And U.S./Japan ASTER Science Team, 2019. ASTER Global Digital Elevation Model V003. <https://doi.org/10.5067/ASTER/ASTGTM.003>
- Neave, D.A., Bali, E., Guðfinnsson, G.H., Halldórsson, S.A., Kahl, M., Schmidt, A.-S., Holtz, F., 2019. Clinopyroxene–Liquid Equilibria and Geothermobarometry in Natural and Experimental Tholeiites: the 2014–2015 Holuhraun Eruption, Iceland. *Journal of Petrology* 60, 1653–1680. <https://doi.org/10.1093/petrology/egz042>
- Neave, D.A., Putirka, K.D., 2017. A new clinopyroxene-liquid barometer, and implications for magma storage pressures under Icelandic rift zones. *American Mineralogist* 102, 777–794. <https://doi.org/10.2138/am-2017-5968>
- Newman, S., Lowenstern, J.B., 2002. VolatileCalc: a silicate melt–H₂O–CO₂ solution model written in Visual Basic for excel. *Computers & Geosciences* 28, 597–604. [https://doi.org/10.1016/S0098-3004\(01\)00081-4](https://doi.org/10.1016/S0098-3004(01)00081-4)

- Nichols, M.L., Malone, S.D., Moran, S.C., Thelen, W.A., Vidale, J.E., 2011. Deep long-period earthquakes beneath Washington and Oregon volcanoes. *Journal of Volcanology and Geothermal Research* 200, 116–128. <https://doi.org/10.1016/j.jvolgeores.2010.12.005>
- Obrebski, M., Abers, G.A., Foster, A., 2015. Magmatic arc structure around Mount Rainier, WA, from the joint inversion of receiver functions and surface wave dispersion. *Geochemistry, Geophysics, Geosystems* 16, 178–194.
- O'Hara, D., Karlstrom, L., Ramsey, D.W., 2020. Time-evolving surface and subsurface signatures of Quaternary volcanism in the Cascades arc. *Geology* 48, 1088–1093. <https://doi.org/10.1130/G47706.1>
- Papale, P., Moretti, R., Barbato, D., 2006. The compositional dependence of the saturation surface of H₂O+CO₂ fluids in silicate melts. *Chemical Geology* 229, 78–95. <https://doi.org/10.1016/j.chemgeo.2006.01.013>
- Park, S.K., Ostos, L.C., 2013. Constraints from magnetotelluric measurements on magmatic processes and upper mantle structure in the vicinity of Lassen volcanic center, northern California. *Geosphere* 9, 382–393. <https://doi.org/10.1130/GES00799.1>
- Parker, A.L., Biggs, J., Lu, Z., 2016. Time-scale and mechanism of subsidence at Lassen Volcanic Center, CA, from InSAR. *Journal of Volcanology and Geothermal Research* 320, 117–127. <https://doi.org/10.1016/j.jvolgeores.2016.04.013>
- Parker, A.L., Biggs, J., Lu, Z., 2014. Investigating long-term subsidence at Medicine Lake Volcano, CA, using multitemporal InSAR. *Geophysical Journal International* 199, 844–859. <https://doi.org/10.1093/gji/ggu304>
- Phillips, M., Till, C.B., 2022. Crustal storage and ascent history of the Mt. Shasta primitive magnesian andesite: implications for arc magma crustal flux rates. *Contrib Mineral Petrol* 177, 9. <https://doi.org/10.1007/s00410-021-01853-x>
- Pitcher, B.W., Kent, A.J.R., 2019. Statistics and segmentation: Using Big Data to assess Cascades arc compositional variability. *Geochimica et Cosmochimica Acta* 265, 443–467. <https://doi.org/10.1016/j.gca.2019.08.035>
- Pitt, A.M., Hill, D.P., Walter, S.W., Johnson, M.J.S., 2002. Midcrustal, Long-period Earthquakes beneath Northern California Volcanic Areas. Presented at the Seismological Research Letters, Vol 73, 2.
- Platt, B., 2020. Constraining Internal Eruption Trigger Mechanisms for Flows at Brokeoff Volcano, Lassen Volcanic Center, California.
- Poland, M., Bawden, G., Liwoski, M., Dzurisin, D., 2004. Newly discovered subsidence at Lassen Peak, southern Cascade Range, California, from InSAR and GPS. Presented at the AGU Fall Meeting, San Fran.
- Poland, M., Bürgmann, R., Dzurisin, D., Lisowski, M., Masterlark, T., Owen, S., Fink, J., 2006. Constraints on the mechanism of long-term, steady subsidence at Medicine Lake volcano, northern California, from GPS, leveling, and InSAR. *Journal of Volcanology and Geothermal Research* 150, 55–78. <https://doi.org/10.1016/j.jvolgeores.2005.07.007>
- Poland, M.P., Lisowski, M., Dzurisin, D., Kramer, R., McLay, M., Pauk, B., 2017. Volcano geodesy in the Cascade arc, USA. *Bull Volcanol* 79, 59. <https://doi.org/10.1007/s00445-017-1140-x>
- Poland, M.P., Miklius, A., Emily, M.-B., 2014. Magma Supply, Storage, and Transport at Shield-Stage Hawaiian Volcanoes, in: *Characteristics of Hawaiian Volcanoes*. pp. 179–234.
- Priest, G.R., Hladky, F.R., Mertzman, S.A., Murray, R.B., Wiley, T.J., 2013. Volcanic signature of Basin and Range extension on the shrinking Cascade arc, Klamath Falls-Keno area, Oregon: VOLCANIC SIGNATURE ON THE SHRINKING CASCADE ARC. *J. Geophys. Res. Solid Earth* 118, 4013–4038. <https://doi.org/10.1002/jgrb.50290>
- Pritchard, M.E., Mather, T.A., McNutt, S.R., Delgado, F.J., Reath, K., 2019. Thoughts on the criteria to determine the origin of volcanic unrest as magmatic or non-magmatic. *Phil. Trans. R. Soc. A* 377, 20180008. <https://doi.org/10.1098/rsta.2018.0008>

- Prueher, L.M., McBirney, A.R., 1988. Relations of cinder cones to the magmatic evolution of Mount Mazama, Crater Lake National Park, Oregon. *Journal of Volcanology and Geothermal Research* 35, 253–268. [https://doi.org/10.1016/0377-0273\(88\)90021-2](https://doi.org/10.1016/0377-0273(88)90021-2)
- Putirka, K., Johnson, M., Kinzler, R., Longhi, J., Walker, D., 1996. Thermobarometry of mafic igneous rocks based on clinopyroxene-liquid equilibria, 0-30 kbar. *Contributions to Mineralogy and Petrology* 123, 92–108. <https://doi.org/10.1007/s004100050145>
- Putirka, K.D., 2008. Thermometers and Barometers for Volcanic Systems. *Reviews in Mineralogy and Geochemistry* 69, 61–120. <https://doi.org/10.2138/rmg.2008.69.3>
- QGIS.org, 2022. QGIS Geographic Information System. <http://www.qgis.org>.
- Quinn, E., 2014. EXPERIMENTAL DETERMINATION OF PRE-ERUPTIVE STORAGE CONDITIONS AND CONTINUOUS DECOMPRESSION OF RHYODACITE MAGMA ERUPTED FROM CHAOS CRAGS, LASSEN VOLCANIC CENTER, CALIFORNIA.
- Rasmussen, D.J., 2019. The Aleutian arc through and through: Subduction dynamics and the generation, storage, and eruption of hydrous magmas.
- Rasmussen, D.J., Plank, T.A., Roman, D.C., Zimmer, M.M., 2022. Magmatic water content controls the pre-eruptive depth of arc magmas. *Science* 375, 1169–1172. <https://doi.org/10.1126/science.abm5174>
- Reeg, H., 2008. Seismic Structure of the Crust and upper Mantle of the Sierra Nevada, California. University of Colorado.
- Riddick, S.N., Schmidt, D.A., 2011. Time-dependent changes in volcanic inflation rate near Three Sisters, Oregon, revealed by InSAR: THREE SISTERS TIME-DEPENDENT INFLATION. *Geochem. Geophys. Geosyst.* 12, n/a-n/a. <https://doi.org/10.1029/2011GC003826>
- Ridolfi, F., 2021. Amp-TB2: An Updated Model for Calcic Amphibole Thermobarometry. *Minerals* 11, 324. <https://doi.org/10.3390/min11030324>
- Ritter, J.R.R., Evans, J.R., 1997. Deep structure of Medicine Lake volcano, California. *Tectonophysics* 275, 221–241. [https://doi.org/10.1016/S0040-1951\(97\)00022-X](https://doi.org/10.1016/S0040-1951(97)00022-X)
- Rohay, A., Malone, S.D., 1977. Seismic velocity anomalies in the vicinity of Mt. Baker, Washington (Abstract).
- Rowe, M., Thornber, C.R., Gooding, D., Pallister, J., 2008. Catalog of Mount St. Helens 2004 - 2005 Tephra Samples with Major- and Trace-Element Geochemistry.
- Rudnick, R.L., 1995. Making continental crust. *Nature* 378, 571–578. <https://doi.org/10.1038/378571a0>
- Ruscitto, D.M., Wallace, P.J., Johnson, E.R., Kent, A.J.R., Bindeman, I.N., 2010. Volatile contents of mafic magmas from cinder cones in the Central Oregon High Cascades: Implications for magma formation and mantle conditions in a hot arc. *Earth and Planetary Science Letters* 298, 153–161. <https://doi.org/10.1016/j.epsl.2010.07.037>
- Ruscitto, D.M., Wallace, P.J., Kent, A.J.R., 2011. Revisiting the compositions and volatile contents of olivine-hosted melt inclusions from the Mount Shasta region: implications for the formation of high-Mg andesites. *Contrib Mineral Petrol* 162, 109–132. <https://doi.org/10.1007/s00410-010-0587-y>
- Rutherford, M.J., Devine, J.D., 2008. Magmatic Conditions and Processes in the Storage Zone of the 2004–2006 Mount St. Helens Dacite, in: *A Volcano Rekindled: The Renewed Eruption of Mount St. Helens, 2004–2006*.
- Rutherford, M.J., Devine, J.D., 1988. The May 18, 1980, eruption of Mount St. Helens: 3. Stability and chemistry of amphibole in the magma chamber. *J. Geophys. Res.* 93, 11949. <https://doi.org/10.1029/JB093iB10p11949>
- Rutherford, M.J., Sigurdsson, H., Carey, S., Davis, A., 1985. The May 18, 1980, eruption of Mount St. Helens: 1. Melt composition and experimental phase equilibria. *J. Geophys. Res.* 90, 2929. <https://doi.org/10.1029/JB090iB04p02929>
- Ryan, W.B.F., Carbotte, S.M., Coplan, J.O., O’Hara, S., Melkonian, A., Arko, R., Weissel, R.A., Ferrini, V., Goodwillie, A., Nitsche, F., Bonczkowski, J., Zemsky, R., 2009. Global Multi-Resolution

- Topography synthesis: GLOBAL MULTI-RESOLUTION TOPOGRAPHY SYNTHESIS. *Geochem. Geophys. Geosyst.* 10, n/a-n/a. <https://doi.org/10.1029/2008GC002332>
- Sas, M., DeBari, S., Clynne, M., Rusk, B., 2017. Using mineral geochemistry to decipher slab, mantle, and crustal input in the generation of high-Mg andesites and basaltic andesites from the northern Cascade Arc. *msam*. <https://doi.org/10.2138/am-2017-5756>
- Scandone, R., Malone, S.D., 1985. Magma supply, magma discharge and readjustment of the feeding system of mount St. Helens during 1980. *Journal of Volcanology and Geothermal Research* 23, 239–262. [https://doi.org/10.1016/0377-0273\(85\)90036-8](https://doi.org/10.1016/0377-0273(85)90036-8)
- Schmidt, M.E., Grunder, A.L., 2011. Deep Mafic Roots to Arc Volcanoes: Mafic Recharge and Differentiation of Basaltic Andesite at North Sister Volcano, Oregon Cascades. *Journal of Petrology* 52, 603–641. <https://doi.org/10.1093/petrology/egq094>
- Schwab, B., Castro, J., 2007. PRE-ERUPTIVE STORAGE CONDITIONS OF 1915 LASSEN PEAK DACITE. Presented at the GSA Denver Annual Meeting.
- Scott, W.E., Gardner, C., Tilling, R.I., Lanphere, M.A., 1997. Geologic history of Mount Hood Volcano. Oregon: A Field-Trip Guidebook:
- Scruggs, M.A., Putirka, K.D., 2018. Eruption triggering by partial crystallization of mafic enclaves at Chaos Crags, Lassen Volcanic Center, California. *American Mineralogist* 103, 1575–1590. <https://doi.org/10.2138/am-2018-6058>
- Shaw, S., 2011. H₂O contents in olivine-hosted melt inclusions from primitive magmas in the Northern Cascade arc.
- Sheppard, P.R., Ort, M.H., Anderson, K.C., Clynne, M.A., May, E.M., 2009. Multiple dendrochronological responses to the eruption of Cinder Cone, Lassen Volcanic National Park, California. *Dendrochronologia* 27, 213–221. <https://doi.org/10.1016/j.dendro.2009.09.001>
- Sherrod, D., Mastin, L., Scott, W., Schilling, S., 1997. Volcano Hazards at Newberry Volcano, Oregon.
- Shishkina, T.A., Botcharnikov, R.E., Holtz, F., Almeev, R.R., Jazwa, A.M., Jakubiak, A.A., 2014. Compositional and pressure effects on the solubility of H₂O and CO₂ in mafic melts. *Chemical Geology* 388, 112–129. <https://doi.org/10.1016/j.chemgeo.2014.09.001>
- Sisson, T.W., Lanphere, M.A., 2000. The geologic history of Mount Rainier volcano.
- Sisson, T.W., Layne, G.D., 1993. H₂O in basalt and basaltic andesite glass inclusions from four subduction-related volcanoes. *Earth and Planetary Science Letters*.
- Sisson, T.W., Salters, V.J.M., Larson, P.B., 2014. Petrogenesis of Mount Rainier andesite: Magma flux and geologic controls on the contrasting differentiation styles at stratovolcanoes of the southern Washington Cascades. *Geological Society of America Bulletin* 126, 122–144. <https://doi.org/10.1130/B30852.1>
- Sisson, T.W., Schmitt, A.K., Danišik, M., Calvert, A.T., Pempena, N., Huang, C.-Y., Shen, C.-C., 2019. Age of the dacite of Sunset Amphitheater, a voluminous Pleistocene tephra from Mount Rainier (USA), and implications for Cascade glacial stratigraphy. *Journal of Volcanology and Geothermal Research* 376, 27–43. <https://doi.org/10.1016/j.jvolgeores.2019.03.003>
- Smith, D., Leeman, W.P., 1993. The origin of Mount St. Helens Andesites. *Journal of Volcanology and Geothermal Research* 55 (3).
- Stanley, W.D., 1984. Tectonic study of Cascade Range and Columbia Plateau in Washington State based upon magnetotelluric soundings. *J. Geophys. Res.* 89, 4447–4460. <https://doi.org/10.1029/JB089iB06p04447>
- Stauber, D.A., Green, S.M., Iyer, H.M., 1988. Three-dimensional *P* velocity structure of the crust below Newberry Volcano, Oregon. *J. Geophys. Res.* 93, 10095–10107. <https://doi.org/10.1029/JB093iB09p10095>
- Stockstill, K., 1999. The Origin and Evolution of the Burroughs Mountain Lava Flow, Mount Rainier, Washington. Michigan State University Masters Thesis.

- Streck, M.J., Leeman, W.P., 2018. Petrology of “Mt. Shasta” high-magnesian andesite (HMA): A product of multi-stage crustal assembly. *American Mineralogist* 103, 216–240. <https://doi.org/10.2138/am-2018-6151>
- Taira, T., Brenguier, F., 2016. Response of hydrothermal system to stress transients at Lassen Volcanic Center, California, inferred from seismic interferometry with ambient noise. *Earth Planets Space* 68, 162. <https://doi.org/10.1186/s40623-016-0538-6>
- Thornber, C.R., Pallister, J., Rowe, M., McConnell, S., Herriott, T.M., Eckberg, A., 2008. Catalog of Mount St. Helens 2004-2007 dome samples with major- and trace-element chemistry.
- Thurber, C., Zhang, H., Brocher, T., Langenheim, V., 2009. Regional three-dimensional seismic velocity model of the crust and uppermost mantle of northern California: N. CALIFORNIA 3-D SEISMIC VELOCITY MODEL. *J. Geophys. Res.* 114. <https://doi.org/10.1029/2008JB005766>
- Till, C.B., Kent, A.J.R., Abers, G.A., Janiszewski, H.A., Gaherty, J.B., Pitcher, B.W., 2019. The causes of spatiotemporal variations in erupted fluxes and compositions along a volcanic arc. *Nat Commun* 10, 1350. <https://doi.org/10.1038/s41467-019-09113-0>
- Turner, S.J., Izbekov, P., Langmuir, C., 2013. The magma plumbing system of Bezymianny Volcano: Insights from a 54-year time series of trace element whole-rock geochemistry and amphibole compositions. *Journal of Volcanology and Geothermal Research* 263, 108–121. <https://doi.org/10.1016/j.jvolgeores.2012.12.014>
- Ulberg, C.W., Creager, K.C., Moran, S.C., Abers, G.A., Thelen, W.A., Levander, A., Kiser, E., Schmandt, B., Hansen, S.M., Crosson, R.S., 2020. Local Source V_p and V_s Tomography in the Mount St. Helens Region With the iMUSH Broadband Array. *Geochem. Geophys. Geosyst.* 21. <https://doi.org/10.1029/2019GC008888>
- Underwood, S.J., Feeley, T.C., Clynne, M.A., 2012. Hydrogen isotope investigation of amphibole and biotite phenocrysts in silicic magmas erupted at Lassen Volcanic Center, California. *Journal of Volcanology and Geothermal Research* 227–228, 32–49. <https://doi.org/10.1016/j.jvolgeores.2012.02.019>
- USGS, 2022. Mt Shasta Hazards.
- Ustunisik, G., Loewen, M.W., Nielsen, R.L., Tepley, F.J., 2016. Interpretation of the provenance of small-scale heterogeneity as documented in a single eruptive unit from Mt. Jefferson, Central Oregon Cascades. *Geochem. Geophys. Geosyst.* 17, 3469–3487. <https://doi.org/10.1002/2016GC006297>
- Venezky, D.Y., Rutherford, M.J., 1997. Preeruption conditions and timing of dacite-andesite magma mixing in the 2.2 ka eruption at Mount Rainier. *J. Geophys. Res.* 102, 20069–20086. <https://doi.org/10.1029/97JB01590>
- Venugopal, S., Schiavi, F., Moune, S., Bolfan-Casanova, N., Druitt, T., Williams-Jones, G., 2020. Melt inclusion vapour bubbles: the hidden reservoir for major and volatile elements. *Sci Rep* 10, 9034. <https://doi.org/10.1038/s41598-020-65226-3>
- Waite, G.P., Moran, S.C., 2009. VP Structure of Mount St. Helens, Washington, USA, imaged with local earthquake tomography. *Journal of Volcanology and Geothermal Research* 182, 113–122. <https://doi.org/10.1016/j.jvolgeores.2009.02.009>
- Waite, R., Mastin, L.G., Beget, J., 1995. Volcanic Hazard Zonation for Glacier Peak Volcano, Washington (USGS Open File report 95-499), Open-File Report.
- Walowski, K.J., Wallace, P.J., Cashman, K.V., Marks, J.K., Clynne, M.A., Ruprecht, P., 2019. Understanding melt evolution and eruption dynamics of the 1666 C.E. eruption of Cinder Cone, Lassen Volcanic National Park, California: Insights from olivine-hosted melt inclusions. *Journal of Volcanology and Geothermal Research* 387, 106665. <https://doi.org/10.1016/j.jvolgeores.2019.106665>
- Walowski, K.J., Wallace, P.J., Clynne, M.A., Rasmussen, D.J., Weis, D., 2016. Slab melting and magma formation beneath the southern Cascade arc. *Earth and Planetary Science Letters* 446, 100–112. <https://doi.org/10.1016/j.epsl.2016.03.044>

- Wang, X., Hou, T., Wang, M., Zhang, C., Zhang, Z., Pan, R., Marxer, F., Zhang, H., 2021. A new clinopyroxene thermobarometer for mafic to intermediate magmatic systems. *Eur. J. Mineral.* 33, 621–637. <https://doi.org/10.5194/ejm-33-621-2021>
- Wanke, M., Clynne, M.A., von Quadt, A., Vennemann, T.W., Bachmann, O., 2019. Geochemical and petrological diversity of mafic magmas from Mount St. Helens. *Contrib Mineral Petrol* 174, 10. <https://doi.org/10.1007/s00410-018-1544-4>
- Waters, L.E., Andrews, B.J., Frey, H.M., 2021. Daly Gaps at South Sister, Oregon, USA, generated via partial melting. *Contrib Mineral Petrol* 176, 52. <https://doi.org/10.1007/s00410-021-01805-5>
- Weaver, C.S., Green, S.M., Iyer, H.M., 1982. Seismicity of Mount Hood and structure as determined from teleseismic *P* wave delay studies. *J. Geophys. Res.* 87, 2782. <https://doi.org/10.1029/JB087iB04p02782>
- Weaver, C.S., Norris, R., Jonientz-Trisler, C., 1990. Results of Seismological Monitoring in the Cascade Range, 1962-1989: Earthquakes, eruptions, avalanches and other curiosities. *Geoscience Canada* 17(3), 158–162.
- White, R., McCausland, W., 2016. Volcano-tectonic earthquakes: A new tool for estimating intrusive volumes and forecasting eruptions. *Journal of Volcanology and Geothermal Research* 309, 139–155. <https://doi.org/10.1016/j.jvolgeores.2015.10.020>
- Wicks, C.W., 2002. Magmatic activity beneath the quiescent Three Sisters volcanic center, central Oregon Cascade Range, USA. *Geophys. Res. Lett.* 29, 1122. <https://doi.org/10.1029/2001GL014205>
- Wieser, P., Iacovino, K., Matthews, S., Moore, G., Allison, C., 2022a. VESical Part II: A critical approach to volatile solubility modelling using an open-source Python3 engine. *Earth and Space Sciences.* 10.1029/2021EA001932
- Wieser, P. E., Edmonds, M., Gansecki, C., Maclennan, J., Jenner, F.E., Kunz, B., Antoshechkina, P., Trusdell, F., Lee, R.L., Eimf, 2022c. Explosive Activity on Kīlauea’s Lower East Rift Zone Fueled by a Volatile-Rich, Dacitic Melt. *Geochem Geophys Geosyst* 23. <https://doi.org/10.1029/2021GC010046>
- Wieser, P.E., Kent, A.J., Till, C., 2023b. Barometers behaving badly II: A critical evaluation of Cpx-only and Cpx-Liq thermobarometry in variably-hydrous arc magmas.
- Wieser, Penny E, Kent, A.J.R., Till, C.B., Donovan, J., Neave, D.A., Blatter, D.L., Krawczynski, M.J., 2023a. Barometers Behaving Badly I: Assessing the Influence of Analytical and Experimental Uncertainty on Clinopyroxene Thermobarometry Calculations at Crustal Conditions. *Journal of Petrology* 64, egac126. <https://doi.org/10.1093/petrology/egac126>
- Wieser, P.E., Lamadrid, H., Maclennan, J., Edmonds, M., Matthews, S., Iacovino, K., Jenner, F.E., Gansecki, C., Trusdell, F., Lee, R.L., Ilyinskaya, E., 2021. Reconstructing Magma Storage Depths for the 2018 Kīlauean Eruption From Melt Inclusion CO₂ Contents: The Importance of Vapor Bubbles. *Geochem Geophys Geosyst* 22. <https://doi.org/10.1029/2020GC009364>
- Wieser, P.E., Petrelli, M., Lubbers, J., Wieser, E., Ozaydin, S., Kent, A., Till, C., 2022b. Thermobar: An open-source Python3 tool for thermobarometry and hygrometry. *Volcanica* 5, 349–384. <https://doi.org/10.30909/vol.05.02.349384>
- Wright, H.M., Bacon, C.R., Vazquez, J.A., Sisson, T.W., 2012. Sixty thousand years of magmatic volatile history before the caldera-forming eruption of Mount Mazama, Crater Lake, Oregon. *Contrib Mineral Petrol* 164, 1027–1052. <https://doi.org/10.1007/s00410-012-0787-8>
- Zhang, H., Thurber, C.H., Shelly, D., Ide, S., Beroza, G.C., Hasegawa, A., 2004. High-resolution subducting-slab structure beneath northern Honshu, Japan, revealed by double-difference tomography. *Geol* 32, 361. <https://doi.org/10.1130/G20261.2>
- Zucca, J.J., Evans, J.R., 1992. Active high-resolution compressional wave attenuation tomography at Newberry Volcano, Central Cascade Range. *J. Geophys. Res.* 97, 11047. <https://doi.org/10.1029/92JB00492>

Geochemistry, Geophysics, Geosystems

Supporting Information for

Geophysical and Geochemical Constraints on Magma Storage Depths along the Cascade Arc: Knowns and Unknowns

Penny E Wieser^{1, 2*}, Adam J.R. Kent², Christy B. Till³, Geoff A. Abers⁴

1. **Corresponding author:** Penny_wieser@berkeley.edu, 541–908–4572. Department of Earth and Planetary Sciences, McCone Hall, UC Berkeley, 94720, USA
2. College of Earth, Ocean and Atmospheric Sciences, Oregon State University, 97331, USA
3. School of Earth and Space Exploration, Arizona State University, Tempe, AZ 85281, USA
4. Earth and Atmospheric Sciences, Cornell University, Ithaca, NY 14850, USA

Contents of this file

Figures S1 to S3
Tables S1

Introduction

Supporting Table 1 provides information on the different solubility models and bubble corrections performed. Supporting Fig 1-3 show additional geochemical plots to supplement the main text. All data and associated Jupyter notebooks for filtering and plotting are provided at GitHub (https://github.com/PennyWieser/Cascade_data_Compilation/tree/main), and will be archived through Zenodo following acceptance.

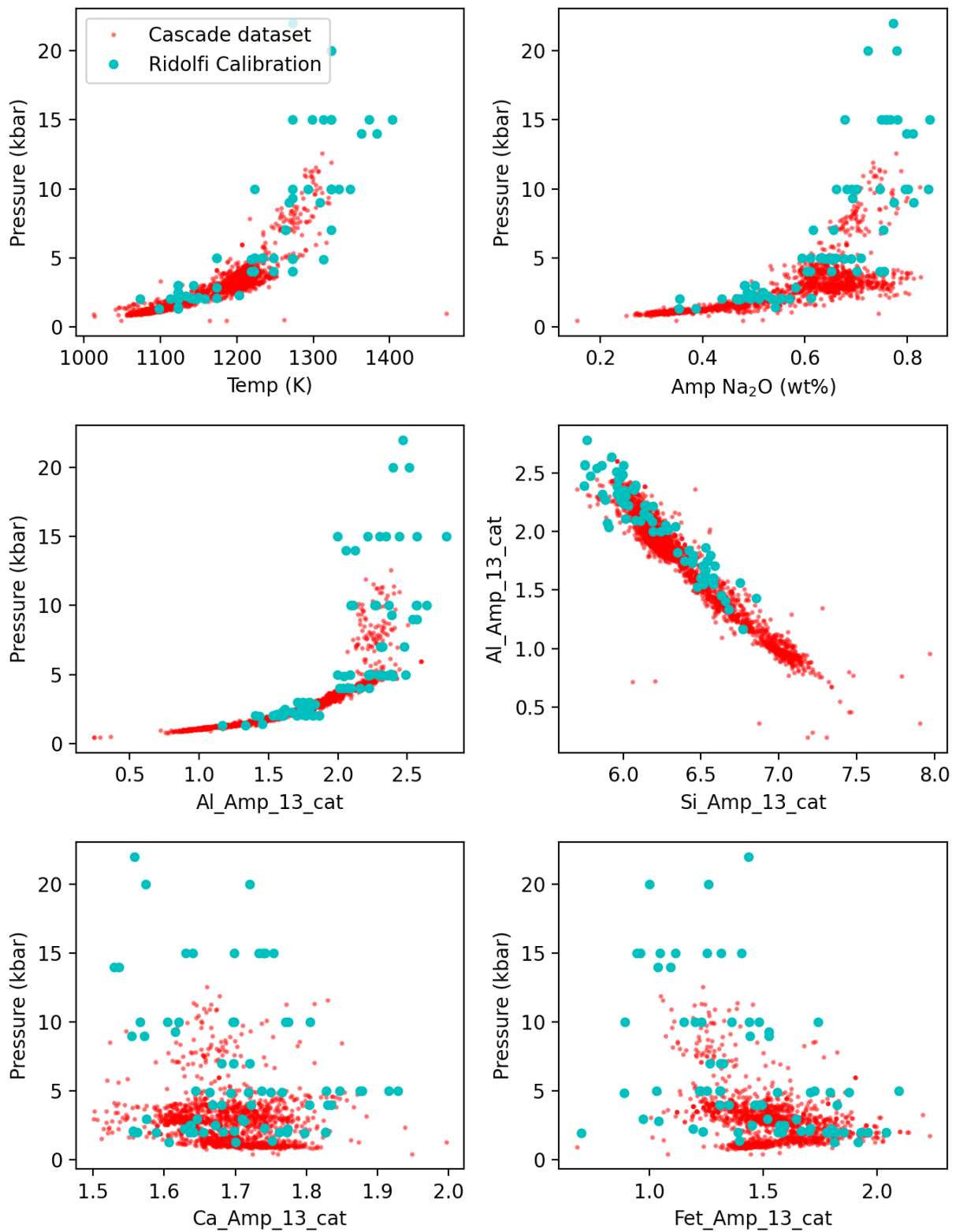


Figure S1 – Cascade amphibole data plotted alongside the calibration dataset of Ridolfi (2021). We apply filters based on the cation fraction of Al and Si, as these are the clearest

places where our data lies outside the calibration range. Specifically, we exclude data with >6.8 For Si, and <1.1 for Al.

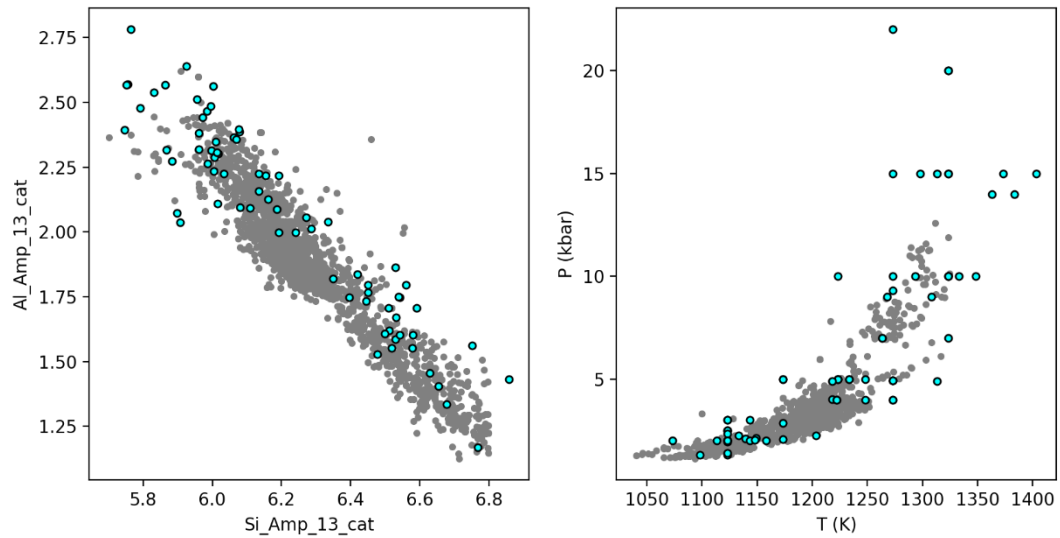


Figure S2 – Applying the additional filters for Si and Al cation fraction results in a filtered dataset (grey) within the calibration range of Ridolfi, 2021.

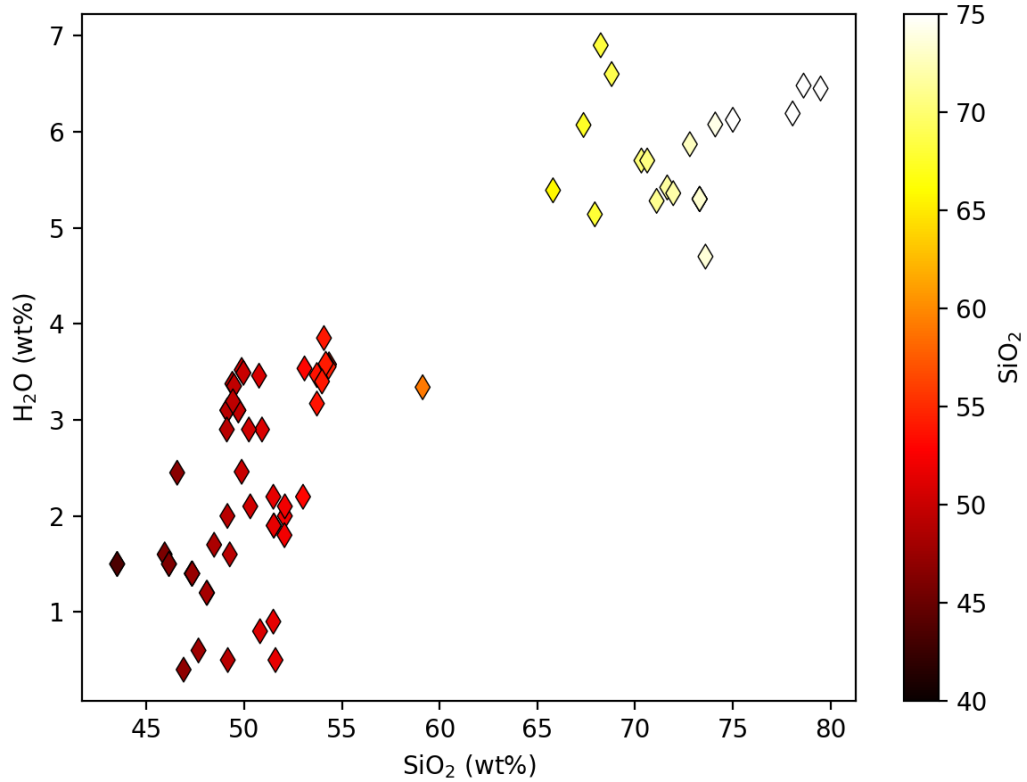


Figure S3 – Correlation between SiO₂ and H₂O for the 3 most H₂O-rich melt inclusions from each volcano.

Reference	Model	Density	Handling of bubbles
Aster et al. 2016	VolatileCalc (doesn't say, but presume basalt)	Don't convert to depths	Measure some at VT,
Walowski et al. (2016)			
Walowski et al. 2019	Isobars overlain with RhyoliteMELTS	Don't convert to depths	Vol bubble=0.0092 ΔT from rhyolite MELTS, then mol% of CO ₂ from rhyolite-MELTS, then equation of state for CO ₂ .
Quinn, 2014	Papale et al. 2006	2650 kg/m ³	None
Ruscitto et al. 2010	Papale et al. 2006	2800 kg/m ³	None
Le Voyer et al. 2010	VolatileCalc (basalt)	Doesn't say	None
Ruscitto et al. 2011	Papale et al. 2006	Doesn't convert to depths	None
Bacon et al. 1992	Cite Newman et al. (1988)	2200 kg/m ³	None
Mandeville et al. 2009	Moore et al. 1998	2300 kg/m ³	None
Wright et al. 2012	VolatileCalc (doesn't say, but assume rhyolite)	2200 kg/m ³	None
Johnson and Cashman, 2020	Papale et al. 2006	2800 kg/m ³	Vol bubble=0.00923 ΔT from rhyolite MELTS, calculate mol% CO ₂ using VolatileCalc,
Koleszar et al. 2012	Papale et al. 2006, Newman and Lowenstern, 1995	Don't convert to depths	None
Blundy et al. (2005)	Newman and Lowenstern (1995),	Doesn't say	None

	presume rhyolite from temperature		
Blundy et al. 2010	Newman and Lowenstern (1995), presume rhyolite from temperature, Papale et al. 2006	Doesn't convert to depths	
Venugopal et al. (2020)	Papale et al. 2006	Don't convert to depths	Raman analyses, but no instrument-specific calibration.

Table S1: Compilation of different solubility models, crustal densities, and handling of bubbles in published cascade melt inclusion studies.